Design of bi-orthogonal rational Discrete Wavelet Transform and the associated applications

by

Nguyen, Nguyen Si Tran

B. Eng. (Information Technology and Telecommunication, with first class Honours),
The University of Adelaide, Australia, 2007

Thesis submitted for the degree of

Doctor of Philosophy

in

Electrical and Electronic Engineering,
Faculty of Engineering, Computer and Mathematical Sciences
The University of Adelaide, Australia

2014

Supervisors:
Dr Brian W.-H. Ng, School of Electrical & Electronic Engineering
Prof Langford B White, School of Electrical & Electronic Engineering

ADELAIDE
UNIVERSITY
AUSTRALIA

Contents

Abstract

Time-frequency analysis has long been a very useful tool in the field of signal processing, especially in dealing with non-stationary signals. Wavelet transform is amongst many time-frequency analysis techniques whose attributes have been well exploited in many classic applications such as de-noising and compression. In recent years, representation sparsity, a measure of the representation's ability to condense signals' energy into few coefficients, has raised much interest from researchers in many fields such as signal processing, information theory and applied mathematics due to its wide range of use. Thus, many classes of time-frequency representations have recently been developed from the conventional ones in maximising the representation sparsity recently. Rational discrete wavelet transform (RADWT), an extended class of the conventional wavelet family, is among those representations. This thesis discusses the design of bi-orthogonal rational discrete wavelet transform which is constructed from finite impulse response (FIR) two-channel rational rate filter banks and the associated potential applications. Techniques for designing the bi-orthogonal rational filter bank are proposed, their advantages and disadvantages are discussed and compared with the existing designs in literature. Experimental examples are provided to illustrate the use of the novel bi-orthogonal RADWT in application such as signal separation. The experiments show sparser signal representations with RADWTs over conventional dyadic discrete wavelet transforms (DWTs). This is then exploited in applications such as de-noising and signal separation based on basis pursuit.

Statement of Originality

I certify that this work contains no material that has been accepted for the award of any other degree or diploma in my name in any university or other tertiary institution and, to the best of my knowledge and belief, contains no material previously published or written by another person, except where due reference has been made in the text. In addition, I certify that no part of this work will in the future, be used in a submission in my name for any other degree or diploma in any university or other tertiary institution without the prior approval of the University of Adelaide and where applicable, any partner institution responsible for the joint award of this degree.

I give consent to this copy of my thesis, when deposited in the University Library, being available for loan, photocopying subject to the provisions of the Copyright Act 1968.

I also give permission for the digital copy of my thesis to be made available on the web, via the University's digital research respiratory, the Library Search and also through web search engines, unless permission has been granted by the University to restrict access for a period of time.

Signed

Date

Acknowledgments

I would like to take the opportunity to express my gratitude to all those people whose support, skills and encouragement has helped me to complete this Thesis successfully.

First, I would like to convey my deep gratitude to my supervisors **Dr Brian Ng W-H** and **Prof Langford B White** for their guidance and support throughout my candidature. With the remarkable knowledge, they have helped me gain valuable research skills throughout my candidature. A special thanks to **Dr Brian Ng W-H** for his pioneering idea and insightful comments, which are good guidance for me to become a successful scientist.

I am grateful to Prof Douglas A. Gray from School of Electrical & Electronic Engineering for his support towards the end of my candidature.

I would also like to express my gratitude to all my friends and colleagues from the School of Electrical & Electronic Engineering at the University of Adelaide for their constant support throughout my candidature.

I gratefully acknowledge the School of Electrical & Electronic Engineering at the University of Adelaide, IEEE South Australia for their financial support and travel grants.

I would like to take the opportunity to extend my gratitude to my parents, sister and friends, especially Shaun Fox, Adrian Wun, Jindou Lee and Gommy for their support and encouragement in helping me going through ups and downs during the journey.

Nguyen Nguyen Si Tran

Thesis Conventions

The following conventions have been adopted in this Thesis:

1. **Spelling.** Australian English spelling conventions have been used, as defined in the Macquarie English Dictionary, A. Delbridge (Ed.), Macquarie Library, North Ryde, NSW, Australia, 2001.

2. **Typesetting.** This document was compiled using LaTeX2e. TeXnicCenter was used as text editor interfaced to LaTeX2e. Adobe Illustrator CS2 and Inkscape was used to produce schematic diagrams and other drawings.

3. **Mathematics.** MATLAB code was written using MATLAB Version R2007b/R2008a; URL: http://www.mathworks.com.

4. **Referencing.** The Harvard style has been adopted for referencing.

Publications

Journal articles

NGUYEN-S. T. N., AND NG-B.-W.-H. (2012). Design of two-band critically sampled rational rate filter banks with multiple regularity orders and associated discrete wavelet transforms, *Signal Processing, IEEE Transactions on*, **60**(7), pp. 3863 –3868.

S. TRAN NGUYEN NGUYEN, AND B.W.-H.NG (2013). Bi-orthogonal rational discrete wavelet transform with multiple regularity orders and application experiments, *Signal Processing (2013)*, http://dx.doi.org/10.1016/j.sigpro.2013.04.001i.

Conference articles

NGUYEN-S., AND NG-B.-H. (2010). Critically sampled discrete wavelet transforms with rational dilation factor of 3/2, *Signal Processing (ICSP), 2010 IEEE 10th International Conference on*, pp. 199 –202.

List of Figures

List of Tables

Chapter 1

Introduction

TIME-frequency analysis is an important tool in the field of signal processing, especially for non-stationary signal analysis. A time-frequency decomposition projects a time signal into a space which facilitates detection (of events), filtering and classification (of phenomena). In the new time-frequency space, the considered signal's components of interest can be well separated since such separation cannot be attained in the original time domain. Hence, thresholding and some other well known kernel methods can be applied for detection, filtering and classification tasks once time-frequency analysis is used in extracting the signals' features. This chapter provides an introduction to the prominent time-frequency analysis methods together with an outline of the thesis.

1.1 Introduction

Wavelet transform is a way of decomposing signals into a linear combination of waveforms which are scaled and shifted versions of a template signal. The coefficients can be analysed or processed in manners appropriate to applications. The transform provides good localisation in time and frequency at multiple resolutions in these domains. The wavelet transform continuously trades off time resolution for frequency resolution as the frequency changes, which differs from other time-frequency analysis such as short time Fourier transform (STFT). The short time Fourier transform maintains constant time-frequency resolution for all frequencies, which is a contrast to wavelet transform. The idea of wavelets was first developed in applied mathematics and attracted great attention soon after across all fields including physics and engineering. Wavelets hence can be approached from engineering perspective (sub-band coding), physics (coherent states) and mathematics (study of Calderon-Zygmund operators) (Daubechies 1992). The wavelet transforms, with a range of attractive features such as multi-scale representations, *piecewise smooth* functions recovery, transform flexibility, have become very successful in applications ranging from biomedical signal analysis (Unser and Aldroubi 1996), statistical analysis (Antoniadis 1997), digital wireless communications (Lakshmanan and Nikookar 2006) and many others (Sandercock *et al.* 2005, Pichot *et al.* 1999, Pichot *et al.* 2001, Belova *et al.* 2007).

For many years, dyadic wavelets and M-band wavelets (Daubechies 1992, Steffen *et al.* 1993) have been the most common, or conventional types. In the field of signal processing, wavelet transform is well known for improving sparsity of signals' representation, defined as one in which small number of coefficients contain large majority of energy. This property has been exploited by many applications, some classical examples are de-noising (Pan *et al.* 1999) and classification (Ghinwa and James 2007, Farooq and Datta 2001). Recently, sparse representation property has been further developed and the uses range from signal separation (O'Grady *et al.* 2005, He *et al.* 2007), compression (Goyal *et al.* 2008, Jiao *et al.* 2007, Blu *et al.* 2008), compressive sampling and signal analysis (Akçakaya and Tarokh 2008a). As a result, there have been interests in developing a different way of representing signals, which departs from the conventional wavelets, to further improve sparsity of representation.

In early 1990s non-uniform filter banks (NUFBs), which have non-integer re-sampling ratios and unequal spectrum partitioning, have received much interest. One of the

earliest works on this topic, presented by Kovacevic and Vetterli, addressed the issues of perfect reconstruction for non-uniform FBs. The authors devised a generalised feasibility test for perfect reconstruction (PR) conditions in a non-uniform FB structure and developed two methods of designing non-uniform FBs, namely direct and indirect methods (Kovacevic and Vetterli 1993). A subsequent direction of research explored the generalisation of the link between iterated *two channel uniform* FBs and *dyadic wavelets* to the *non-uniform* case (Blu 1993). Iterated non-uniform FBs, or iterated rational FBs (RFBs) with regularity factors can be viewed as approximate wavelet transforms with rational dilation factors. Such a transform is named *rational discrete wavelet transform* (RADWT), which is a weaker form of wavelet transform as they only satisfy approximately the conditions for conventional wavelets (Blu 1998). The biggest challenge for designing RADWTs is the issue of *shift variance*. The phenomenon refers to the cases where the designed filter of a rational rate FB does not converge to a unique wavelet function (Blu 1993), details of which will be discussed in chapter 2.

This thesis aims to advance the design of PR *non-orthogonal critically-sampled RADWT* or *bi-orthogonal RADWT* which satisfy regularity conditions; either name will be used interchangeably throughout the thesis. The FB is bi-orthogonal because in PR critically-sampled FBs, the synthesis bank is the inverse of analysis bank and inverse matrices automatically involve bi-orthogonality (Strang and Nguyen 1996). Specifically, there are no works in the literature on the subject of designing bi-orthogonal RFB structures that we are aware of, let alone the iterated version. In this thesis, design challenges such as *the issue of shift variance* in RADWTs is addressed and results are presented. Three approaches to solving non-linear constraint optimisation are proposed for the problem of designing bi-orthogonal rational FBs satisfying regularity conditions. The resulting RADWTs provide constant Q-transforms as similar to the conventional dyadic counterpart, where Q denotes the *quality factor* of the transform. This quality factor Q is approximately two in dyadic wavelet transform and greater in RADWT case. The ability to adjust Q flexibly can be useful in the analysis of many oscillatory signals such as speech or EEG signals (Selesnick 2011a). This flexibility of Q in RADWT and its applications are discussed in details in the thesis (chapter 4). Experimental examples of sparse signal representation based on our proposed bi-orthogonal RADWT are presented in chapter 5.

1.2 Open questions to address

To help understand the underlying role of bi-orthogonal RADWT in the family of RADWTs and in the field of time-frequency analysis, this thesis will address the following questions

- The issue of *shift-variance* in constructing RADWT – how is it dealt with in bi-orthogonal RADWT designs? What do we gain by relaxing orthogonality as compared to RADWTs in existing literature?
- Bi-orthogonal rational filter bank design and the corresponding non-linear constraint optimisation – how is the resultant non-convex optimisation problem dealt with?
- How is regularity order imposed on a bi-orthogonal rational filter bank structure?
- Which types of signals can benefit from our designed bi-orthogonal RADWTs and which contexts can they be used in?
- In which context are constant Q transforms useful? What does flexibility of Q value in constant Q transforms contribute?
- Why are dyadic/rational wavelet transforms necessary? What advantages can they bring as compared to other time-frequency analysis techniques?

1.3 Overview of the thesis

The thesis is outlined as follows:

- In chapter 1, we present the outline of the thesis along with some background on time frequency analysis, which ends with discussion on rational discrete wavelet transform and their applications.
- Chapter 2 provides a review of the literature on this topic with the challenges for constructing rational DWTs.
- In chapter 3, two channel $(\frac{q-1}{q}, \frac{1}{q})$ RFB and its corresponding wavelet is considered. Motivation for such choice of re-sampling parameters is briefly discussed.

This chapter begins with the construction of the FB design problem into a non-linear optimisation problem, then describes two solving methods and design results.

- In chapter 4, the general two channel $(\frac{p}{q}, \frac{q-p}{q})$ rate changing RFB and their corresponding wavelets are discussed. Hence, flexible Q factor transform is enabled. An iterative routine for solving the design problem in this case is considered and design results are presented.

- Applications such as de-noising, signal separation based on l_1 optimisation or basis pursuit with bi-orthogonal RADWTs constructed dictionary are discussed in chapter 5.

- Chapter 6 presents thesis conclusion and contains suggestions for potential future work.

1.4 Background on Time-frequency analysis

Fourier transform has long been a fundamental tool for signal analysis whose applications vary across many fields and applications (Terras 1999, Folland 2009). The Fourier transform expands signals into a basis formed by complex sinusoids, which form an orthogonal basis. However, Fourier analysis has several notable shortcomings for the analysis of non-stationary signals, most notably being the lack of time information in the frequency representation. In other words, although all frequencies present in a signal can be determined by Fourier analysis, their times of appearance are unknown. Gibbs phenomenon, which refers to the appearance of overshoots in truncated Fourier expansions when representing signals with discontinuities, is another issue in practice. In analysing non-stationary signals, there is often strong interest in knowing when the different frequency components occur. For example, as the time information of the signal in the transform is not represented, the Fourier transform requires a large number of basis vector components to represent short pulse-like signals, which expands the representation cost and raises processing requirements. In another example such as music signals, notes of certain frequencies are heard for some finite interval of time and they are then replaced by some other notes. Processing of these signals are not usually interested in the overall contribution of the notes or frequencies but rather the timing and duration of these notes. Hence, it is necessary to develop representation

schemes that contain both time and frequency information; such schemes are collectively known as joint time-frequency representations.

Several time-frequency representations have been proposed and developed over the past few decades such as Wigner-ville distribution (WVD) (Stankovic 1994, Kumar and Prabhu 1997), short time Fourier transform (STFT) or windowed Fourier transform (Kwok and Jones 2000, Rothwell *et al.* 1998, Durak and Arikan 2003), and wavelet transform (Mallat 1989b).

In what follows, we provide a short discussion on short time Fourier analysis and wavelet transform. The first technique is one of the earliest time-frequency representations, developed based on the classical Fourier analysis since Dennis Gabor suggested to expand signals into a set of functions which are concentrated in both time and frequency (Gabor 1946). Short Time Fourier transforms (STFTs) have since become wide-spread in practice due to their computational simplicity (Liu 1993, Amin and Feng 1995, Chen *et al.* 1993). The later technique, wavelet transform, is another important time-frequency representation, which was originally proposed as time-scale representation (Daubechies 1990, Mallat 1989b). This representation provides properties that could not be achieved in STFTs, details of which are discussed in section 1.4.2.

1.4.1 Short Time Fourier analysis

Short Time Fourier Transform is a signal decomposition technique that is designed to overcome the aforementioned issues of purely time or frequency representations. The STFT's basis functions, defined as $e^{-j\omega t}w(t-\tau)$, are modulated versions of a window function $w(t)$ (Portnoff 1980). We can consider the transform as signal $s(t)$ being multiplied with the window function $w(t)$, which is usually compactly supported, and Fourier transform is then applied to the product $w(t)s(t)$. The major advantage of such transform is the decomposition localisation, which is suitable for input signals whose energy is concentrated in certain regions of the time-frequency plane. The transform coefficients will be near zero in other regions of the time-frequency plane and so contain little energy; they can be computed as

$$c_{m,n} = \int_{-\infty}^{+\infty} e^{-jm\omega_0 t} w(t - nt_0) s(t)\, \mathrm{d}t \tag{1.1}$$

for parameters $m, n \in \mathbb{Z}$ and $w(t)$ is called the window function or *envelop function*. The coefficients $\{c_{m,n}\}$ of (1.1) represent the original signal $s(t)$ in the new domain. However, one can question how completely and easily can the signal $s(t)$ be reconstructed from the set of coefficients $c_{m,n}$ and how well $\{c_{m,n}\}$ define $s(t)$. The originally proposed Gabor's distribution, which is a special case of STFT with $w(t)$ being chosen to be Gaussian window without compact support and $\omega_0 t_0 = 2\pi$, leads to unstable reconstruction (Raab 1982). In other examples, if $\omega_0 t_0 < 2\pi$, reconstruction stability can be attained and the time-frequency localisation properties of STFT became very useful in many applications (Davis and Heller 1979).

In addressing the issue of reconstruction in STFT, Daubechies (Daubechies 1990) adopted the analysis of *coherent states*, used in many areas of theoretical physics, which are defined as

$$w^{(p,q)}(x) = e^{jpx} w(x - q), \tag{1.2}$$

where the family of *coherent states* $w^{(p,q)}(x)$ are obtained by function $w(x)$ being transformed by p and translated by q. If the continuous parameters (p, q) in (1.2), which determine the *phase space* setting of the *coherent states* $w^{(p,q)}(x)$, are discretised to reduce the transform's redundancy as $p = mp_0$, $q = nq_0$ for $m, n \in \mathbb{Z}$; $p_0, q_0 > 0$ and $p_0 q_0 < 2\pi$, the functions $w^{(p,q)}(x)$ will give rise to a frame for any function $w(x) \in L^2(\mathbb{R})$ (Daubechies 1990). Hence, reconstruction stability is guaranteed; $w^{(p,q)}(x)$ can be written as

$$w_{(m,n)}(x) = e^{jp_0 mx} w(x - q_0 n). \tag{1.3}$$

If we let $p_0 = \omega_0, q_0 = t_0$ and x equal to time t, we obtain the expression of STFT in (1.1) and the reconstruction condition becomes $\omega_0 t_0 < 2\pi$ and the transform is referred to as *over-sampling*. If $\omega_0 t_0 = 2\pi$, the transform is *critically-sampled* (Qian and Chen 1999), for which case $w(.)$ is required to either not very smooth or it does not decay very fast to attain a frame (Daubechies 1990). In order words, orthogonal basis or *critical-sampling* transform can only be achieved with window function $w(.)$ being poorly localised. Hence, over-sampling STFT is often used to attain better behaved window functions $w(.)$ (Vetterli and Herley 1992).

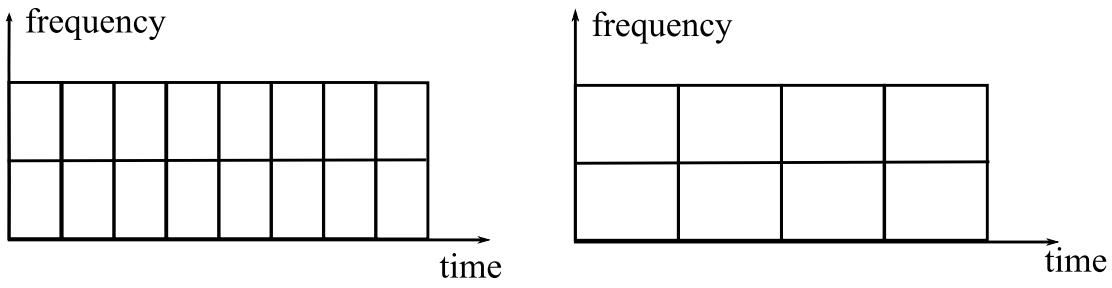

Figure 1.1. Time-frequency plane of the short-time frequency analysis. Two different tilings are shown, corresponding to different choices for windows and modulation frequencies.

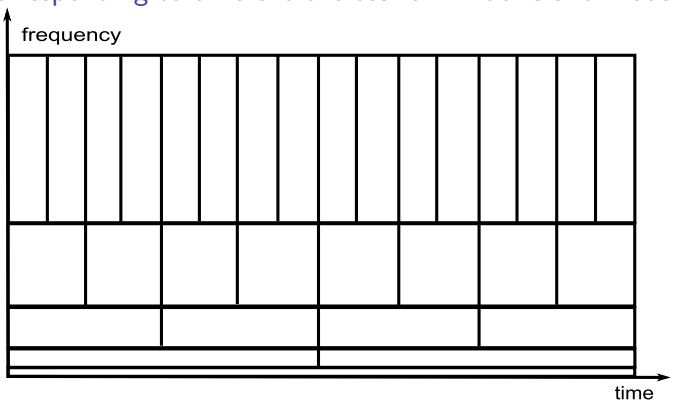

Figure 1.2. Time-frequency plane of the dyadic wavelet transform. The frequency resolution is much finer in low frequency and it corresponds to longer time basis function. At high frequency, the time interval of the basis function is shorter; it corresponds to coarser frequency resolution and better time resolution.

1.4.2 Wavelet transforms

One limitation of STFTs however is that, because a single window is used for all frequencies, the resolution of the analysis is constant across the frequency axis as illustrated in the Fig. 1.1. Such constant resolution can be a disadvantage for STFTs, for example when dealing with discontinuous signals. Such signal discontinuities can be effectively isolated by using transform of short-time, high-frequency and long-time, low-frequency basis functions, which are the attributes of wavelet functions (Strang and Nguyen 1996). Besides, wavelet functions with good time and frequency localisation can be constructed even with *critical sampling* transform (Vetterli and Kovacevic 1995). The wavelet basis functions are obtained from a single prototype wavelet by translation and dilation (Mallat 1989b), which are defined as

$$\psi_{a,b}(t) = \frac{1}{\sqrt{a}}\psi(\frac{t-b}{a}), \tag{1.4}$$

where $a \in \mathbb{R}^+, b \in \mathbb{R}$; $\psi(.)$ represents the mother wavelet function, which is required to satisfy the admissibility condition

$$\int_{-\infty}^{+\infty} \frac{|\Psi(\omega)|^2}{|\omega|} d\omega < \infty, \tag{1.5}$$

where $\Psi(\omega)$ represents the Fourier Transform of $\psi(t)$; 1.5 implies that

$$|\Psi(\omega)|^2_{\omega=0} = 0, \tag{1.6}$$

which results in wavelet spectrum being band-pass. It consequently implies that low frequencies cannot be represented using wavelet functions. The father wavelet function is defined to complement the wavelet function (Mallat 1989b), as it neatly fits into the low pass region of the spectrum that is left uncovered by wavelet functions. The admissibility condition of father wavelet functions is stated as

$$\int_{-\infty}^{+\infty} \phi(t) dt = 1. \tag{1.7}$$

The discretised version of the wavelet function expression in (1.4) is defined as

$$\psi_{m,n}(t) = a_0^{-m/2} \psi(a_0^{-m} t - n b_0) \qquad \text{for } m, n \in \mathbb{Z}, \tag{1.8}$$

which in this case, shows no absolute limitation for a_0, b_0 to constitute a frame, unlike in STFT case which needs $p_0 q_0 \leq 2\pi$. In order words, a frame can be constituted for any arbitrary pair of a_0, b_0. To take the argument further, it is also shown that for arbitrary choices of $a_0 > 1, b_0 > 0$, tight frames can be constructed (Daubechies 1990). For example, an orthogonal basis was constituted for $a_0 = 2, b_0 = 1$ (Meyer 1989). In what follows, a very attractive attribute of wavelet transforms used in computer vision and image processing, will be discussed.

1.4.2.1 Multi-resolution of wavelet transforms

The concept of multi-resolution analysis (MRA) was first introduced by Mallat (Mallat 1989b). In a MRA, let V_0 be the space that is spanned by basis functions $\{\phi_0(t-k), k \in \mathbb{Z}\}$, defined as $\phi_0(t) = \phi(t)$ being the father wavelet function (i.e. $b_0 = 1$). If a signal $f_0(t) \in V_0$, it follows that $f_0(t)$ can be expanded as a linear combination of $\{\phi_0(t-k), k \in \mathbb{Z}\}$. If we define V_j as the space spanned by $\{\phi_j(t-k) = \phi(a_0^j t - k), k \in \mathbb{Z}, a_0 > 1\}$, then the scaled function $f_j(t) = f_0(a_0^j t)$ is in V_j. MRA defines a nested sequence of subspaces $\ldots, V_{-1}, V_0, V_1, V_2, \ldots, V_j$ such that

$$\ldots \subset V_0 \subset V_1 \subset \ldots \subset V_{j-1} \subset V_j \ldots \tag{1.9}$$

If W_{j-1} is defined to be the orthogonal complement space of V_{j-1} , then V_j is equivalent to the "sum" of V_{j-1} and W_{j-1}, defined as

$$V_j = V_{j-1} \oplus W_{j-1}. \tag{1.10}$$

Physically, W_{j-1} defines the detail of signal while V_{j-1} defines the approximation of a signal at level $j-1$. Hence, (1.9) implies that the approximations at level $j-1$, spanned by $\{\phi_{j-1,k}\}_{k\in\mathbb{Z}}$, combine with details at level $j-1$, spanned by $\{\psi_{j-1,k}\}_{k\in\mathbb{Z}}$, to form the approximation of the signal at the finer level j.

Another interpretation of $f_j(t)$ is the projection of the original function $f(t)$ on the subspace V_j and it is then said to be represented at the j^{th} resolution level. The larger the value of j, the finer its resolution. The signal's projection onto V_j corresponds to a time scale $\Delta t = a_0^{-j}$ in the representation. Since $f_j(t)$ can be seen as an approximation of the function $f(t)$ on V_j, the error of such approximation can be shown to satisfy (Strang and Nguyen 1996)

$$\left\| f(t) - f_j(t) \right\| \approx C(\Delta t)^p \left\| f^{(p)}(t) \right\|, \tag{1.11}$$

where p and constant C depends on the choice of wavelet functions (or filters of the corresponding filter banks); $\|\cdot\|$ represents general L^n-norm operation since wavelets are unconditional basis for function space L^n (Strang and Nguyen 1996); $f^{(p)}(t)$ represents the p^{th} derivative of the function $f(t)$ with respect to t. It is clear that piecewise smooth functions are better approximated by wavelet basis compared to Fourier analysis. One important result of the multi-resolution analysis is if we apply successive approximation recursively as shown in (1.9), the nested subspaces which include all the details at all resolutions converge to $L^2(\mathbb{R})$ space when $j \to \infty$. If we let $a_0 = 2$, the above result can be interpreted as: whenever there are sequence of spaces satisfying MRA conditions, there exists an orthonormal basis for $L^2(\mathbb{R})$ defined as

$$\psi_{m,n}(t) = 2^{\frac{m}{2}}\psi(2^m t - n) \qquad \text{for } m, n \in \mathbb{Z}, \tag{1.12}$$

such that $\psi_{m,n}(t)$ is the orthonormal basis for W_m, which is the orthogonal complement space of V_m satisfying (1.10) (Vetterli and Kovacevic 1995). This contributes to one of the techniques of constructing wavelets, namely construction of wavelets using Fourier technique. The example wavelets constructed based on this technique include Meyer's wavelets and wavelets for spline spaces, discussed in (Vetterli and Kovacevic 1995).

1.4.2.2 Wavelet transforms and Filter banks

One of the links between wavelet transform and signal processing was first recognised by Daubechies and Mallat (Mallat 1989a, Daubechies 1988), whose result provides an alternative for performing wavelet decompositions through filter bank analysis or sub-band decomposition. Furthermore, the result suggests that wavelets are intimately connected to the existing body of knowledge on filter banks. Thus, an alternative to direct constructions as typified by the approach based on Fourier transform and MRA, it is equally valid to start with discrete-time filters. The filters, if designed to satisfy certain conditions, will lead to continuous-time wavelets when iterated.

In Fig. 1.3, a uniform two channel filter bank is shown. Typically, $\{H_{LP}, F_{LP}\}$ are low-pass filters while $\{H_{HP}, F_{HP}\}$ are complementary high-pass filters. Such two channel filter bank is known as critically sampled, since the down-sampling factors in both channels are equal to the number of channels.

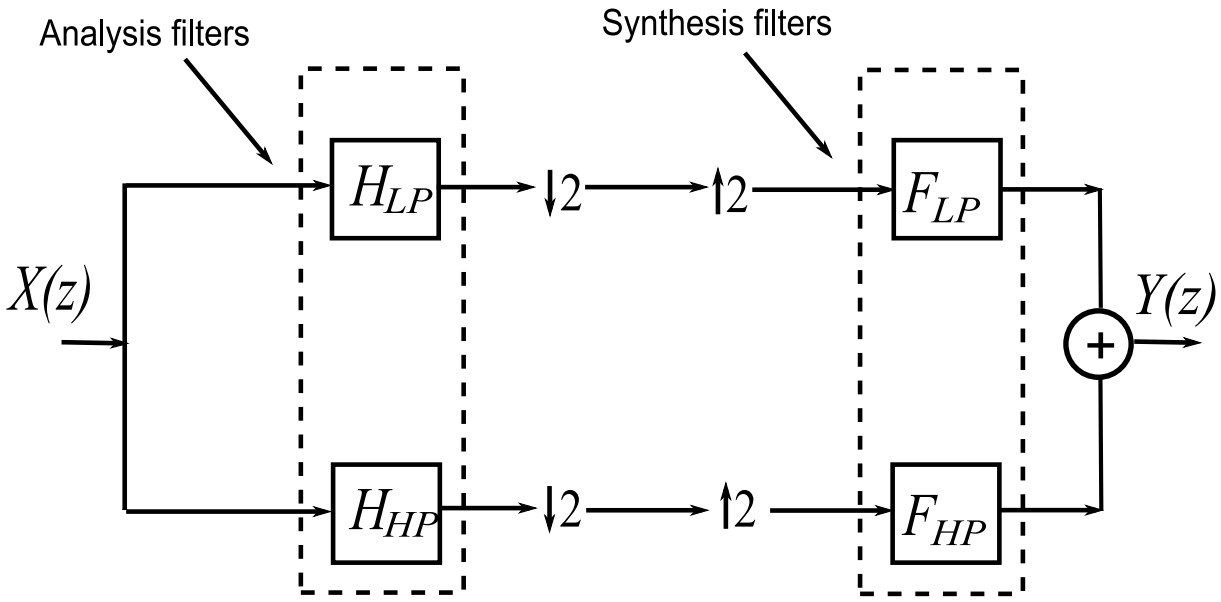

Figure 1.3. Critically sampled uniform two-channel filter bank. Left filters form the analysis bank, while the right ones form the synthesis bank.

Perfect reconstruction (PR) condition is the most fundamental consideration in designing filter banks. This condition requires the output signal $y[n]$ to be a delayed version of input signal $x[n]$. Thus, it is necessary to cancel aliasing and amplitude distortions caused by re-sampling and filtering operations in the filter banks; PR conditions can

be defined in matrix form, namely alias component (AC) matrix, as

$$\begin{bmatrix} H_{LP}(z) & H_{HP}(z) \\ H_{LP}(-z) & H_{HP}(-z) \end{bmatrix} \begin{bmatrix} F_{LP}(z) \\ F_{HP}(z) \end{bmatrix} = \begin{bmatrix} 2z^{-l} \\ 0 \end{bmatrix} \tag{1.13}$$

From (1.13), it can be observed that there are many possible sets of $\{H_{LP}, H_{HP}, F_{LP}, F_{HP}\}$, that satisfy the required PR conditions. A common design approach is to start with imposing additional constraints on the filter set. Hence, for automatic aliasing cancellation a set of relationships between analysis and synthesis filters is imposed. A classic choice, as discussed in (Strang and Nguyen 1996), is

$$F_{LP}(z) = H_{HP}(-z) \qquad F_{HP}(z) = -H_{LP}(-z), \tag{1.14}$$

which can be straightforward to verify as we substitute (1.14) into the *aliasing cancellation* condition as

$$\begin{aligned} H_{LP}(-z)F_{LP}(z) + H_{HP}(-z)F_{HP}(z) &= 0 \\ \Rightarrow H_{LP}(-z)H_{HP}(-z) - H_{HP}(-z)H_{LP}(-z) &= 0, \end{aligned} \tag{1.15}$$

In addition, (1.14) can guarantee that designing high-pass filter H_{HP} results in low-pass filter F_{LP} and similarly, designing low-pass filter H_{LP} will lead to high-pass filter F_{HP}. Hence, the problem of designing PR filter banks reduces to designing filters H_{LP}, H_{HP} that satisfy

$$H_{LP}(z)H_{HP}(-z) - H_{LP}(-z)H_{HP}(z) = 2z^{-l}. \tag{1.16}$$

Let $P(z) = H_{LP}(z)H_{HP}(-z)$, (1.16) can be written as

$$P(z) - P(-z) = 2z^{-l} \tag{1.17}$$

and the problem of designing PR filter bank can thus be summarised as

1. Design half band filter $P(z)$ that satisfies (1.17),
2. Factor $P(z)$ into $H_{LP}(z), H_{HP}(z)$ and find the corresponding $F_{LP}(z), F_{HP}(z)$ using (1.14).

The design in step 1 corresponds to many choices of $\{H_{LP}, H_{HP}\}$. Hence, further constraints can be imposed on the filter set $\{H_{LP}, H_{HP}\}$ as Smith and Barnwell (Smith and

Barnwell 1984) imposed an additional relationship between the analysis low-pass and high-pass as

$$H_{HP}(z) = -z^{-N} H_{LP}(-z^{-1}). \tag{1.18}$$

The choices in (1.14), (1.18) essentially transform the perfect reconstruction design problem into a design of half-band filter, which is then followed by spectral factorisation to attain the analysis and synthesis banks. A famous example of this approach leads to the design of maximally flat filters and the associated Daubechies wavelets (Daubechies 1992).

If $\{H_{LP}, H_{HP}\}$ are not related to each other as in (1.18), the two channel filter banks resulting from the design are non-orthogonal filter banks with PR, known as bi-orthogonal filter banks. In case of two channel bi-orthogonal filter banks, the loss of orthogonality is compensated for by the existence of linear phase solutions for the analysis and synthesis filters. For two channel filter bank, orthogonality and linear phase filters cannot be simultaneously attained (Strang and Nguyen 1996). In terms of practical applications, linear phase, bi-orthogonal filter banks are well-suited to image compression, where phase distortions need to be carefully controlled.

Two scale equation and cascade algorithm

The PR condition for two channel FBs is only one of the essential criteria necessary for the construction of wavelets. Since the construction of dyadic wavelets based on two channel FBs is the main concern in this section, the wavelets parameters are set to be $a_0 = 2, b_0 = 1$.

Let $\phi(t) \in V_0$ and $\psi(t) \in W_0$ be scaling and wavelet functions which satisfy the MRA condition, respectively. Hence $V_0 \subset V_1, V_0 \oplus W_0 = V_1$ and the functions $\phi(t), \psi(t)$ can be expressed as a linear combination of $\{\phi_{1,n}(t) = \sqrt{2}\phi(2t-n)\}_{n\in\mathbb{Z}}$:

$$\phi(t) = \sum_n \sqrt{2}\mathbf{c}[n]\phi(2t-n) \qquad \psi(t) = \sum_n \sqrt{2}\mathbf{d}[n]\phi(2t-n), \tag{1.19}$$

where $\mathbf{c}[n], \mathbf{d}[n]$ represent the coefficients of the two linear expressions; (1.19) denotes *dilation equations* or *two scale equations*. In solving such equations, the *cascade algorithm* is a common method (Strang and Nguyen 1996), which can be described with

$$\phi^{(i+1)}(t) = \sum_n \sqrt{2}\mathbf{c}[n]\phi^{(i)}(2t-n) = 2\sum_n \mathbf{h}[n]\phi^{(i)}(2t-n), \tag{1.20}$$

for $\mathbf{h}[n] = \frac{\mathbf{c}[n]}{2}$. The initial function $\phi^{(0)}(t)$ is normally chosen to be the box function, defined to be 1 on the interval $[0,1]$ and zero everywhere else. The father wavelet function

$\phi(t)$ is defined as $\phi^{(i)}(t) \to \phi(t)$ as $i \to \infty$, if the algorithm converges. In order words, $\phi(t), \psi(t)$ exist only if the cascade algorithm (1.20) converges, which is determined by $\mathbf{h}[n]$ or $\mathbf{c}[n]$ of (1.20) and the choice of function $\phi^{(0)}(t)$. Moreover, when convergence happens, it can be shown that (Vetterli and Kovacevic 1995) $\mathbf{c}[n], \mathbf{d}[n]$ in the two scale equations in (1.19) correspond to the impulse responses of the low-pass and high-pass filters in an orthogonal two-channel filter bank. This is similar to the structure illustrated in 1.3 for $\{H_{LP}, H_{HP}, F_{LP}, F_{HP}\}$ satisfying PR and orthogonal conditions. As a result, $\mathbf{c}[n], \mathbf{d}[n]$ can be considered as scaled impulse responses of H_{LP}, H_{HP} with a $\sqrt{2}$ scaling, respectively. F_{LP}, F_{HP} can be obtained from the PR relationships, some examples are those described in (1.14), (1.16), and (1.18).

The *regularity* condition is required to guarantee that the cascade algorithm in (1.20) converges and $\phi^{(i)}(t)$ converges to a piecewise smooth function $\phi(t)$ in $L^2(\mathbb{R})$ as $i \to \infty$. If we consider cascade algorithm (1.20) in Fourier domain as

$$\Phi^{(i+1)}(\omega) = \Big(\sum_n \mathbf{h}[n] e^{-jn\omega/2}\Big)\Phi^{(i)}\Big(\frac{\omega}{2}\Big) = H\Big(\frac{\omega}{2}\Big)\Phi^{(i)}\Big(\frac{\omega}{2}\Big), \tag{1.21}$$

where $\Phi^{(i+1)}(\omega)$, $\Phi^{(i)}(\omega)$, $H(\omega)$ are Fourier transforms of $\phi^{(i+1)}(t)$, $\phi^{(i)}(t)$, $\mathbf{h}[n]$, respectively; (1.21) provides the relationship between $\Phi^{(i)}(\omega)$ and $\Phi^{(i+1)}(\omega)$; thus we can write $\Phi^{(i)}(\omega)$ in in terms of $\Phi^{(0)}(\omega)$ as

$$\Phi^{(i)}(\omega) = \Big[\prod_{n=1}^{i} H\Big(\frac{\omega}{2^n}\Big)\Big]\Phi^{(0)}\Big(\frac{\omega}{2^i}\Big). \tag{1.22}$$

Hence, the convergence of $\phi^{(i)}(t) \to \phi(t)$ of cascade algorithm in (1.20) is equivalent to the $\Phi^{(i)}(\omega)$ approaches $\Phi(\omega)$ as $i \to \infty$. Such convergence depends on the behavior of the product $\big[\prod_{n=1}^{\infty} H(\frac{\omega}{2^n})\big]\Phi^{(0)}(\frac{\omega}{2^i})$ of (1.22) or

$$\Phi(\omega) = \Big[\prod_{n=1}^{\infty} H\Big(\frac{\omega}{2^n}\Big)\Big]\Phi^{(0)}(0) \tag{1.23}$$

as $i \to \infty$. Daubechies (Daubechies 1988) proposed the necessary and sufficient conditions for filter $H(\omega)$ for a well-behaved $\Phi(\omega)$, which are

$$H(0) = 1, \tag{1.24}$$

$$\text{and} \qquad H(\omega) = \Big(\frac{1+e^{j\omega}}{2}\Big)^N R(\omega), \quad \sup_{\omega\in[0,2\pi]} |R(\omega)| < 2^{N-1}. \tag{1.25}$$

(1.24) is required since $H(\frac{\omega}{2^\infty})$ of the product sequence approaches $H(0)$ and the product will approach infinity at $\omega = 0$ if such condition fails; (1.25) is known as the *regularity condition*. Such condition represents the smoothing part of the function as the

product $\left[\prod_{n=1}^{\infty} H(\frac{\omega}{2^n})\right]$, for $H(\omega)$ satisfying (1.25), becomes

$$\prod_{n=1}^{\infty}\left(\frac{1+e^{j\frac{\omega}{2^n}}}{2}\right)^N \prod_{n=1}^{\infty} R(\frac{\omega}{2^n}) = \left(\frac{\sin(\frac{\omega}{2})}{\frac{\omega}{2}}\right)^N \prod_{n=1}^{\infty} R(\frac{\omega}{2^n}). \tag{1.26}$$

Hence, the RHS of (1.26) along with the bound condition on $|R(\omega)|$ described in (1.25) guarantee that the product $|\prod_{n=1}^{\infty} H(\frac{\omega}{2^n})|$ in (1.23) is bounded above. Thus the corresponding $\lim_{i\to\infty} \phi^{(i)}(t)$ exists and converges to a point-wise continuous father wavelet function $\phi(t)$ (Vetterli and Kovacevic 1995). The parameter N, namely *regularity order*, of the regularity condition in (1.25) plays a critical role in the resulting wavelets. It determines the smoothness of the resulting father wavelet function $\phi(t)$ and thus the accuracy p, as defined in (1.11), of the approximation of piecewise functions based on multi-resolution analysis.

Some dyadic wavelet examples based on two-channel FBs

The PR and regularity conditions discussed above are required for constructing dyadic wavelets based on two-channel filter banks. In the literature, some famous examples include

1. *Daubechies wavelets (max-flat filters)*: In two-channel filter bank and dyadic wavelets, max-flat (Daubechies) filters (Daubechies 1992) form an important family of filters that result in an outstanding wavelets family since the closed form solution of the max-flat filter can be attained with respect to any N regularity orders being imposed in the designed finite impulse response (FIR) filter with minimal length. The key features of this family are:

   (a) The unitariness of the polyphase matrix constructed from the filters

   (b) FIR filters leading to wavelets of finite support

   (c) Frequency response is maximally flat at $\omega = 0$ and $\omega = \pi$. This feature is crucial since it determines the convergence, and maximises the regularity order of the designed filter.

2. *Bi-orthogonal wavelets and bi-orthogonal filter banks*: The filter bank structure consists of bi-orthogonal filters, thus bi-orthogonal wavelet is expected. In the orthogonal case, the synthesis wavelets are the same as analysis wavelets. In contrast, for the bi-orthogonal case if $\phi(t), \psi(t)$ are the analysis scaling and wavelet functions, then there exist $\tilde{\phi}(t), \tilde{\psi}(t)$ for synthesis scaling and wavelet functions, respectively. Some key features of this family include

(a) The orthogonal property of the filters' polyphase matrix is relaxed. However, linear phase can be attained(Antonini *et al.* 1992). Note that linear phase is not achievable for orthogonal filter banks.

(b) For any level j of MRA, if the analysis father wavelet functions $\{\phi_{j,k}(t)\}_{k\in\mathbb{Z}}$ and wavelet functions $\{\psi_{j,k}(t)\}_{k\in\mathbb{Z}}$ span the subspaces V_j, W_j, then the synthesis scaling and wavelet functions $\{\tilde{\phi}_{j,k}(t)\}_{k\in\mathbb{Z}}$, $\{\tilde{\psi}_{j,k}(t)\}_{k\in\mathbb{Z}}$ span the corresponding dual subspaces $\tilde{V}_j, \tilde{W}_j$, such that

$$V_j \perp \tilde{W}_j, \quad W_j \perp \tilde{V}_j, \tag{1.27}$$

$$V_j + W_j = V_{j+1}, \quad \tilde{V}_j + \tilde{W}_j = \tilde{V}_{j+1}, \tag{1.28}$$

in which the sums are direct sums but not orthogonal sums as in the orthogonal case in (1.10). This implies that the bi-orthogonal wavelet series expansions are

$$x(t) = \sum_{j=-\infty}^{+\infty} \sum_{k=-\infty}^{+\infty} < x, \psi_{j,k} > \tilde{\psi}_{j,k}. \tag{1.29}$$

1.4.3 Wavelet transforms based on uniform M-channel FBs

In wavelet transforms, signals are decomposed into channels that have equal bandwidths on logarithmic scale which leads to constant Q transform[1]. For example, in dyadic wavelet, centre frequencies of the decomposed sub-bands are separated by whole octaves. Thus, high frequency channel will have wide bandwidth while low frequency has narrow bandwidth. However, it may be of interest to have narrow bandwidth at high frequency which cannot be achieved with dyadic wavelet decompositions, especially when dealing with applications of input signals such as long narrowband RF signals. In such cases, M-band ($M > 2$) wavelet transform may be considered. The transform offers more energy compactness and it offers narrower sub-band decomposition in high frequency components as compared to dyadic wavelet transform. The construction of M-band wavelets, based on uniform M-channel filter bank, is discussed in this section. This section does not include the mathematical derivations of the construction of M-channel FB but the focus is on the historical development of such FB design techniques and their features. This is used to help set the context of the work in this thesis. The uniform M channel filter bank is illustrated in Fig. 1.4. M-channel filter banks have been extensively investigated. In an early paper,

[1]The parameter Q represent quality factor, defined as the ratio between centre frequency and the bandwidth of the sub-band being considered

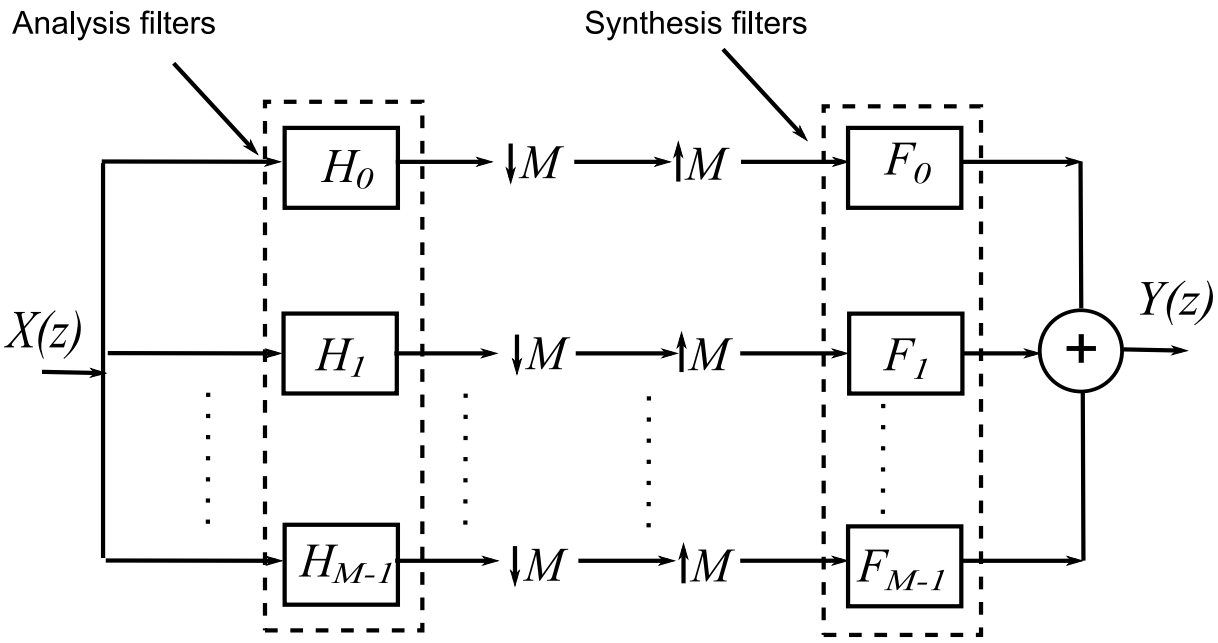

Figure 1.4. A Uniform M-channel filter bank.

Vaidyanathan (Vaidyanathan 1987b) developed the perfect reconstruction conditions for M-channel maximally decimated quadrature mirror filters, in which polyphase components of analysis filters are constrained to be FIR and the overall structure being lossless. The power complementarity property is a necessary condition. The losslessness condition, also equivalent to para-unitariness of the associated polyphase matrix, represents a very special class of uniform M-channel filter banks, which were well investigated in (Vaidyanathan 1987a), (Vetterli 1987). The para-unitary property is attractive since it guarantees perfect reconstruction and orthogonality of the filters, which leads to a popular approach for designing uniform M-channel filter bank, namely regular M-channel FB design based on lattice structure, and thus construction of M-band wavelet bases (Oraintara *et al.* 2001). Even though this approach is based on the condition of para-unitary FB, it emphasises a major departure from the original M-channel design (Vaidyanathan 1987a) as regularity factors are imposed on the filters. Some key features of the design technique includes:

- The filter banks obtained are both orthogonal and linear phase. This differs from the two-channel orthogonal cases where orthogonality and linear phase properties cannot be together attained.
- Stop-band energy can be optimised through free lattice parameters of the lattice structure optimisation design method (Oraintara *et al.* 2001)

- Only relatively low orders of regularity (at most two orders) can be imposed in the published designs (Oraintara *et al.* 2001) since the imposing of regularity conditions is transformed to conditions of lattice coefficients in the lattice structure. Such transform increases the complexity of the design, especially in cases of higher order of regularity.

Steffen and Hellller (Steffen *et al.* 1993) designed regular M-channel filter banks using a different approach. The design method was a generalisation of minimal length K-regular two-band Daubechies to M-band case. The method is to impose the regularity condition directly into the low-pass filter and then derive a general scheme for a minimal length regular M-band wavelet bases. Band pass and high pass filters can be obtained from low-pass filter by a Gram-Schimidt process (Chui. 1992). The major departure from two-band wavelet design, in which high-pass channel can be uniquely determined once low-pass filter is designed, is the greater freedom in choosing the band-and high-pass filters that match the designed low-pass filter in M-band case. The key features of this technique can be summarised as

- The regularity order can be imposed with mathematical exactness; the minimum length low pass filters with arbitrary K-order regularity in the M-band wavelet is analytically obtained (Steffen *et al.* 1993).
- The main disadvantage is of poor stop band attenuation when minimal length designs are sought.

1.4.4 Rational rate filter banks (RFB) and rational discrete wavelets

Motivation of RFB or non-uniform FB (NUFB): Multi-rate digital signal processing techniques are often used in the analysis of non-stationary signals, with applications in fields such as speech and image compression and telecommunications. Historically, the most common multi-rate systems use dyadic scaling of re-sampling rates, which lead to sub-bands with centre frequencies separated by whole octaves. In many applications, however, it may be possible to obtain greater sparsity in the sub-band decomposition for non-dyadic structures. The analysis of certain classes of signals, such as natural speech, electrocardiographic (ECG) recordings and image textures, can benefit from filter banks with rational re-sampling factors (Baussard *et al.* 2004, Yu and White 2005, Yu and White 2006, Selesnick 2010, Ghinwa and James 2007, Selesnick

2011c), where the sub-band bandwidths can be varied more gradually than in uniform filter banks. For example, iterated rational filter banks with tuneable Q-factors have recently been used to enhance sparsity in the representation of EEG and speech signals (Selesnick 2011c, Selesnick 2011a).

An M-channel non-uniform FB or rational rate FB is illustrated in Fig. 1.5. As similar to the uniform counter part, let $\{N_0, \ldots, N_{M-1}\}$ denote analysis low-pass, band-pass and high-pass filters while $\{S_0, \ldots, S_{M-1}\}$ denote synthesis low-pass, band-pass and high-pass filters, respectively. The FB is critically-sampled, thus requiring the rate changing parameters to satisfy $\sum_{i=0}^{M-1} \frac{p_i}{q_i} = 1$; if $\sum_{i=0}^{M-1} \frac{p_i}{q_i} > 1$, the structure is over-complete.

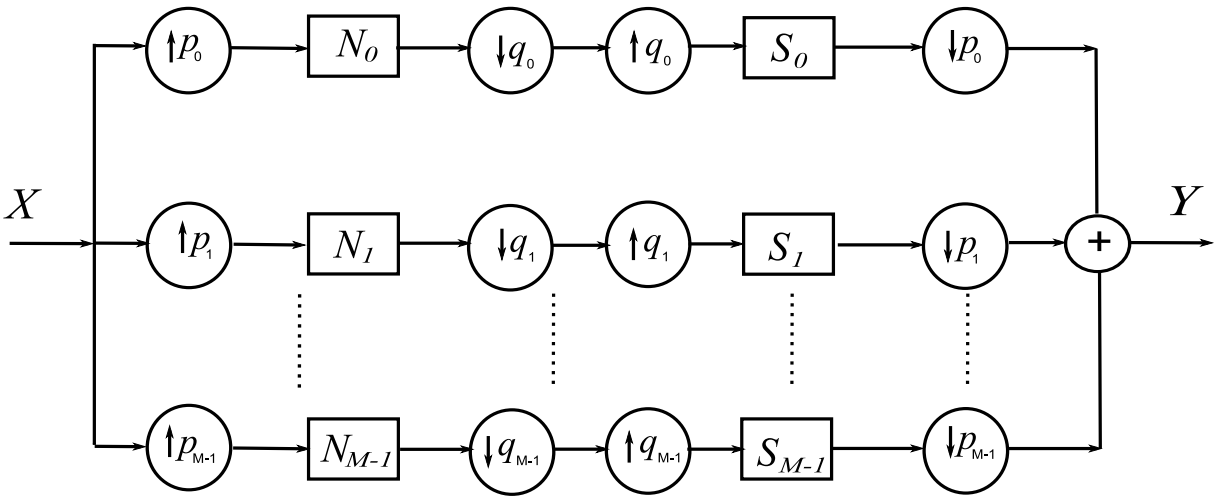

Figure 1.5. Non-uniform M-channel filter bank.

Unlike uniform FB whereas the frequency spectrum is usually equally partitioned amongst the FB channels, RFBs offer more flexible frequency partitioning. This can be advantageous in analysing real world signals such as speech audio. For example, in Fig. 1.6 a comparison between dyadic and rational dilation wavelets on speech signal representation is illustrated. Sparsity measure of GINI index as discussed in (Hurley and Rickard 2009) is used in which high value of GINI index denotes sparser representation. The experiment compares a 6/5 RADWT with other common dyadic wavelet transforms such as Daubechies and bi-orthogonal wavelets in terms of speech signal representation sparsity, details of which are discussed in section 5.2.1. The experiment shows sparser representation obtained by using 6/5 RADWT as compared to the dyadic counterpart since such RADWT can approximate the psychoacoustic bark scale (Fastl and Zwicker 2007). Figure 1.6 shows that the sparsity measure resulted from the

RADWT distributes at higher values (sparser representation) compared to the dyadic transforms and the lowest values (least sparse) of non-transformed data as expected.

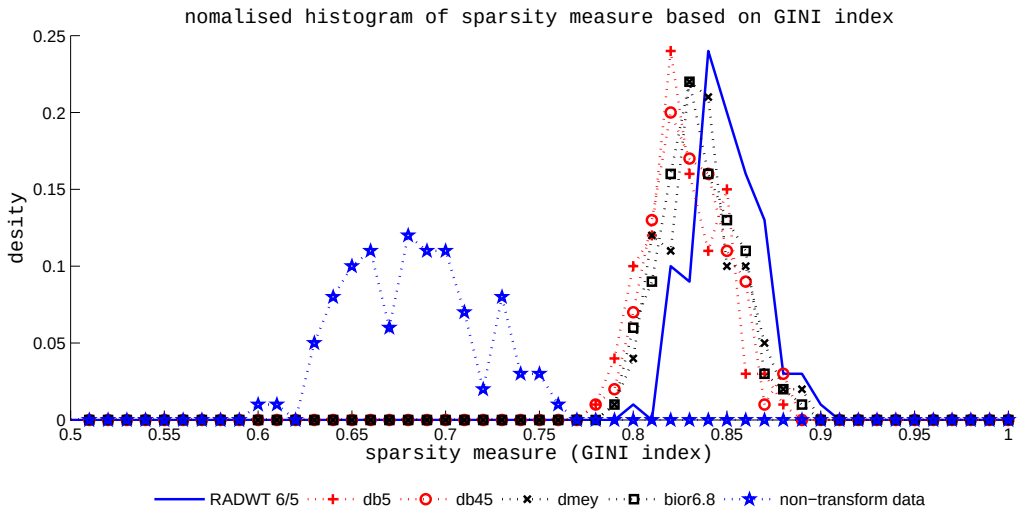

Figure 1.6. The normalised histogram of the signals' sparsity measure. Blue solid trace represents sparsity measures of the coefficients resulted from 6/5 RADWT transform on TIMIT signals; $+, \circ, \times, \diamond, \star$ traces represent the results of dyadic wavelets `db5`, `db45`, `dmey` and `bior6.8`

Due to the flexibility in frequency partitioning, iterated RFBs can result in decomposition with better flexibility to accommodate various signals' characteristics, especially those of an oscillatory nature; Fig. 1.7 (bottom) illustrates the frequency decomposition of the Daubechies dyadic wavelets `db4`, produced by iterating a uniform two-channel FB, and 7/6 RADWT, produced by iterating $(\frac{6}{7}, \frac{1}{7})$ RFB in Fig. 1.7 (top), of dilation factor 2 and $\frac{7}{6}$, respectively. By adjusting the rate changing parameters, RADWTs with more flexible dilation factors can be attained as compared to the conventional dyadic wavelet transform.

There have been many works (Blu 1998, Kovacevic and Vetterli 1993, Saadat Mehr and Chen 2000, Bayram and Selesnick 2009c, Princen 1994, Wada 1995, Bayram and Selesnick 2009b, Argenti and Del Re 1998, Bayram and Selesnick 2007, Zhong *et al.* 2010, Bregovic *et al.* 2008) on the design of non-uniform or rational FB, driven by specific applications. Therefore, the designs in the literature are varied and quite often involve different trade-offs. For example, in image processing applications, linear phase property is highly desirable, and so certain NUFBs are designed with filters satisfying linear phase and PR conditions. However, PR condition can be relaxed in return

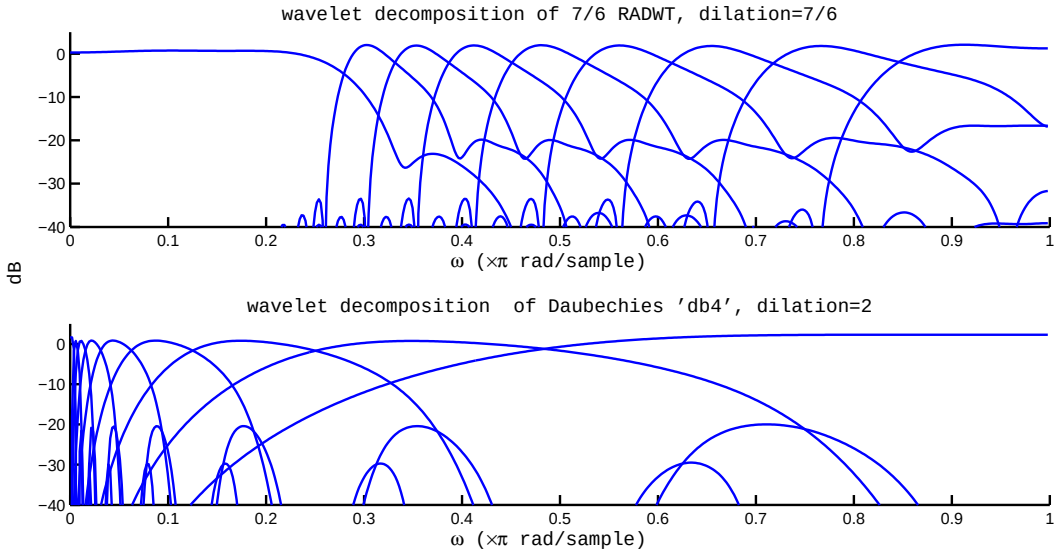

Figure 1.7. RADWTs versus dyadic wavelet transforms frequency decomposition. Top panel represents 7/6 RADWT frequency decomposition while bottom represents dyadic db4's.

for reduced computational complexity, which leads to nearly perfect reconstructing NUFBs (Zhong *et al.* 2010, Bregovic *et al.* 2008). Iterated NUFBs also attracted much interest since they can improve the sparsity of representation for signals with an oscillatory nature, such as speech and EEG signals. The literature on iterated RFB can be summarised as:

- Auscher (Auscher 1992) first attempted to design RADWT in frequency domain which associates to IIR filters with non-compact support.
- Blu (Blu 1998) designed an orthogonal RADWT based on FIR filters with imposed regularity order being restricted to one.
- Bayram and Selesnick initially proposed to design minimal length over-complete RADWT (Bayram and Selesnick 2009c) with arbitrary regularity and close-form expression of the filters can be attained. Later works include (Bayram and Selesnick 2009b) as orthogonal FBs are attained with K regularity order. However, stop-band attenuation is sacrificed in the above two designs.
- In (Bayram and Selesnick 2009a) and (Selesnick 2011a) by Bayram and Selesnick, RADWTs are designed in frequency domain with some amount of transform redundancy

- In (Nguyen and Ng 2012, Nguyen and Ng 2010) and (Nguyen and Ng 2013), we designed bi-orthogonal RADWTs based on FIR filters and with optimised stop-band filters.

1.5 Contributions and Publications

The main contribution of this thesis include:

1. Design of two-channel bi-orthogonal rational FBs, with rational rate changes in the two-channel satisfying $(\frac{q-1}{q}, \frac{1}{q})$ $(q \in \mathbb{N}, q \geq 3)$, which can lead to rational discrete wavelet transforms. Arbitrary K regularity orders are imposed on the filters which differentiates the proposed designs to those in the literature. Such a design approach results in critically-sampled RADWT with adjustable smoothness and offers *better frequency resolution* transform as compared to dyadic wavelets. This comes from the fact that the designed rational dilation factor is $\frac{q}{q-1} < 2$ for any $q \geq 3$. The rational re-sampling factors at the two channels are set to $(\frac{q-1}{q}, \frac{1}{q})$ in order to maximise the fine frequency decomposition when the FB is iterated for a given value of $q \geq 3$. The detailed design and two methods of solving the non-linear constraint optimisation, arisen from the PR conditions of the FB structure, is presented in chapter 3. Portions of this work has been published in

   - **Nguyen-S.**, and Ng-B.-H. (2010). Critically sampled discrete wavelet transforms with rational dilation factor of 3/2, *Signal Processing (ICSP), 2010 IEEE 10th International Conference on*, pp. 199 –202.

   - **Nguyen-S. T. N.**, and Ng-B.-H. (2012). Design of two-band critically sampled rational rate filter banks with multiple regularity orders and associated discrete wavelet transforms, *Signal Processing, IEEE Transactions on*, **60**(7), pp. 3863 –3868.

2. The adjustable Q factor transform is considered as the re-sampling rate parameters are generalised to $(\frac{p_0}{M}, \frac{p_1}{M})$ for $p_0 + p_1 = M$ and co-prime pairs p_0, M and p_1, M . An iterative algorithm is proposed to solve the optimisation problem arisen from this design. Generalised conditions for imposing regularity on the RFB structure is discussed. This work will be covered in chapter 4, and some parts of this appeared in

- **S. Tran Nguyen Nguyen**, and B.W.-H.Ng (2013). Bi-orthogonal rational discrete wavelet transform with multiple regularity orders and application experiments, *Signal Processing (2013)*, http://dx.doi.org/10.1016/j.sigpro.2013.04.001i.

3. The sparse representation of signals based on the proposed RADWTs is exploited. We have shown that speech and chirp signals are amongst the signals which can benefit from the designed bi-orthogonal RADWT. Chapter 5 will further discuss on this topic. Parts of this work appears in

   - **S. Tran Nguyen Nguyen**, and B.W.-H.Ng (2013). Bi-orthogonal rational discrete wavelet transform with multiple regularity orders and application experiments, *Signal Processing (2013)*, http://dx.doi.org/10.1016/j.sigpro.2013.04.001i.

1.6 Chapter summary

This chapter provides fundamental and some historical background on time-frequency analysis in which STFTs, wavelet transforms are amongst the known techniques. The advantages of wavelet transform over STFTs are discussed. In the family of wavelets, orthogonal, bi-orthogonal dyadic wavelets, M-band wavelets form the conventional wavelets, which were thoroughly investigated by many authors from both mathematic and signal processing perspectives. RADWTs, which are the main focus in this thesis, have been developed more recently with the view to increase representation sparsity over the conventional type wavelets for some types of signals. In that context, the thesis outline and contributions are also presented in this chapter. A brief summary of literature on M-band wavelets, rational DWTs is presented to emphasise the novelty of the work presented in the thesis. In chapter 2, a detailed review of RADWT literature will be presented.

Chapter 2

Iterated RFB - Design challenges and literature works

IN this chapter, the design challenges of iterated RFBs and RADWTs are discussed. A summary on this topic's literature is provided with discussions on the key features of each technique. The literature review provides a framework that provides a suitable background for the work described later in this thesis.

2.1 Iterated rational filter bank designs - Design challenges

There are two main issues associated with the design of iterated RFB. First, designing perfect reconstruction (PR) filter banks with rational re-sampling factors is not straightforward. Unlike uniform FBs which do not suffer from aliasing if the filters are assumed to have ideal brick wall responses, the non-integer re-sampling ratios in a RFB structure can potentially produce aliasing which render PR impossible even with such brick wall filters. A feasibility test to determine necessary conditions for perfect reconstruction with respect to the rational re-sampling rates was established (Kovacevic and Vetterli 1993). The second issue is specifically concerned with iterating RFB. The use of rational re-sampling ratios in iterating FB leads to the issue of *loss of shift invariance*, which was first discussed in (Blu 1993). Consequently, the translated father wavelet functions $\{\phi_{j,k}(t)\}_{k\in\mathbb{Z}}$ will no longer constitute a basis or frame for V_j. Additionally, the issue results in non-uniqueness of the limit function as the filters are iterated. In practice, such design issue can be mitigated by strictly controlling the shift error, hence it is critical for this to be constrained during the design process.

2.1.1 Aliasing in NUFBs structure – summary of necessary conditions for PR non-uniform FB

A general analysis side M-channel RFB is illustrated in Fig. 2.1 (a) and the desired spectrum partitioning is shown in Fig. 2.1 (b). Let the analysis filters $\{N_0, N_1, \ldots, N_{M-1}\}$ be real valued FIR filters with contiguous pass-band and the filter bank is critically-sampled. Consider the the following examples:

Example 2.1.1. (*aliasing of RFB): Let* $M = 2, p_0 = 3, p_1 = 2, q_0 = q_1 = 5$, *which corresponds to a two channel RFB with rational re-sampling ratios* $(\frac{3}{5}, \frac{2}{5})$. *The structure is illustrated in Fig. 2.2 (a).*

Let the channels with N_0, N_1 pick up low-pass spectra and high frequencies of the input signal's spectrum, respectively. If the input signal $X(\omega)$ is up-sampled by 2, the resulting input spectrum $X(2\omega)$ will be compressed to the frequency band of $[-\frac{\pi}{2}, \frac{\pi}{2}]$ and periodic for every π. Hence to extract the expected high-pass spectrum of the original signal, the filter N_1 should have pass band response in the frequency bands

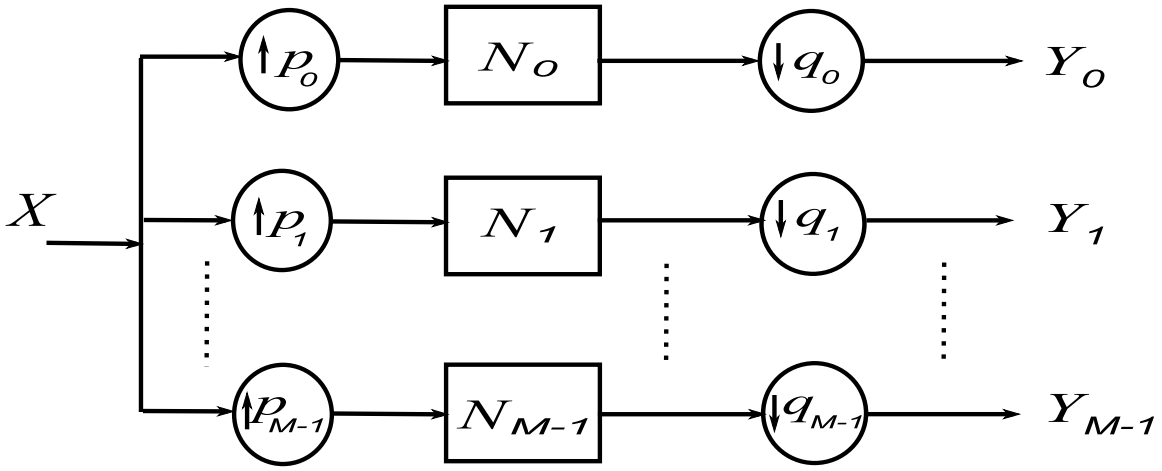

(a) M-channel NUFB

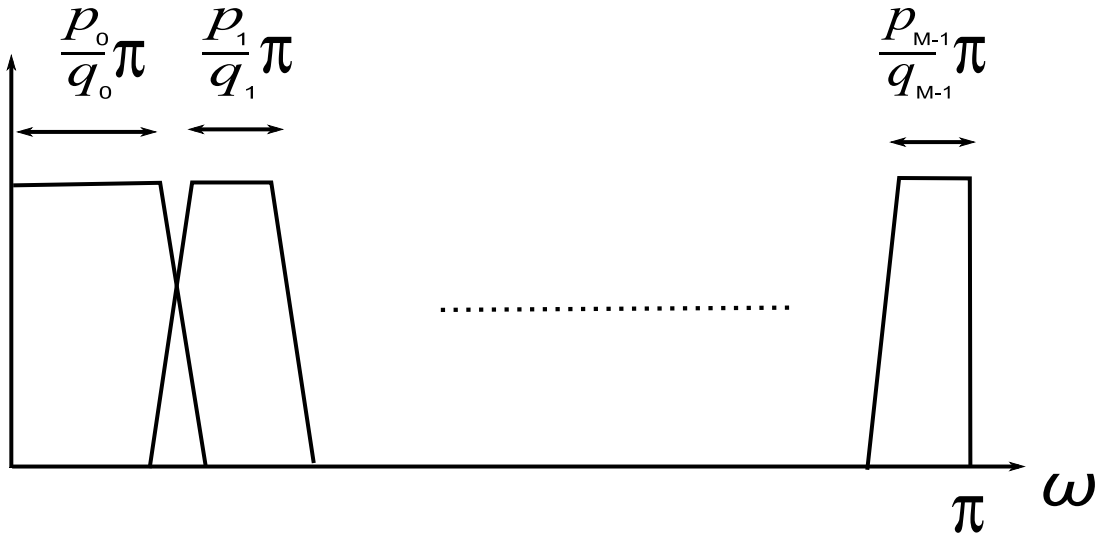

(b) NUFB M-channel spectra

Figure 2.1. Analysis M-channel NUFB (a) and the desired spectrum splitting (b).

$[-\frac{\pi}{2}, -\frac{3\pi}{10}]$ and $[\frac{3\pi}{10}, \frac{\pi}{2}]$ as illustrated in Fig. 2.2 (b). At the output of the filter, the signal is down-sampled by 5. The positive half at frequency band $[\frac{3\pi}{10}, \frac{\pi}{2}]$ is expanded to $[\frac{3\pi}{2}, \frac{5\pi}{2}]$ as a result.

Consider the extracted negative band of the filter N_1 output, as a result of down-sampling operation by 5 the extracted frequency band is relocated at $[\frac{-5\pi}{2}, \frac{-3\pi}{2}]$. The frequency band is equivalent to that at $[\frac{-5\pi}{2}, \frac{-3\pi}{2}] + 2\pi = [\frac{3\pi}{2}, \frac{5\pi}{2}]$. However, the frequency edge $\frac{3\pi}{2}$ corresponds to the original input spectrum at $-\frac{\pi}{2}$ which is at a higher frequency component compared to that at $\frac{5\pi}{2}$ edge. Hence, the negative band results in the extracted signal locating in frequency band of $[\frac{3\pi}{2}, \frac{5\pi}{2}]$, similar to the positive band,

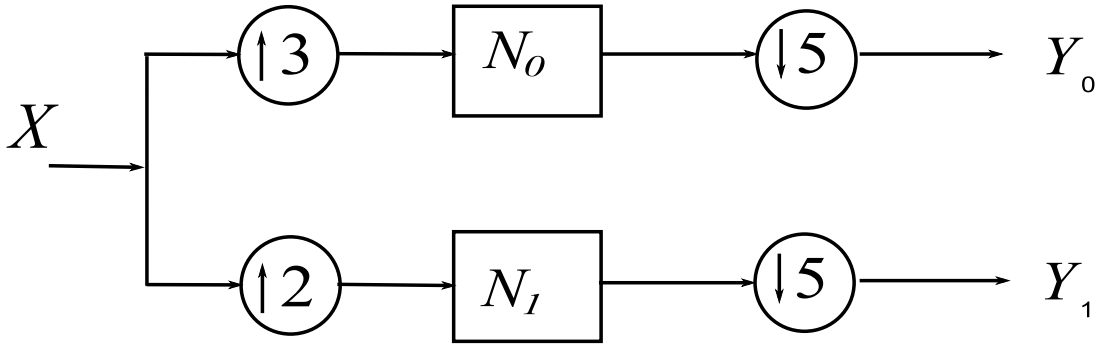

(a) Analysis side of an $(\frac{3}{5}, \frac{2}{5})$ RFB structure

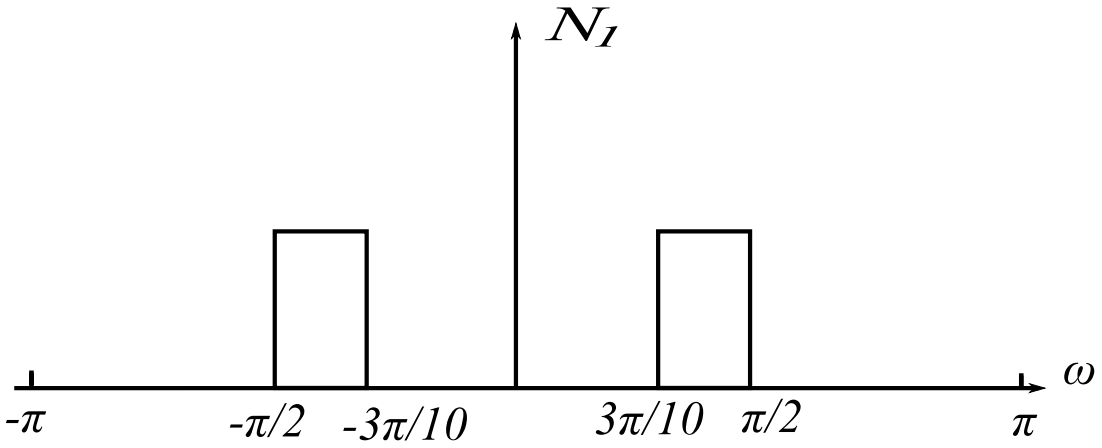

(b) $(\frac{3}{5}, \frac{2}{5})$ RFB desired band-pass response

Figure 2.2. Two-channel NUFB with rational rate changing $(\frac{3}{5}, \frac{2}{5})$(a) and the desired spectrum at the output of N_1 filter (assumed ideal filter N_1) (b).

however with reversed frequency order. Such overlapping renders perfect reconstruction impossible.

Note that if N_1 is to extract signal occupying frequency bands $\pm[\frac{\pi}{2}, \frac{7\pi}{10}]$, the similar overlapping will occur at frequency region of $[\frac{\pi}{2}, \frac{3\pi}{2}]$, which again renders perfect reconstruction impossible.

Such aliasing in the high-pass response can be avoided for a slight adjustment in the filter rate changing parameters. Consider the following example:

Example 2.1.2. *Consider a three channel RFB with* $M = 3, p_0 = 2, p_1 = 2, p_2 = 1$ *and* $q_0 = q_1 = q_2 = 5$*; the corresponding three channel RFB has rational re-sampling ratios of* $(\frac{2}{5}, \frac{2}{5}, \frac{1}{5})$*. The structure is illustrated in Fig. 2.3*

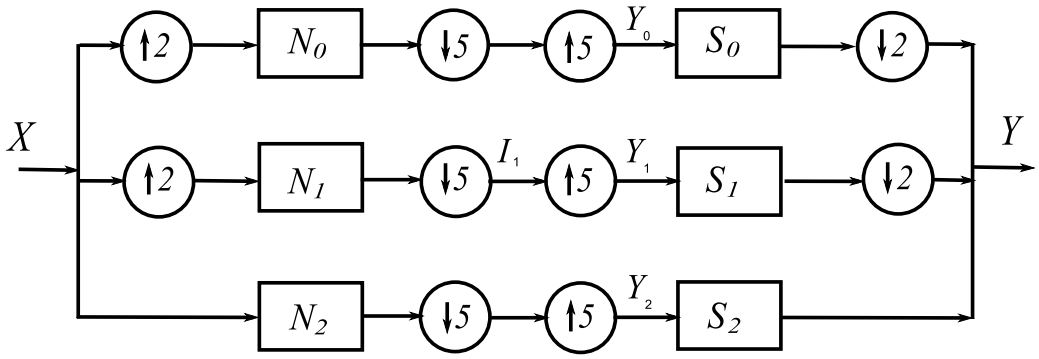

(a) 3-channel $(\frac{2}{5}, \frac{2}{5}, \frac{1}{5})$ RFB

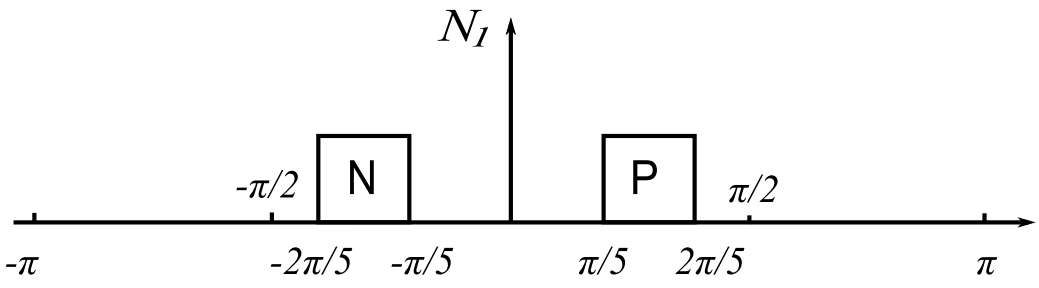

(b) $(\frac{2}{5}, \frac{2}{5}, \frac{1}{5})$ RFB desired band-pass response

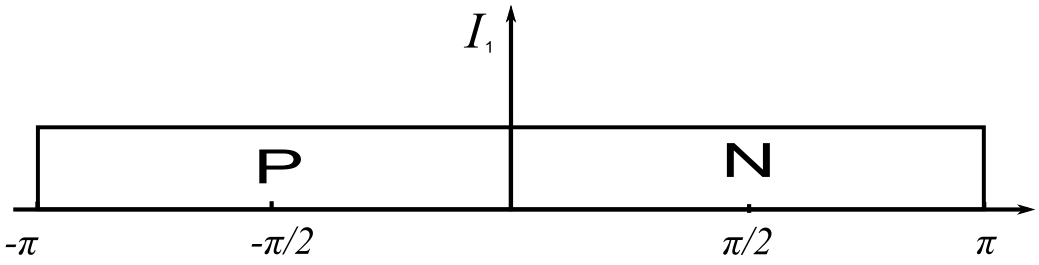

(c) Frequency response at the output of the down-sampling operation, i.e. I_1

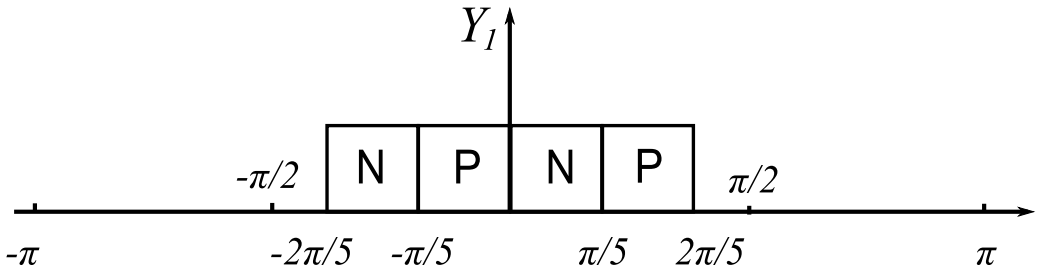

(d) Frequency response of Y_1

Figure 2.3. (a) Three-channel NUFB with rational rate changing $(\frac{2}{5}, \frac{2}{5}, \frac{1}{5})$ and (b) the desired spectrum at the output of N_1 filter (assumed ideal band-pass filter N_1); (c) illustrates the response at I_1 after the down-sampling operation while (d) represents the response at Y_1.

Consider the band-pass filter N_1 of structure Fig. 2.3 (a). The extracted frequency band is $\pm[-\frac{2\pi}{5}, -\frac{\pi}{5}]$. We denote N and P for negative and positive bands of the considered real filter as shown in Fig. 2.3 (b). Note that up-sampling of input signal by

two resulting in the original extracted band-pass frequency bands at $\pm[\frac{2\pi}{5}, \frac{4\pi}{5}]$ being compressed to the $[-\frac{2\pi}{5}, -\frac{\pi}{5}]$ and $[\frac{\pi}{5}, \frac{2\pi}{5}]$, hence the required band of filter N_1. Since down-sampling by 5 results in the signal's spectrum being expanded by 5, the P and N frequency bands at the N_1 filter output are expanded to $[\pi, 2\pi]$ and $[0, \pi]$, respectively. Note that 2π shifting has been done to the resulting frequency bands to bring them within the fundamental Nyquist's zone $[-\pi, \pi]$. This is illustrated in Fig. 2.3 (c). At this stage, no aliasing has occurred for this structure. Fig. 2.3 (d) illustrates the response Y_1 after up-sampling operation. If S_1 has similar frequency response as N_1, the frequency bands as similar to those at the output of N_1 will be extracted and the order of positive and negative frequency bands are also picked up correctly. Hence, no aliasing occurs in this case.

Note that for the low-pass channel (corresponding to filters N_0, S_0), in which the extracted frequency band of interest is in $[-\frac{\pi}{5}, \frac{\pi}{5}]$, there is no aliasing caused by the down-sampling operation by 5. In the high-pass channel (corresponding to filters N_2, S_2), the extracted frequency bands are $\pm[\frac{4\pi}{5}, \pi]$. Down-sampling by 5 results in the bands being relocated to frequency regions of $[0, \pi]$ and $[-\pi, 0]$, for positive and negative frequency bands, respectively. Similarly, as a result of the up-sampling 5, the response is compressed by 5 in a similar manner but in a reverse P and N order of that in Fig. 2.3 (d). These can be correctly reconstructed again if S_2 has the same response as N_2.

In summary, it is possible for a critically-sampled M-channel RFB structure with real filters, to extract in the following frequency bands of input signal (Kovacevic and Vetterli 1993) for any channel $i = 0 \ldots, M-1$:

$$X_i : \left[\frac{k}{q}\pi, \frac{k+p}{q}\pi\right] \tag{2.1}$$

if there exist l, s such that one of the following pairs of conditions is satisfied,

$$k = sp - lq, \qquad l = 2t, \tag{2.2}$$

$$k - q = lq - sp, \qquad l = 2t + 1, \tag{2.3}$$

where $l = 0, \ldots, p-1; s = 0, \ldots, q-1$; and $k = 0, \ldots, q-p$. If the solution exists for (2.2) or (2.3), then the filters are required to have pass-bands

$$N_i, S_i : \left[\frac{s}{q}, \frac{s+1}{q}\right]. \tag{2.4}$$

In example 2.1.1, extracting the spectrum from $[\frac{3}{10}\pi, \frac{5}{10}\pi]$ in channel 1 (i.e. $i = 1$) gives $k = 3, q = 10, p = 2$. It can be verified that there exists no $l \in [0, p-1], s \in [0, q-1]$ that satisfy either (2.2) or (2.3).

In example 2.1.2, the following solutions of s, l can be found

- For low-pass channel consisting of S_0, N_0, the interested spectrum to be extracted is $[0, \frac{\pi}{5}]$, hence $k = 0, q = 5, p = 1$ and the corresponding solution for (2.2) are $s = 0, l = 0$.
- For band-pass channel consisting of S_1, N_1, the extracted spectrum is $[\frac{\pi}{5}, \frac{2\pi}{5}]$, hence $k = 1, q = 5, p = 1$ and the corresponding solution for (2.2) are $s = 1, l = 0$.
- For high-pass channel with S_2, N_2, the spectrum of interest to be extracted is $[\frac{4\pi}{5}, \pi]$, hence $k = 4, q = 5, p = 1$ and the corresponding solution for (2.2) are $s = 4, l = 0$.

The required frequency responses of the filters are illustrated in Fig. 2.4.

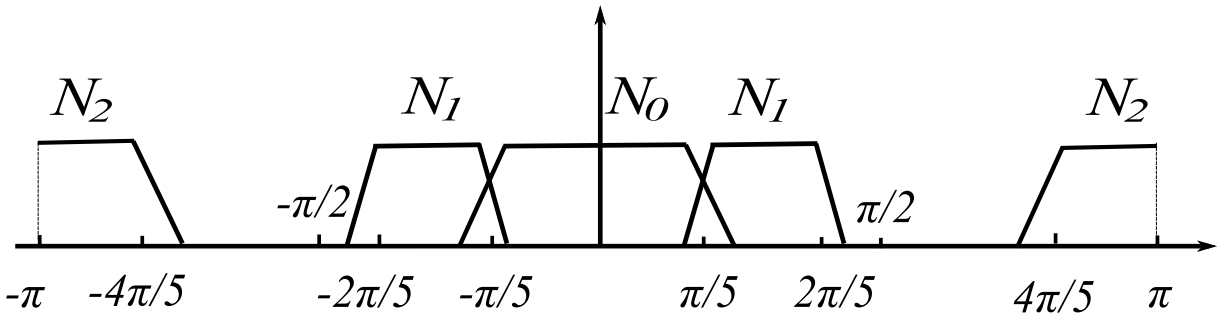

Figure 2.4. Three-channel NUFB with rational rate changing $(\frac{2}{5}, \frac{2}{5}, \frac{1}{5})$ and the required filters' frequency responses; N_0, N_1, N_2 represent low-pass, band-pass and high-pass filters, respectively. Note that S_0, S_1, S_2 are required to have the same responses of the illustrated N_0, N_1, N_2, respectively.

2.1.2 The issue of shift variance in iterated RFB

In iterated RFBs, the term *shift-variance* takes on a different meaning to the dyadic case. For dyadic wavelet transform this term refers to the high dependence of wavelet coefficients on the time of appearance of the input signal. Delays in the input signal can cause significant changes in the wavelet coefficients, which is caused by the subsampling operation by 2 in dyadic discrete wavelet decompositions. In RADWTs, the

term refers to whether iterations of the filters in a RFB converge to a single limit function (Blu 1993). An iterated two-channel RFB is illustrated in Fig. 2.5 for which critically sampled requirement is satisfied if $p_0 + p_1 = M$.

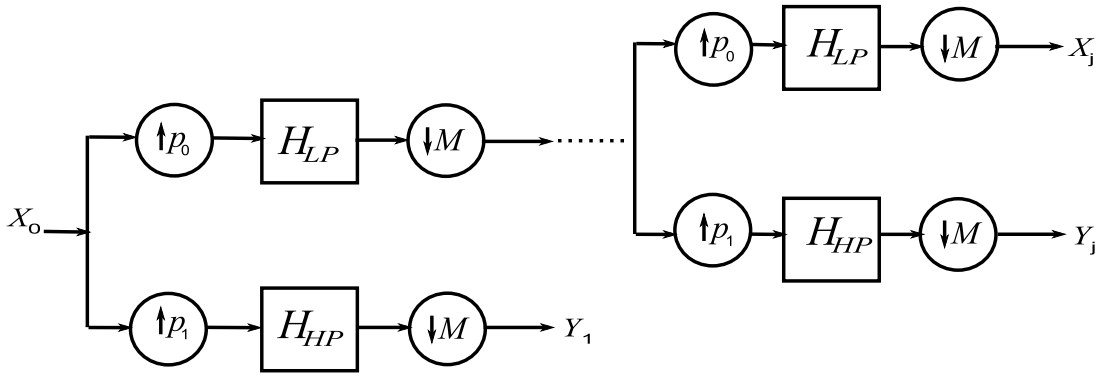

Figure 2.5. Iterated rational two-channel filter bank on the analysis side; $p_0 + p_1 = M$ represents a critically-sampled rational FB structure for co-prime pairs (p_0, M) and (p_1, M).

The manner of the iterations on low-pass filter H_{LP} in a RFB structure as in Fig. 2.5 is similar to that of dyadic wavelet decomposition. After j iterations, the resulting structure corresponds to an $(j+1)$-band filter bank. The simplified version of such iteration on the low-pass analysis filter H_{LP} is shown in Fig. 2.6 (a). For the co-prime pair (p_0, M), the j-stage iterated structure can be grouped together to form the equivalent structure as in Fig. 2.6 (b). This transformation can be proved using basic properties of up or down sampling operators, summarised in (Vaidyanathan 1993). $H_{LP}^{(j)}$ is defined as (Blu 1993)

$$H_{LP}^{(j)}(z) = H_{LP}(z^{({p_0}^{j-1})})H_{LP}(z^{(M{p_0}^{j-2})}) \dots H_{LP}(z^{(M^{j-1})}). \tag{2.5}$$

Let the output $X_j(z)$ and filter $H_{LP}^{(j)}(z)$ of the transformed low-pass iteration of Fig. 2.6 (b) be defined as $X_j(z) = \sum_n \mathbf{x}_j[n]z^{-n}$ and $H_{LP}^{(j)}(z) = \sum_n \mathbf{h}_j[n]z^{-n}$, respectively. Hence, $\mathbf{x}_j$ can be written in terms of $\mathbf{x}_0$ as

$$\mathbf{x}_j[n] = \sum_k \mathbf{h}_j[nM^j - k{p_0}^j]\mathbf{x}_0[k], \tag{2.6}$$

where $X_0(z) = \sum_n \mathbf{x}_0[n]z^{-n}$. Consider low-pass iteration on the synthesis side with synthesis low-pass filter being the same as the analysis filter H_{LP}, for a delayed impulse input $X_0(z) = z^{-s}$ the output $\mathbf{x}_{j,s}$ can be written as

$$\mathbf{x}_{j,s}[n] = \mathbf{h}_j[n{p_0}^j - sM^j]. \tag{2.7}$$

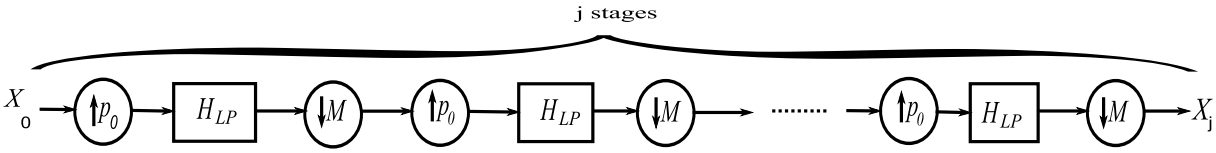

(a) $j-$stage iterated analysis low-pass filter in a $(\frac{p_0}{M}, \frac{p_1}{M})$ RFB structure

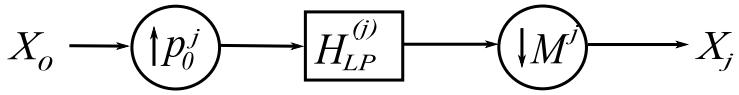

(b) Equivalent filtering operation

Figure 2.6. (a)j-stage iterated rational filter bank on the analysis low-pass filter and (b) the equivalent structure for co-prime pair (p_0, M).

If $p_0 = 1$, the the entire problem becomes constructing the father wavelet function from a uniform M-channel FB structure with a low-pass filter $H_{LP}(z)$. $\{\mathbf{x}_{j,s}\}_{s\in\mathbb{Z}}$ of (2.7) define the discrete father wavelet $\mathbf{h}_j[n]$ and its translated versions $\mathbf{h}_j[n - sM^j]$, which spans the subspace V_j of a multi-resolution analysis described by (1.9) in section 1.4.2.1. If $p_0 > 1$, (2.7) shows that there exists ${p_0}^j$ father wavelet functions which corresponds to ${p_0}^j$ polyphase components of $\mathbf{h}_j$. It is precisely this complication that defines *shift variance* of iterated a RFB, for it prevents an iterated RFB from behaving as a wavelet transform in conventional sense.

However, it is argued that (Blu 1998, Bayram and Selesnick 2009c) by minimising the error between the ${p_0}^j$ discrete sequences defined in (2.7) as s varies, we can attain an approximate discrete wavelet transform for rational dilation case. This forms the family of RADWTs which have been discussed by many authors in the literature (Blu 1998, Bayram and Selesnick 2009c, Bayram and Selesnick 2009b).

Fig. 2.7 (a) illustrates the *shift-variance* issue of iterated RFBs. The father wavelet and its translated version are not shifted versions of each other as in conventional wavelets. In Fig. 2.7 (b), the shift-error is minimised to approximate RADWTs. It has been shown (Blu 1993) that the *shift error* can be minimised if the designed filter has

- good frequency selectivity and
- at least one regularity factor.

Good frequency selectivity refers to filters with narrow transition-band and high stop-band attenuation. A rational FB is said to possess regularity factors if the low-pass analysis and synthesis filters preserve the discrete time polynomial of order $K-1$, for

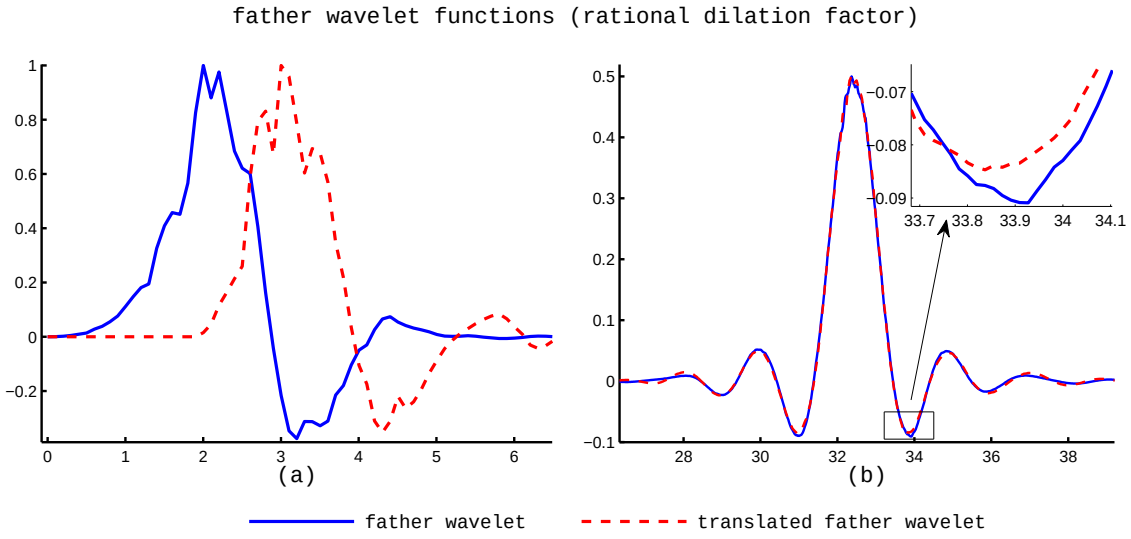

Figure 2.7. (a) iterated rational FB on the low-pass filter and its translated version (without minimising shift-error) (b) iterated rational FB and its translated version on the same interval (with shift-error being minimised).

which K represents the *regularity order*. Simultaneously, the analysis high-pass channel annihilates the discrete time polynomial of order $K-1$. Thus, for rational FBs as in Fig. 2.5, the analysis low-pass and high-pass filters possess K regularity order if and only if they satisfy the following conditions (Bayram and Selesnick 2009c, Steffen *et al.* 1993)

$$H_{LP}(z) = (1 + z^{-1} + \ldots + z^{-(p_0-1)})^K P_0(z), \tag{2.8}$$

$$H_{HP}(z) = (1 - z^{-1})^K Q(z), \tag{2.9}$$

and the synthesis low-pass filter is required to be divisible by

$$(1 + z^{-1} + \ldots + z^{-(M-1)})^K. \tag{2.10}$$

2.2 Existing Design approaches in the literature

The topic of designing rational filter banks has been addressed by many authors (Blu 1998, Kovacevic and Vetterli 1993, Saadat Mehr and Chen 2000, Bayram and Selesnick 2009c, Princen 1994, Wada 1995, Bayram and Selesnick 2009b, Argenti and Del Re 1998, Bayram and Selesnick 2007). In that context, several approaches have attempted to impose regularity orders on the design of RFB (Bayram and Selesnick 2007, Bayram and Selesnick 2009b, Bayram and Selesnick 2009c, Bayram and Selesnick 2009a, Blu 1998).

Among these designs, Bayram and Selesnick (Bayram and Selesnick 2009b) attained K-regular RFB with finite impulse response (FIR) filters in an orthonormal structure using matrix factorisation, but this approach did not explicitly address the shift-variance issue and hence frequency selectivity as reported in other papers on rational DWT (Blu 1993, Blu 1998, Bayram and Selesnick 2009c, Bayram and Selesnick 2009a). Furthermore, the design leads to near PR when K regularity orders are imposed on the FB structure.

Bayram's other designs (Bayram and Selesnick 2007, Bayram and Selesnick 2009c, Bayram and Selesnick 2009a) are over-complete RFBs with arbitrary K regularity orders, and the associated expansive decompositions can be undesirable for applications such as signal compression. Blu's design from an iterative optimisation algorithm resulted in orthonormal RFBs which were approximately shift-invariant, although this algorithm is reported to diverge for regularity orders greater than one (Blu 1998).

In this section, iterated RFB designs in the literature are presented and discussed. The summary of the designs' key features are separated into classes. This classification is based on 1) redundancy of the eventual filter banks and 2) compactness of filter support which can either be compact (FIR) and non-compact (IIR).

2.2.1 Critically sampled RFBs and RADWTs

Orthogonal RADWTs with compact support

One of the earliest approaches on RADWTs is presented in (Blu 1998), in which the resultant design approximates rational DWT and satisfies PR, possesses regularity factors and are orthogonal. The FB consists of FIR filters, which are designed based on an iterative algorithm. The designed filters are frequency selective and their iterations lead to wavelet functions which are approximately shift-invariant. The FB structure is shown in Fig. 2.8. The filters $H(z), G(z)$ represent analysis low-pass and high-pass filters, respectively. The synthesis filters are time-reversed versions of the analysis filters. Some key features of such designs include:

- the design algorithm is recursive and consists of a sequence of convex optimisation routines. At each iteration, the low-pass filter's stop band energy is optimised against some linear constraints;

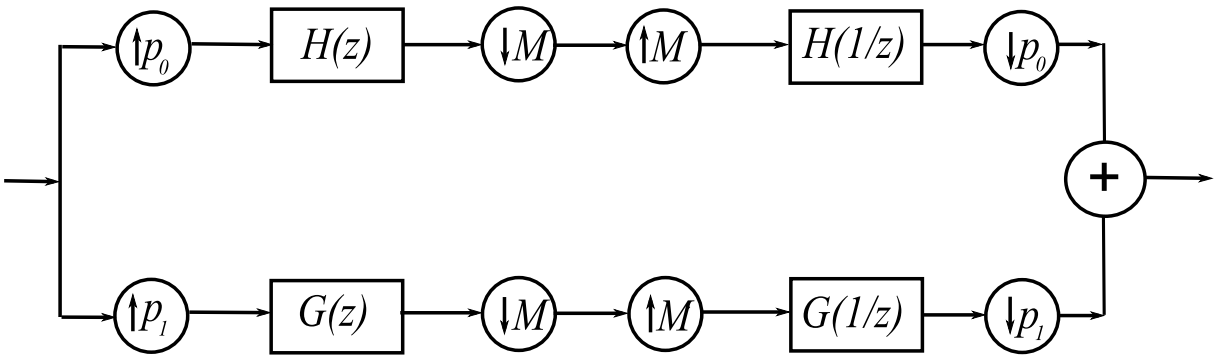

Figure 2.8. Rational FB structure of (Blu 1998) literature design; $H(z), G(z)$ represent analysis low-pass and high-pass filters, respectively; $p_0 + p_1 = M$.

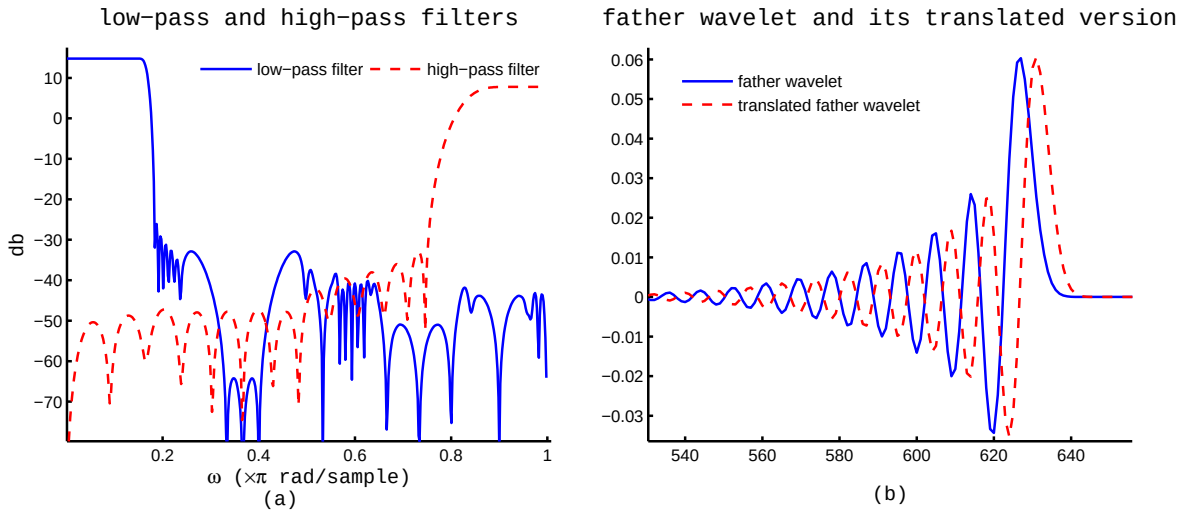

Figure 2.9. (a) Frequency response of low-pass $H(z)$ and high-pass $G(z)$ of the design example based on (Blu 1998)(b) corresponding father wavelet and its translated version.

- the filter bank is orthogonal and thus has a para-unitary polyphase matrix. Hence, the high-pass filter can be attained from factorisation of the polyphase matrix in the manner described in (Vaidyanathan 1993) once the low-pass filter is designed;

- the algorithm is independent of initialisations and it diverges if more than one regularity order is imposed on the filters.

Fig. 2.9 (a) illustrates the low-pass and high-pass filters' responses of a rational FB design for $p_0 = 5, p_1 = 1, M = 6$. The low-pass filter $H(z)$ has good frequency selectivity, which results in approximately shift-invariant father wavelet functions as shown in Fig. 2.9 (b). In summary, the design approach successfully led to orthogonal rational

FBs with good frequency selectivity and possessing regularity orders. However, the convergence of this approach is limited to filters with one regularity order.

In an attempt to overcome the limitation of only one regularity order, an algorithm was proposed (Bayram and Selesnick 2009b) to design orthogonal rational FB with arbitrary regularity orders. In this approach, the rational rate filter bank is decomposed into the equivalent uniform filter bank, whose filters from each analysis and synthesis side are DFT-modulated versions of each others. The approach shows poorer stop-band performance as compared to (Blu 1998), provided the total length of filters are similar. More importantly, the algorithm's output does depend on the initialisation of the design algorithm and the resultant FB only satisfies PR condition approximately, i.e. only near PR filter banks. A comparison between the two filters resulted from the two algorithms is shown in Fig. 2.10.

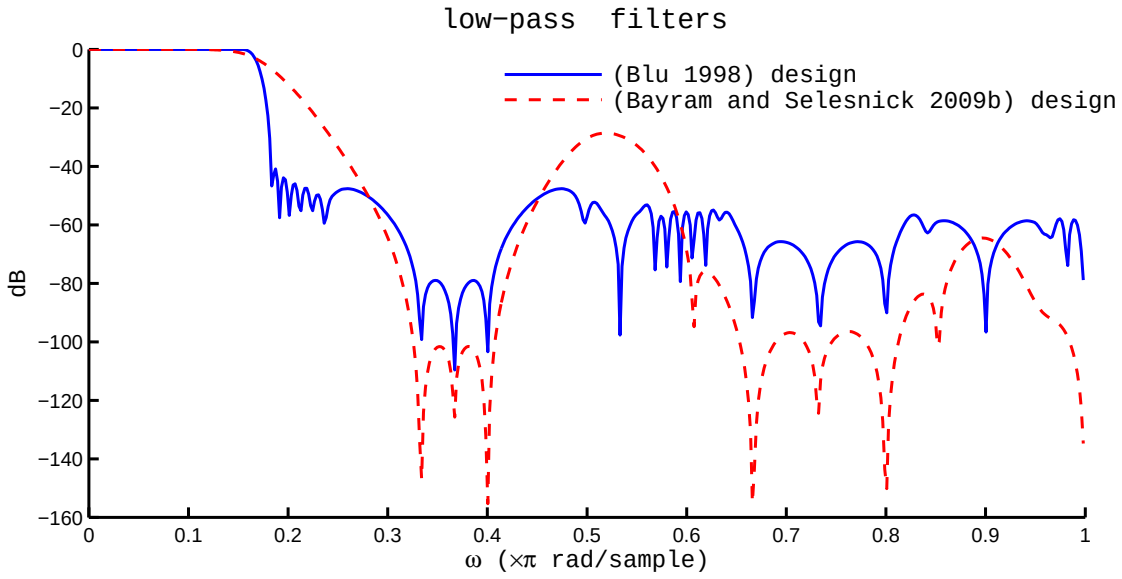

Figure 2.10. Blue solid trace represents Blu's design (Blu 1998) (one regularity order) while red dashed trace represents design in (Bayram and Selesnick 2009b) (two regularity orders); FB rate changing factors are $(\frac{5}{6}, \frac{1}{6})$

Orthogonal RADWTs with non-compact support

Auscher (Auscher 1992) first attempted to construct RADWTs in the Fourier domain, which leads to non-compact support wavelet functions. For a rational dilation factor, defined by a ratio $\frac{p}{q}$ for $p, q \in \mathbb{N}, p = q + 1$, let function $\chi(\omega)$ be an even function in

$C^{\infty}(\mathbb{R})$, defined as

$$\chi(\omega) = \begin{cases} 0 & \text{for} \quad \omega \in [0, (q-\epsilon)\pi) \\ \frac{\pi}{4} + \beta(\omega - q\pi) & \text{for} \quad \omega \in [(q-\epsilon)\pi, (q+\epsilon)\pi) \\ \frac{1}{2} & \text{for} \quad \omega \in [(q+\epsilon)\pi, \frac{p}{q}(q-\epsilon)\pi) \\ \frac{\pi}{4} - \beta(\frac{q}{p}\omega - q\pi) & \text{for} \quad \omega \in [\frac{p}{q}(q-\epsilon)\pi, \frac{p}{q}(q+\epsilon)\pi) \\ 0 & \text{for} \quad \omega \in [\frac{p}{q}(q+\epsilon)\pi, +\infty) \end{cases} \tag{2.11}$$

for $\epsilon \in (0, \frac{1}{\frac{p}{q}+1}]$ and

$$\beta(\omega) = \frac{\pi}{4} \qquad \forall \omega \in [\epsilon\pi, +\infty) \tag{2.12}$$

Hence, the scaling and wavelet functions are defined as

$$\Phi(\omega) = \begin{cases} \cos(\chi(\omega)) & \text{for} \quad |\omega| \leq (q-\epsilon)\pi \\ 0 & \text{for} \quad \text{elsewhere} \end{cases} \tag{2.13}$$

$$\Psi(\omega) = \text{sgn}(\omega)\sin(\chi(\omega))e^{j\omega/2} \tag{2.14}$$

Fig. 2.11 illustrates the scaling and wavelet functions constructed using this approach

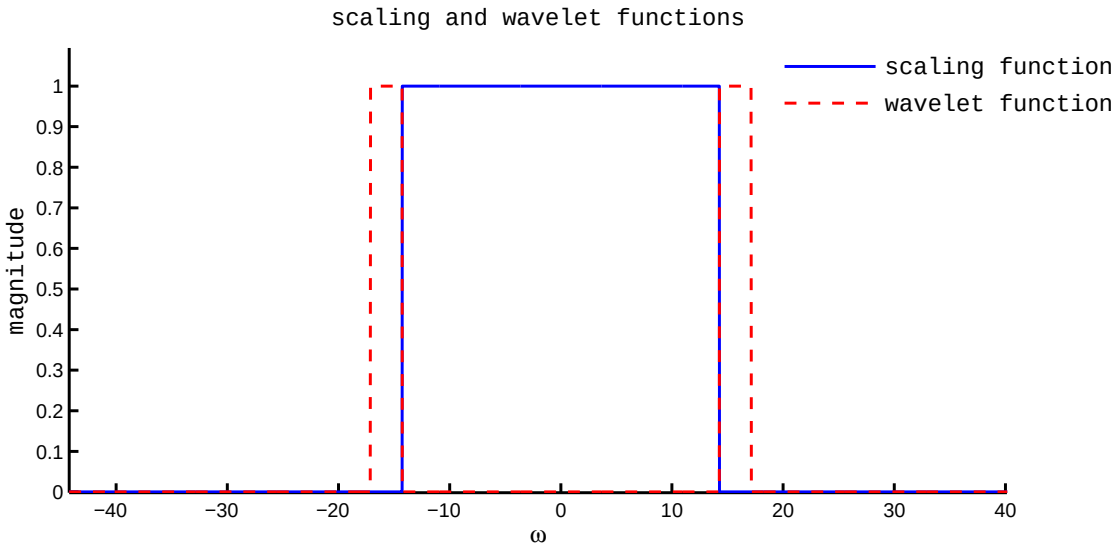

Figure 2.11. Blue solid trace represents father wavelet function while red trace illustrates the wavelet function, both of which are designed based on (Auscher 1992) with rational dilation factor of $\frac{6}{5}$

with $\epsilon = \frac{q}{2q+1}$. Even though the obtained functions are not compactly supported in

time, the design approach leads to a MRA with rational dilation factor $\frac{p}{q}$. The designed wavelet functions have shown to possess infinite number of regularity orders since the frequency responses are precisely zero in all stop-band regions.

In summary, FIR based design offers compact support to the resulting wavelet functions even though the obtained RADWTs only satisfy *shift invariance* approximately. On the other hand, if the wavelet functions are constructed in Fourier domain, a MRA with rational scaling factors can be obtained at the expense of needing infinite impulse response (IIR) filters.

2.2.2 Overcomplete RFB – redundant RADWTs

Redundant [2] RADWTs with compact support

The topic of over-complete DWT with rational dilation factor was first addressed by Bayram and Selesnick in (Bayram and Selesnick 2009c), whose filters are designed to possess the following properties

- perfect reconstruction;
- self inverting FIR filters and compact support of basis functions;
- high-pass filters are designed based on matrix spectral factorisation;
- possess arbitrary number of (K) regularity orders with minimal length filters and closed form solutions for low-pass filters, hence mathematical exactness;
- for a RADWT design with rational dilation factor of $\frac{M}{p_0}$ for $p_0, M \in \mathbb{N}$, the redundancy factor of the transform is always $\frac{p_0+M}{M}$.

The rational FB structure is illustrated in Fig. 2.12, in which $H(z), G_n(z), n = 0, \ldots, M-2$ represent the low-pass and high-pass analysis filters, respectively. The synthesis filters are time-reversed versions of the analysis filters. Consider the following example, in which a rational FB with $p_0 = 2, M = 3$ and $K = 4$ regularity orders is designed based on (Bayram and Selesnick 2009c). The filters are shown in Fig. 2.13. In Fig. 2.13 (a), only the response of $G_0(z)$ high-pass filter is shown since $G_1(z), G_2(z)$ have very

[2] In this section, the terms over-complete and redundant are used interchangeably to denote RADWTs with some redundancy.

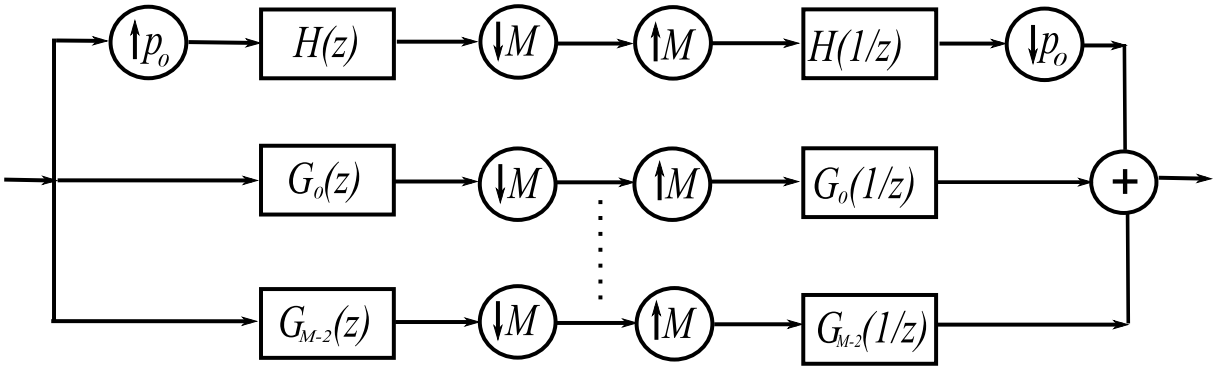

Figure 2.12. Rational FB structure of (Bayram and Selesnick 2009c) literature design; $H(z), G_n(z)$, $n = 0, \ldots, M-2$ represent high-pass and low-pass filters, respectively.

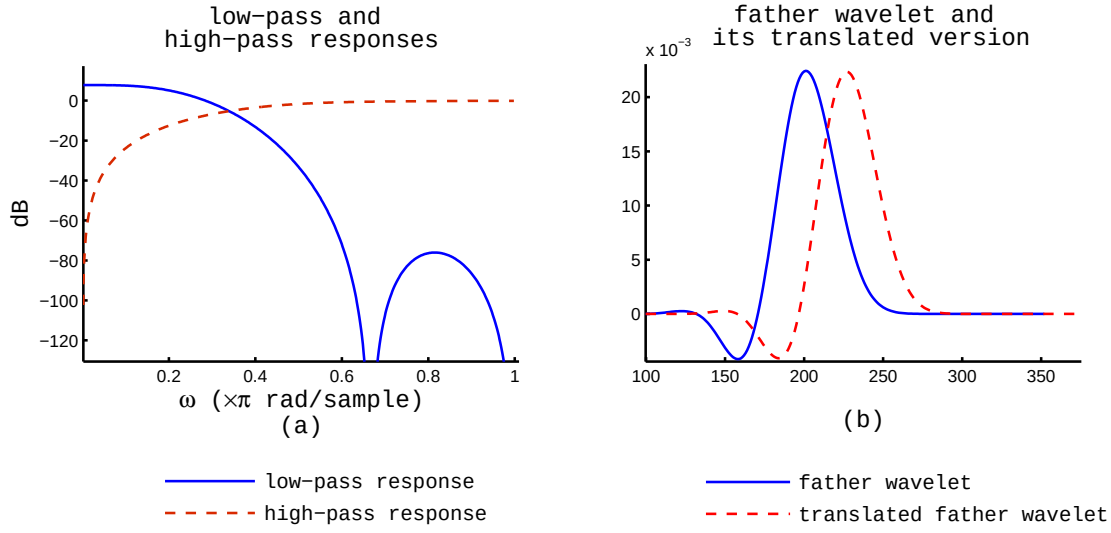

Figure 2.13. (a) Frequency response of low-pass $H(z)$ and high-pass $G_0(z)$ of the design example based on (Bayram and Selesnick 2009c) and (b) corresponding father wavelet and its translated version.

similar frequency responses. The frequency response for low-pass filter $H(z)$ is shown with good stop band attenuation. Its regularity property is illustrated as $H(\omega)$ has zeros at $(\omega = 2\pi/3, \pi)$, which corresponds to conditions (2.8), (2.10) for $M = 3, p_0 = 2$. The filter $H(\omega)$ is required to satisfy both (2.8), (2.10) for analysis and synthesis filters since the previous filter is time-reversed version of the latter. The filter $G_0(z)$ is also shown, from Fig. 2.13 (a) to have zeros at $\omega = 0$ as a result of (2.9). Fig.2.13 (b) shows the iterated low-pass filter or discrete father wavelet and the translated version, which approximates the shifted version of the father wavelet function.

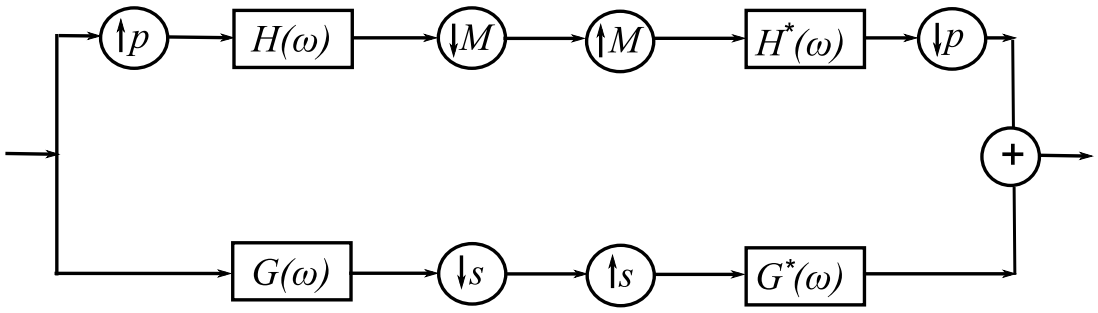

Figure 2.14. Rational FB structure of (Bayram and Selesnick 2009a) literature design; $H(\omega), G(\omega)$ represent low-pass and high-pass filters, respectively.

One notable disadvantage of the design lies in the pass-band region of the low-pass filter, which is required to pass frequencies in the region $[0, \frac{\pi}{3}]$. In this design, no optimisation is imposed on the frequency characteristic of the resulting filter at the expense of minimal length filters and exact closed form formula. This leads to filters with poor pass-band and transition-band responses as illustrated in Fig. 2.13(a).

Redundant RADWTs in Fourier domain (non-compact support wavelet functions)

Blu (Blu 1993) found that the construction of wavelet transform with rational dilation factors can only be approximately attained with FIR filters since the resulting wavelet functions are not perfectly shifted versions of each other. Hence, multi-resolution analysis cannot be achieved perfectly for rational dilation factors. However, Auscher (Auscher 1992) showed that MRA is achievable even in rational dilation cases if the the wavelet functions are to be designed in Fourier domain, implying IIR filters. Bayram and Selesnick extended the design idea, and allowed some degree of transform redundancy (Bayram and Selesnick 2009a). The approach, which leads to RADWTs and MRA with rational dilation factor, is constructed based on a single band-limited filter. The allowed redundancy can be adjusted to provide adjustable Q-factor [3] of the RADWT. This shows an improvement as compared to the approach in (Bayram and Selesnick 2009c). Fig. 2.14 illustrates the design FB structure and its parameters p, M, s, which determine the transform's Q factor and its redundancy. For integer values p, M, s, the quality factor Q and the redundancy factor r of transform, is defined as (Bayram and Selesnick 2009a)

$$Q = \sqrt{\frac{p}{M}} \frac{1}{1 - \frac{p}{M}} \quad \text{and} \quad r = \frac{1}{s} \frac{1}{1 - \frac{p}{M}} \tag{2.15}$$

[3] The quality factor Q factor is defined to be the ratio of centre frequency and the spectrum's bandwidth.

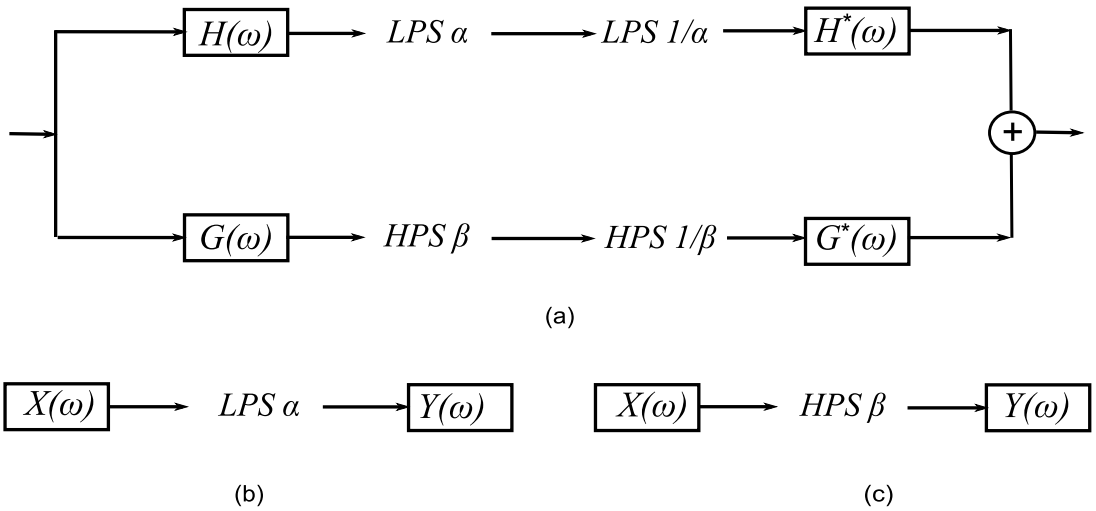

Figure 2.15. (a) FB structure of (Selesnick 2011a) literature design; $H(\omega), G(\omega)$, represent low-pass and high-pass filters, respectively; LPS and HPS represent low-pass scaling and high-pass scaling by factors α, β, respectively (i.e. if f_s is the input signal's sampling frequency, LPS by α gives a new sampling rate of αf_s); (b),(c) represent the low-pass and high-pass scaling operation diagrams.

for

$$1 - \frac{1}{s} > \left(\frac{p}{M}\right)^2. \tag{2.16}$$

If (2.16) is not satisfied, the resulting Fourier transform of the wavelet functions will not have flat band-pass responses as the FB is iterated. Hence, Q factor cannot be algebraically computed as in (2.15) but having to be estimated numerically. In such case, Q factor is dependent on the values of p, M and s.

In (Selesnick 2011a), Selesnick proposed a design of tunable Q wavelet transform, also in the Fourier domain. The FB structure is illustrated in Fig. 2.15. The design approach introduces the idea of low-pass and high-pass scalings, which can be straightforwardly performed in the frequency domain. For example, if the low-pass scaling operation by α is performed as shown in Fig. 2.15 (b) on input signal $X(\omega)$, defined as the discrete Fourier transform of input sequence $\mathbf{x}$, then the output signal can be obtained as (Selesnick 2011a)

$$Y(\omega) = X(\alpha\omega), \qquad |\omega| \leq \pi, \qquad \text{for} \quad 0 < \alpha \leq 1, \tag{2.17}$$

$$Y(\omega) = \begin{cases} X(\alpha\omega), & |\omega| \leq \frac{\pi}{\alpha} \\ 0 & \frac{\pi}{\alpha} < |\omega| \leq \pi \end{cases} \qquad \text{for} \quad \alpha \geq 1, \tag{2.18}$$

where $Y(\omega)$ denotes the discrete time Fourier transform of the output sequence $\mathbf{y}$ of sampling rate αf_s, provided f_s being the input signal's sampling frequency. Similarly,

if high-pass scaling is performed as in Fig. 2.15 (c), the output of such operation can be obtained as (Selesnick 2011a)

$$Y(\omega) = \begin{cases} X(\beta\omega + (1-\beta)\pi), & 0 < \omega < \pi, \quad 0 < \beta \leq 1 \\ X(\beta\omega - (1-\beta)\pi), & -\pi < \omega < 0, \quad 0 < \beta \leq 1 \end{cases}, \tag{2.19}$$

and

$$Y(\omega) = \begin{cases} 0, & |\omega| \leq (1-\frac{1}{\beta})\pi, \quad \beta > 1 \\ X(\beta\omega + (1-\beta)\pi), & (1-\frac{1}{\beta})\pi < \omega < \pi, \quad \beta > 1 \\ X(\beta\omega - (1-\beta)\pi), & -\pi < \omega < -(1-\frac{1}{\beta})\pi, \quad \beta > 1 \end{cases}. \tag{2.20}$$

Note that $Y(\pi) = X(\pi)$ for high-pass scaling, which preserves the high-pass response when performing high-pass scaling. Likewise, $Y(0) = X(0)$ for low-pass scaling illustrates that low-pass response should be preserved in low-pass scaling operation. The FB structure satisfies perfect reconstruction if the low pass and high pass filters $H(\omega), G(\omega)$ satisfy

$$|H(\omega)| = 1, \quad \text{for} \quad |\omega| \leq (1-\beta)\pi, \tag{2.21}$$

$$H(\omega) = 0, \quad \text{for} \quad \alpha\pi \leq |\omega| \leq \pi, \tag{2.22}$$

$$G(\omega) = 0, \quad \text{for} \quad |\omega| \leq (1-\beta)\pi, \tag{2.23}$$

$$|G(\omega)| = 1, \quad \text{for} \quad \alpha\pi \leq |\omega| \leq \pi. \tag{2.24}$$

The design parameters α, β determine the filters' frequency responses (i.e. the transition band widths) and relate to the transform redundancy and quality Q factors as

$$\beta = \frac{2}{Q+1}, \qquad \alpha = 1 - \frac{\beta}{r} \tag{2.25}$$

Once the quality factor Q and redundancy factor r are specified, the corresponding design parameters α, β can be computed, hence the filters' responses. This is an attractive property of the design method as quality factor Q and redundancy factor r are directly specified as opposed to the approach presented in (Bayram and Selesnick 2009a).

Table 2.1 summarises properties of the design approaches in the literature, note that in all the approaches, the arbitrary K regularity orders can be imposed except for (Blu 1998) that K is restricted to 1.

2.3 Chapter summary

In this chapter, critical conditions for designing rational filter bank with regularity orders are addressed and such FBs can be iterated to form rational DWTs. This chapter

Table 2.1. Approaches in the literature for the design of RFBs leading to RADWTs

	Bi-orthogonal/ Orthogonal	Redundant/ critically-sampled	FIR/ IIR FB	PR
(Blu 1998)	Orthogonal	Critically sampled	FIR FB	PR
(Bayram and Selesnick 2009b)	Orthogonal	Critically sampled	FIR FB	near PR
(Auscher 1992)	Orthogonal	Critically sampled	IIR FB	PR
(Bayram and Selesnick 2009c)	Non-orthogonal (tight frame)	redundant	FIR FB	PR
(Bayram and Selesnick 2009a)	Non-orthogonal (tight frame)	redundant	IIR FB	PR
(Selesnick 2011a)	Tight frame	redundant	IIR FB	PR
Proposed approach	Bi-orthogonal	critically-sampled	FIR FB	PR

provides literature review of various designs of rational DTWs and presents outlines of their key features. The construction of rational wavelet transforms in Fourier domain shows good advantages in attaining MRA with rational scaling factors as opposed to the designs based on FIR FBs. However, non-compact support of the resulting wavelet functions in time domain is a notable disadvantage, which can lead to reconstruction errors when dealing with finite length signals. Therefore, construction of RADWTs based on FIR filters is desirable and it is possible to to implement these in time domain, perhaps in real time. It should be noted that all designs in literature are based on FIR orthogonal structure and high-pass filters are designed based on polynomial matrix spectral factorisation. Even though this approach is reasonable in theory, the resulting schemes can be involved when implemented. In this thesis, we propose to design RADWTs based on a FIR bi-orthogonal structure with the inclusion of arbitrary K regularity orders. The analysis filters are designed based on non-linear constrained optimisation, after which the synthesis filters can be straightforwardly computed. The rational DWT family and the corresponding filter banks will be presented in details in the next chapters.

Chapter 3

Bi-orthogonal RFB for Fine Frequency Decomposition: the $\left(\frac{q-1}{q}, \frac{1}{q}\right)$ case

IN this chapter, the design of bi-orthogonal FIR rational rate filter banks with the inclusion of K regularity orders is presented. The FB design is formulated as a nonlinear constrained optimisation problem. Two methods for solving this optimisation are proposed and discussed. The designs obtained from these methods are comprehensively evaluated against the RFBs resulting from the existing approaches.

3.1 Introduction and motivation

The majority of wavelet designs in the literature are based on integer scaling ratios. In the associated multi-resolution analysis, the scaling and wavelet functions between successive levels are scaled by a given integer, with dyadic scale being by far the most common. However, non-integer scaling ratios, equivalent to rational re-sampling rate changes in a discretised implementation, produce sub-bands which offer better decomposition of spectrum. This is a significant advantage for many applications (Baussard *et al.* 2004, Yu and White 2005, Yu and White 2006). This chapter presents an approach to design critically sampled two-channel FIR RFBs, with perfect reconstruction (PR), for rate change schemes satisfying $((q-1)/q, 1/q)$, $q > 2$. Such a RFB is depicted in Fig. 3.1. Such choice of re-sampling ratios is selected to maximise the fine frequency decomposition property offered by rational wavelet transform over the conventional dyadic case. In the literature, several designs of perfect reconstruction FIR RFB are based on factorisation of either a para-unitary or spectral matrix (Bayram and Selesnick 2007, Bayram and Selesnick 2009b, Bayram and Selesnick 2009c, Blu 1998), which require the synthesis filters to be time reversed versions of the analysis filters. The features of these designs are summarised in chapter 2. The approach presented in this chapter discards this time reversal property to attain more degrees of freedom for optimising the filters' frequency selectivity. Instead, the analysis filters are designed using non-linear constrained optimisation over the samples of their impulse response, and the synthesis filters are then formed from products of modulated analysis filters to ensure PR. The linear and non-linear constraints arise from regularity and PR conditions, respectively. Two techniques are proposed for solving the optimisation problem to improve the robustness against initialisations when designing K-regular PR RFBs.

This chapter is organised as follows, in section 3.2, the structure of PR RFB and related conditions such as regularity orders are discussed, followed by a formulation of the design optimisation problem. Section 3.3 describes two approaches for solving the optimisation problems and compares their advantages and disadvantages. Section 3.4 presents the design results and comparisons with the existing approaches and discussions. Section 3.5 discusses the RADWT shift error and the design computational complexity. Section 3.6 contains the concluding remarks.

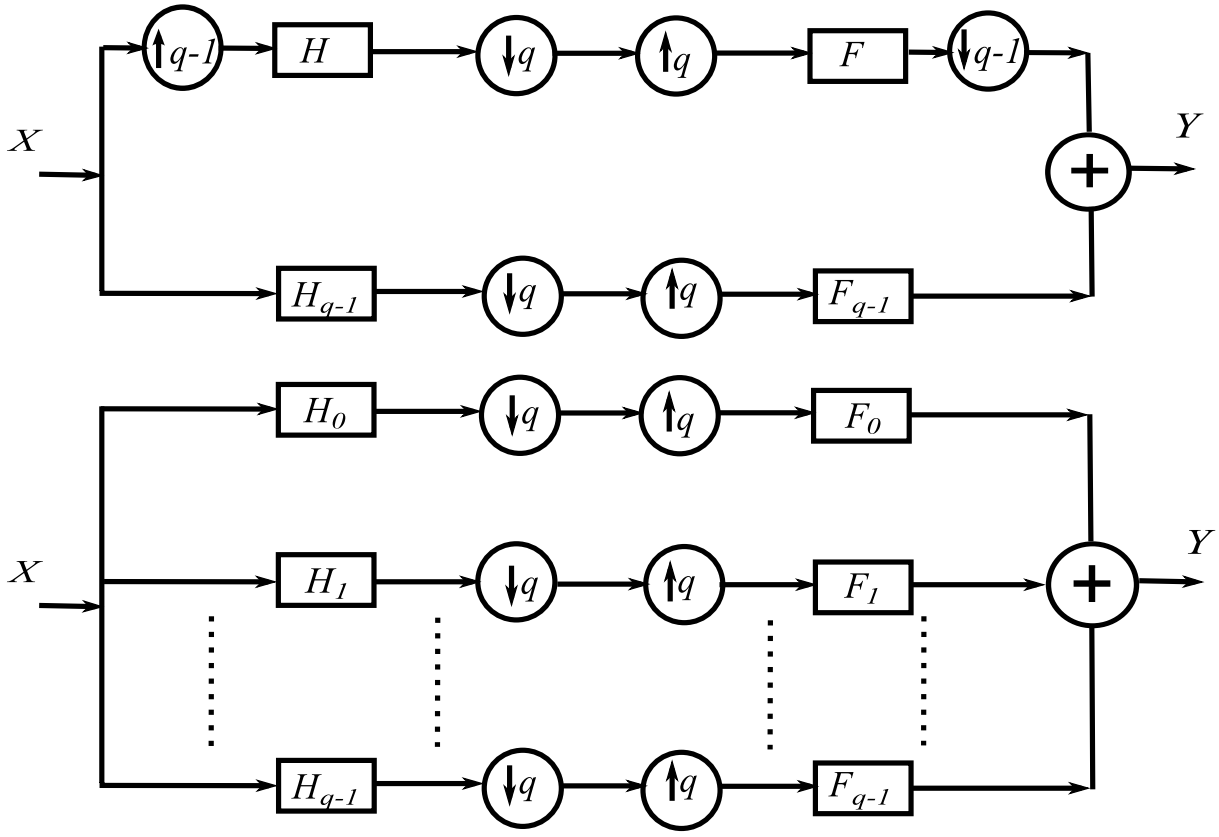

Figure 3.1. Rational rate filter bank with rate changing of $(\frac{q-1}{q}, \frac{1}{q})$ (i.e $p_0 = 1, p_1 = q-1$) (top panel) and its equivalent uniform q-channel FB (bottom).

3.2 Design of two-channel rational filter banks

Let us start with a lemma that allows a critically sampled non-orthogonal two channel RFB be transformed to an equivalent q-channel uniform FB.

Lemma 3.2.1. *The PR rational FB in Fig. 3.2(a) design is equivalent to designing a PR q-channel structure in Fig. 3.2(b) if and only if*

$$H_{LP}(z) = \sum_{n=0}^{p_0-1} z^{qn} H_n(z^{p_0}), \qquad F_{LP}(z) = \sum_{n=0}^{p_0-1} z^{-qn} F_n(z^{p_0}) \tag{3.1}$$

$$H_{HP}(z) = \sum_{n=0}^{p_1-1} z^{qn} H_{n+p_0}(z^{p_1}), \qquad F_{HP}(z) = \sum_{n=0}^{p_1-1} z^{-qn} F_{n+p_0}(z^{p_1}) \tag{3.2}$$

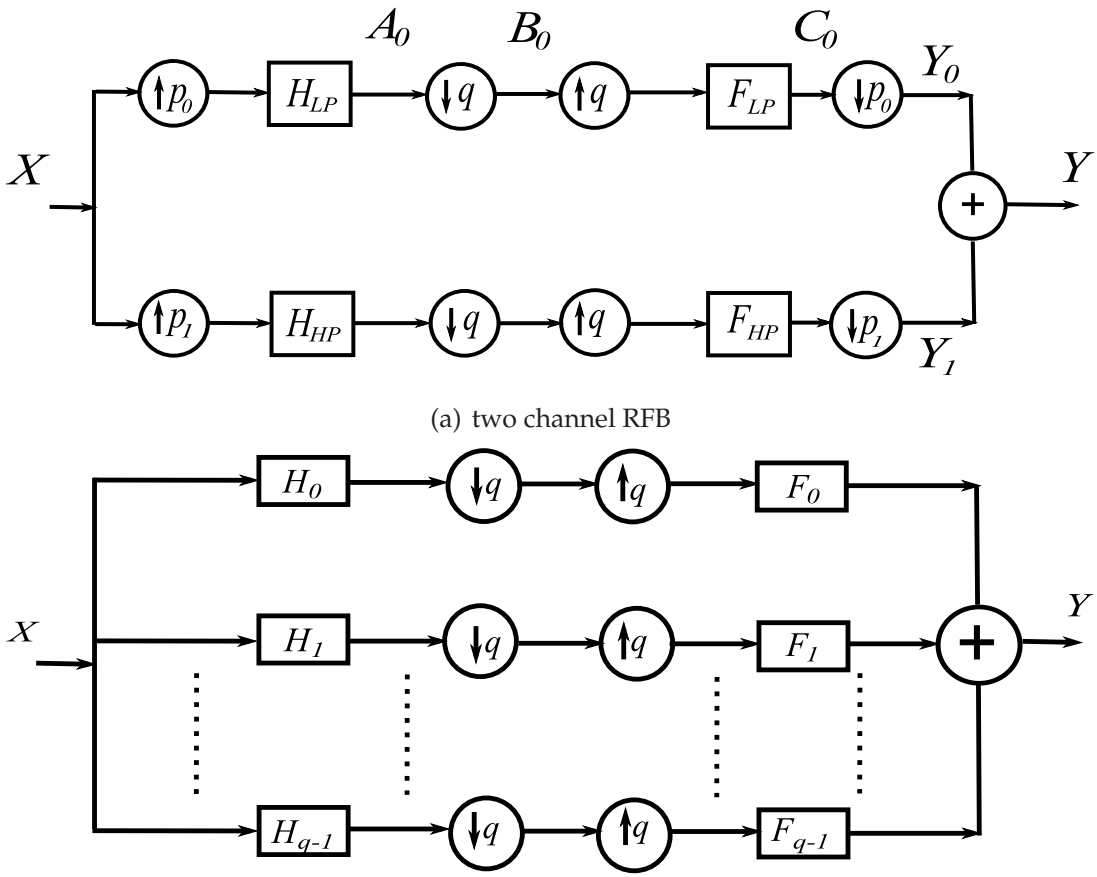

(a) two channel RFB

(b) equivalent uniform q-channel FB

Figure 3.2. Rational rate filter bank with rate changing of $(\frac{p_0}{q}, \frac{p_1}{q})$ for coprime pairs (p_0, q) and (p_1, q) (a) and the equivalent uniform q-channel FB (b).

Proof. We define $W = e^{-j2\pi/q}, W_{p_0} = e^{-j2\pi/p_0}, W_{p_1} = e^{-j2\pi/p_1}$ where $p_0 + p_1 = q$. It is straightforward to show the following holds for FB in Fig. 3.2(b)

$$Y(z) = \frac{1}{q}\Big[X(z)\sum_{n=0}^{q-1} H_n(z)F_n(z) + X(zW)\sum_{n=0}^{q-1} H_n(zW)F_n(z) + \dots + X(zW^{q-1})\sum_{n=0}^{q-1} H_n(zW^{q-1})F_n(z)\Big]. \tag{3.3}$$

Consider the low-pass channel of the RFB structure in Fig. 3.2(a), let $A_0(z) = X(z^{p_0})H_{LP}(z)$ which is the output of the up-sampling by p_0 and followed by $H_{LP}(z)$ filtering, if $B_0(z)$ denotes the output of the subsequent down-sampling by q operation it can be written

as

$$\begin{aligned} B_0(z) &= \frac{1}{q}\Big[A_0(z^{1/q}) + A_0(z^{1/q}W) + \ldots + A_0(z^{1/q}W^{q-1})\Big] \\ &= \frac{1}{q}\Big[X(z^{p_0/q})H_{LP}(z^{1/q}) + X(z^{p_0/q}W^{p_0})H_{LP}(z^{1/q}W) + \ldots + \\ &+ X(z^{p_0/q}W^{(q-1)p_0})H_{LP}(z^{1/q}W^{q-1})\Big]. \end{aligned} \tag{3.4}$$

Hence, the output $C_0(z)$ of the filter by $F_{LP}(z)$ is

$$\begin{aligned} C_0(z) &= B_0(z^q)F_{LP}(z) \\ &= \frac{1}{q}\Big[X(z^{p_0})H_{LP}(z) + X(z^{p_0}W^{p_0})H_{LP}(zW) + \ldots + \\ &+ X(z^{p_0}W^{(q-1)p_0})H_{LP}(zW^{q-1})\Big]F_{LP}(z). \end{aligned} \tag{3.5}$$

$Y_0(z)$ of Fig. 3.2(a) can be written as

$$\begin{aligned} Y_0(z) &= \frac{1}{p_0}\Big[C_0(z^{\frac{1}{p_0}}) + C_0(z^{\frac{1}{p_0}}W_{p_0}) + \ldots + C_0(z^{\frac{1}{p_0}}W_{p_0}^{p_0-1})\Big] \\ &= \frac{1}{qp_0}\Big[X(z)\sum_{n=0}^{p_0-1}\Big(H_{LP}(z^{\frac{1}{p_0}}W_{p_0}^n)F_{LP}(z^{\frac{1}{p_0}}W_{p_0}^n)\Big) + X(zW^{p_0})\sum_{n=0}^{p_0-1}\Big(H_{LP}(z^{\frac{1}{p_0}}W_{p_0}^nW) \\ &F_{LP}(z^{\frac{1}{p_0}}W_{p_0}^n)\Big) + \ldots + X(zW^{(q-1)p_0})\sum_{n=0}^{p_0-1}\Big(H_{LP}(z^{\frac{1}{p_0}}W_{p_0}^nW^{q-1})F_{LP}(z^{\frac{1}{p_0}}W_{p_0}^n)\Big)\Big] \end{aligned} \tag{3.6}$$

Consider one component of the sum in (3.6), denoted as

$$S_k(z) = X(zW^{kp_0})\sum_{n=0}^{p_0-1}\Big(H_{LP}(z^{\frac{1}{p_0}}W_{p_0}^nW^k)F_{LP}(z^{\frac{1}{p_0}}W_{p_0}^n)\Big) \tag{3.7}$$

Substituting (3.1), (3.2) into H_{LP}, F_{LP} give

$$\begin{aligned} S_k(z) &= X(zW^{kp_0})\sum_{n=0}^{p_0-1}\Big[\sum_{l=0}^{p_0-1}\Big((z^{\frac{1}{p_0}}W_{p_0}^nW^k)^{ql}H_l[(z^{\frac{1}{p_0}}W_{p_0}^nW^k)^{p_0}]\Big)\times \\ &\sum_{m=0}^{p_0-1}\Big((z^{\frac{1}{p_0}}W_{p_0}^n)^{-qm}F_m[(z^{\frac{1}{p_0}}W_{p_0}^n)^{p_0}]\Big)\Big] \\ &= X(zW^{kp_0})\sum_{n=0}^{p_0-1}\Big[\sum_{l=0}^{p_0-1}\Big(z^{\frac{ql}{p_0}}W_{p_0}^{lnq}H_l(zW^{kp_0})\Big)\sum_{m=0}^{p_0-1}\Big(z^{\frac{-qm}{p_0}}W_{p_0}^{-mnq}F_m(z)\Big)\Big], \end{aligned} \tag{3.8}$$

since $W^q = 1$, $W_{p_0}^{p_0} = 1$. The product of the two sum in (3.8) will result in a sum of products, in which each product component is

$$H_l(zW^{kp_0})F_m(z)z^{\frac{q(l-m)}{p_0}}\sum_{n=0}^{p_0-1}W_{p_0}^{nq(l-m)}, \tag{3.9}$$

for $l, m = 0, \dots p_0 - 1$. Note that when $l \neq m$, the sum $\sum_{n=0}^{p_0-1} W_{p_0}^{nq(l-m)}$ equals to 0. Hence, $S_k(z)$ is simplified to

$$S_k(z) = X(zW^{kp_0}) \sum_{n=0}^{p_0-1} H_n(zW^{kp_0}) F_n(z).$$

Thus $Y_0(z)$ can re-written as

$$Y_0(z) = \frac{1}{qp_0}\Big[X(z) \sum_{n=0}^{p_0-1} \Big(H_n(z)F_n(z)\Big) + X(zW^{p_0}) \sum_{n=0}^{p_0-1} \Big(H_n(zW^{p_0})F_n(z)\Big) + \dots$$
$$+ X(zW^{(q-1)p_0}) \sum_{n=0}^{p_0-1} \Big(H_n(zW^{(q-1)p_0})F_n(z)\Big)\Big]. \tag{3.10}$$

Similarly, $Y_1(z)$ of the high-pass channel can be simplified to

$$Y_1(z) = \frac{1}{qp_1}\Big[X(z) \sum_{n=0}^{p_1-1} \Big(H_{n+p_0}(z)F_{n+p_0}(z)\Big) + X(zW^{p_1}) \sum_{n=1}^{p_1-1} \Big(H_{n+p_0}(zW^{p_1})F_{n+p_0}(z)\Big) + \dots$$
$$+ X(zW^{(q-1)p_1}) \sum_{n=0}^{p_1-1} \Big(H_{n+p_0}(zW^{(q-1)p_1})F_{n+p_0}(z)\Big)\Big]. \tag{3.11}$$

Combining (3.10) and (3.11) gives us $Y(z)$ as written in (3.3) □

As a result of lemma 3.2.1, and with $p_0 = 1, p_1 = q - 1$, the uniform q-channel and 2-channel rational FBs in Fig. 3.1 are equivalent if the following conditions are satisfied

$$H(z) = \sum_{n=0}^{q-2} z^{qn} H_n(z^{q-1}), \qquad F(z) = \sum_{n=0}^{q-2} z^{-qn} F_n(z^{q-1}) \tag{3.12}$$

3.2.1 Perfect reconstruction filter bank

The PR condition of the two channel RFB structure is constructed from the equivalent uniform q-channel FB. The uniform q-channel FB in Fig. 3.1 satisfies PR if the synthesis and analysis filters satisfy (Saghizadeh and Willson 1998):

$$F_m(z) = (-1)^m \det \mathbf{A}_{-(0,m)}, \tag{3.13}$$
$$R_m(z) = F_m(z)H_m(z), \tag{3.14}$$

such that $R_m(z)$ is a q^{th}-band filter[4] for some $m = 0, \cdots, q-1$; $\mathbf{A}(z)$ is the alias component (AC) matrix:

$$\mathbf{A}(z) = \begin{bmatrix} H_0(z) & H_1(z) & \cdots & H_{q-1}(z) \\ H_0(zW) & H_1(zW) & \cdots & H_{q-1}(zW) \\ \vdots & \vdots & \vdots & \vdots \\ H_0(zW^{q-1}) & H_1(zW^{q-1}) & \cdots & H_{q-1}(zW^{q-1}) \end{bmatrix}, \tag{3.15}$$

where $W = e^{j2\pi/q}$ and $\mathbf{A}_{-(0,m)}$ denotes matrix $\mathbf{A}$ with row 0 and column m deleted. Such choice of analysis/synthesis relationship (3.13) guarantees the FB structure is alias free and synthesis filters are real coefficient FIR if the analysis filters are real FIR filters. If $\mathbf{h}$ and $\mathbf{h}_{q-1}$ are the column vectors representing the impulse responses of the analysis low- and high-pass filters of the RFB structure in Fig. 3.1, respectively and r_m represents the impulse response of the filter $R_m(z)$ of equation (3.14), the PR condition can be formulated as

$$r_{m,k}(\mathbf{h}, \mathbf{h}_{q-1}) \equiv \begin{bmatrix} \mathbf{0}_{k_0-1}^t & \alpha & \mathbf{0}_{B-k_0}^t \end{bmatrix}^t, \tag{3.16}$$

where $r_{m,k}$ denotes the k-th q-polyphase component of the impulse response r_m of $R_m(z)$, $\mathbf{0}_l$ is a zero vector of length l; B and k_0 are positive integers. In other words, one of the q polyphase components of r_m is required to equal to a pure delay. Note that the condition in (3.16) is only required to satisfy one integer index value $m \in [0, q-1]$ as satisfying for one results in satisfying for all others due to the relationship in (3.13).

From (3.13), (3.14) we can write $R_m(z)$ as $(-1)^m \det \mathbf{A}_{-(0,m)} H_m(z)$, where $\mathbf{A}$ is a $q \times q$ matrix of $H_m(zW^k)$ entries ($k = 0, \ldots, q-1$). Hence, if we consider the impulse response of $H_m(z)$ as unknowns, the impulse response of $R_m(z)$ will be a function of $H_m(z)$'s for $m = 0, \ldots, q-1$ with the unknowns' highest order being q.

3.2.2 Vanishing moments and regularity orders

A rational wavelet transform is defined to have K vanishing moments if the corresponding RFB satisfies: 1) the analysis high-pass filter possesses a factor of $(1 - z^{-1})^K$, and 2) the analysis and synthesis low-pass filters are divisible by $(1 + z^{-1} + \cdots + z^{-(q-2)})^K$ and $(1 + z^{-1} + \cdots + z^{-(q-1)})^K$, respectively (Bayram and Selesnick 2009c). It is customary to normalise the analysis low-pass filter's response to be $\sqrt{q-1}$ at $\omega = 0$

[4] q^{th}-band filter is defined as filters with pass-band response in the region of $[\frac{k_0\pi}{q}, \frac{k_1\pi}{q}]$ for intergers $k_0, k_1; k_0 < k_1 \leq q$ and one of its q-polyphase is a pure delay

and analysis high-pass filter's response to be 1 at $\omega = \pi$, respectively. Expanding these requirements in terms of the filter impulse responses results in the *linear* constraints on the design (Blu 1998). The vector form for the vanishing moment conditions can be written as:

$$\mathbf{T}\begin{bmatrix}\mathbf{h}^t & \mathbf{h}_{q-1}^t\end{bmatrix}^t = \begin{bmatrix}\mathbf{0}^t & \sqrt{q-1} & 1\end{bmatrix}^t, \tag{3.17}$$

where $\mathbf{T}$ is a $((q-1)K+2) \times (N_0+N_1)$ matrix, and N_0, N_1 are the analysis low-pass and high-pass filters' lengths, respectively.

In orthogonal RFB designs (Blu 1998, Bayram and Selesnick 2009b), the analysis and synthesis low-pass filters are time-reversed versions of each other, and so share the same number of regularity factors. In the absence of this time-reversal relationship, it raised the possibility of needing to explicitly impose regularity factors on *both* the synthesis and analysis banks when performing a bi-orthogonal design. This would significantly raise the complexity of the design process. However, in the proposed bi-orthogonal structure, imposing the regularity factors on the analysis filters will result in the synthesis filters possessing regularity factors of the same order, courtesy of the following lemma.

Lemma 3.2.2. *If the analysis high-pass and low-pass filters of a RFB possess regularity factors as discussed above, i.e. they are divisible by* $(1-z^{-1})^K$ *and* $(1+z^{-1}+\cdots+z^{-(q-2)})^K$, *respectively, then the synthesis low-pass filter will also possess regularity factors or it is divisible* $(1+z^{-1}+\cdots+z^{-(q-1)})^K$, *provided that the analysis and synthesis filters satisfy the relationships in* (3.12) *and* (3.13).

Proof. From (3.12) and (3.13), the synthesis low-pass filter can be expressed in terms of the AC matrix as

$$\begin{aligned} F(z) = \det \mathbf{A}_{-(0,0)}(z^{q-1}) - z^{-q}\det \mathbf{A}_{-(0,1)}(z^{q-1}) + \cdots \\ + z^{-q(q-2)}(-1)^{q-2}\det \mathbf{A}_{-(0,q-2)}(z^{q-1}), \end{aligned} \tag{3.18}$$

where $\mathbf{A}$ is the AC matrix, defined as in (3.15). It can be shown that A.1 $F(z)$ can be expanded to

$$\begin{aligned} F(z) = \frac{q-1}{c}\big[&z^{-k_0}(-1)^{(q-2)}H_{q-1}(z^{q-1}W)\det \mathbf{C}_{-(0,0)} \\ &+ z^{-k_1}(-1)^{(1+q-2)}H_{q-1}(z^{q-1}W^2)\det \mathbf{C}_{-(1,0)} \\ &+ \cdots + z^{-k_{q-2}}(-1)^{(2q-4)}H_{q-1}(z^{q-1}W^{q-1})\det \mathbf{C}_{-(q-2,0)}\big], \end{aligned} \tag{3.19}$$

where

$$\mathbf{C} = \begin{bmatrix} H(zW^{q-1}) & H(zW^{q-1}W_p) & \cdots & H(zW^{q-1}W_p^{q-2}) \\ H(zW^{q-2}) & H(zW^{q-2}W_p^{q-2}) & \cdots & H(zW^{q-2}W_p) \\ \vdots & \vdots & \vdots & \vdots \\ H(zW) & H(zWW_p) & \cdots & H(zWW_p^{q-2}) \end{bmatrix} \tag{3.20}$$

and $W = e^{j2\pi/q}$, $W_p = e^{j2\pi/(q-1)}$, c is a constant, $k_0, \cdots, k_{q-2} \in \mathcal{Z}$. (3.19) can be verified by substituting a specific value of $q \geq 3$ and expanding the corresponding determinant of $\mathbf{C}$. For example, for $q = 3$, (3.19) holds for $k_0 = k_1 = 3, c = -2$. Since $H(z)$ is divisible by $(z^{q-2} + \cdots + z + 1)^K$ and $H_{q-1}(z)$ is divisible by $(z-1)^K$, there exists $T_0(z)$ and $T_1(z)$ such that

$$H(z) = [(z - W_p) \ldots (z - W_p^{(q-2)})]^K T_1(z), \tag{3.21}$$

$$H_{q-1}(z) = (z-1)^K T_0(z). \tag{3.22}$$

We need to show that if (3.19)–(3.22) are satisfied, then $F(z)$ will be divisible by $(1 + z + \cdots + z^{q-1})^K$. Consider the first term of the sum in (3.19), define

$$P_1(z) = H_{q-1}(z^{q-1}W) \det \mathbf{C}_{-(0,0)} = (z^{q-1}W - 1)^K T_0(z^{q-1}W) \det \mathbf{C}_{-(0,0)}. \tag{3.23}$$

Therefore, $P_1(z)$ will have K zeros at $z^{q-1} = W^{-1} = e^{-j2\pi/q}$ or equivalently, at frequencies $\omega_{n_0} = \frac{-2\pi}{q(q-1)} + \frac{2\pi n_0}{(q-1)}$ for $n_0 = 1, \cdots, q-1$. From (3.20):

$$\begin{aligned} \det \mathbf{C}_{-(0,0)} &= \det \begin{bmatrix} H(zW^{q-2}W_p) & \cdots & H(zW^{q-2}W_p^{q-2}) \\ \vdots & \vdots & \vdots \\ H(zWW_p) & \cdots & H(zWW_p^{q-2}) \end{bmatrix} \\ &= \sum_m (-1)^m \underbrace{\prod_{n_1,n_2=1}^{q-2} H(zW^{n_1}W_p^{n_2})}_{N_m}, \end{aligned} \tag{3.24}$$

where any N_m is a product term which contains terms of the form $H(zW^l W_p^{n_2})H(zW^{n_1}W_p^l)$ for arbitrary integers $1 \leq l, n_1, n_2 \leq q-2$. Substitute (3.21) into (3.24):

$$\begin{aligned} \det \mathbf{C}_{-(0,0)} &= \sum_m (-1)^m \prod_{n_1,n_2=1}^{q-2} \left[(zW^{n_1}W_p^{n_2} - W_p) \ldots (zW^{n_1}W_p^{n_2} - W_p^{(q-2)}) \right]^K T_1(zW^{n_1}W_p^{n_2}) \\ &= \sum_m (-1)^m \Big\{ \prod_{n_1,n_2,n_3=1}^{q-2} (zW^{n_1}W_p^{n_2} - W_p^{n_3})^K T_1(zW^{n_1}W_p^{n_2}) \Big\}. \end{aligned} \tag{3.25}$$

Therefore, each product term N_m of $\det \mathbf{C}_{-(0,0)}$ will have zeros at $\omega_{n_1n_2n_3} = \frac{2\pi n_3}{(q-1)} - \left[\frac{2\pi n_1}{q} + \frac{2\pi n_2}{(q-1)} \right]$; $n_1, n_2, n_3 = 1, \cdots, q-2$ and $p = q-1$. As a consequence, it is

always possible to find common zeros at frequencies $\omega_{n_1 n_2 n_3} = -\frac{2\pi n_1}{q}$ by choosing $n_1 \in [1, q-2]$ and $n_3 = n_2$. In other words, $\det \mathbf{C}_{-(0,0)}$ will have K-multiple zeros at $\omega = -\frac{2\pi}{q}, \cdots, -\frac{2(q-2)\pi}{q}$, or equivalently, at $\frac{l2\pi}{q}$, $2 \leq l \leq q-2$. Including the common zeros at $2\pi/q$ from high-pass filter $H_{q-1}(z^{q-1}W)$ discussed earlier, $P_1(z)$ will therefore have K-multiple zeros at frequencies $\frac{l2\pi}{q}$, $1 \leq l \leq q-2$. By similar arguments, it is straight forward to show that other product terms of $F(z)$ will have zeros at the above frequencies. It follows that the synthesis low-pass filter has K regularity factors. □

This result allows us to design a bi-orthogonal RFB by designing the analysis side with K regularity factors independently. The synthesis side is then fully determined from (3.12)–(3.13) and will automatically have K regularity factors as well. This forms the strategy underlying the design approach presented in this chapter.

3.2.3 Least square optimisation

The issue of shift-variance of rational DWTs has been discussed in literature (Blu 1993, Blu 1998, Bayram and Selesnick 2009c) and this is summarised in chapter 2. This property prevents the iterated RFB to behave like a rational DWT, as the iterated RFB will not converge to a unique wavelet function. An illustration of the shift-variance issue is shown in Fig. 2.7 of chapter 2.

To suppress this effect, it has been shown (Blu 1993, Blu 1998, Bayram and Selesnick 2009c) that good frequency selectivity in the RFB filters reduces the shift error, defined as the maximum of absolute error between the $(q-1)^i$ discrete time sequences being shifted on the same interval (Blu 1993). Our proposed design approach therefore seeks to achieve good frequency selectivity by using least squares optimisation, with the objective function being defined as:

$$f = \alpha_0 \int_{\omega_{sLP}}^{\pi} |H(\omega)|^2 \, \mathrm{d}\omega + \alpha_1 \int_{0}^{\omega_{sHP}} |H_{q-1}(\omega)|^2 \, \mathrm{d}\omega, \tag{3.26}$$

where $\omega_{sLP} = \frac{\pi}{q} + \Delta\omega_{LP}$, $\omega_{sHP} = \frac{(q-1)\pi}{q} - \Delta\omega_{HP}$ are the stop-band edge frequencies of the analysis low-pass and high-pass filters, respectively, and α_0, $\alpha_1 \geq 0$ are adjustable weights. In vector form, the objective function can be written as:

$$f(\mathbf{h}, \mathbf{h}_{q-1}) = \alpha_0 \mathbf{h}^t \mathbf{M_{LP}} \mathbf{h} + \alpha_1 \mathbf{h}_{q-1}^t \mathbf{M_{HP}} \mathbf{h}_{q-1}, \tag{3.27}$$

where $\mathbf{M_{LP}}$ and $\mathbf{M_{HP}}$ are positive semi-definite matrices whose entries depend solely on design parameters ω_{sLP} and ω_{sHP}, respectively. The matrices are defined as

$$\left[\mathbf{M_{LP}}\right]_{i,j} = \begin{cases} -\frac{2\sin((i-j)\omega_{sLP})}{\pi(i-j)} & i \neq j \\ 2\left(1 - \frac{\omega_{sLP}}{\pi}\right) & i = j \end{cases}, \tag{3.28}$$

$$\left[\mathbf{M_{HP}}\right]_{i,j} = \begin{cases} \frac{2\sin((i-j)\omega_{sHP})}{\pi(i-j)} & i \neq j \\ \frac{2\omega_{sHP}}{\pi} & i = j \end{cases}. \tag{3.29}$$

The RFB design problem, which we label as **(P)**, can be formulated as an optimisation problem that minimises $f(\mathbf{h}, \mathbf{h}_{q-1})$ in (3.27), subject to the conditions in (3.16)–(3.17).

3.3 Solving the design problem

The optimisation problem **(P)** is non-convex since the PR constraints (3.16) have highest order $q \geq 3$ and hence are non-convex. Nonlinear optimisation is the term used to describe problems whose objective or constraint functions are nonlinear where the convexity is not guaranteed. For such problems, effective methods to find the global solution are also not guaranteed.

In this chapter, we propose two approaches to solve problem **(P)**: **local optimisation** and **linearisation**. The first approach, local optimisation approach abandons finding the global solution of the problem in favor of finding 'good enough' local solution based on an appropriate initialisation to the problem. In the latter, a compromise is made by fixing some variables of the multivariate problem to reduce the order of the non-linear constraints to one, thus leading to a two stage method of solution.

3.3.1 Local optimisation of the non-linear problem

The local optimisation approach proceeds in two stages. An approximate optimum is first found by solving a simplified sub-problem, which is then used to initialise a line-search algorithm to find a solution to the original problem [5]. This proposed approach aims to improve the robustness against initialisation of the optimisation problem $(\mathbf{P})$ by first solving a convex sub-problem $(\mathbf{P}_0)$, this sub-problem is obtained by removing

[5] fmincon and the active-set (line search) sub-algorithm of Matlab is used as the optimisation algorithm

the PR constraint (3.16) from (**P**). Instead, convex constraints (3.30) are introduced to ensure the global solution found by $(\mathbf{P}_0)$ satisfy the PR condition approximately.

The proposed RFB satisfies PR if $R_m(z)$ described in (3.14) is a q^{th}-band filter, or equivalently, one of its q-polyphase components is a pure delay (see (3.16)). Therefore, if we choose $m = q-1$, $R_{q-1}(z)$ is required to be approximately q^{th}-band as a result of $(\mathbf{P}_0)$ with pass-band response in the region of $[\frac{q-1}{q}\pi, \pi]$. This can be achieved by individually requiring the respective q-polyphase components of $\mathbf{h}$ and $\mathbf{h}_{q-1}$ to approximate pure delays, within some set tolerance bounds in the coefficient values. Such bounding constraints are convex:

$$|\mathbf{h}(m_0)| \leq \epsilon_{LP}, \quad \left|\mathbf{h}_{q-1}(m_1)\right| \leq \epsilon_{HP}, \tag{3.30}$$

Hence, $(\mathbf{P}_0)$ can be formulated as

Problem $(\mathbf{P}_0)$

$$\min_{\mathbf{h},\mathbf{h_{q-1}}} f(\mathbf{h}, \mathbf{h_{q-1}}) \text{ as defined in (3.27), subject to (3.17), and}$$

$$|\mathbf{h}(m_0)| \leq \epsilon_{LP}, \quad \left|\mathbf{h_{q-1}}(m_1)\right| \leq \epsilon_{HP}$$

for

$$\begin{cases} m_0 = L_0 \pm kq, & 0 \leq m_0 \leq N_0, L_0 = \lfloor N_0/2 \rfloor \pm c_0 \\ m_1 = L_1 \pm kq, & 0 \leq m_1 \leq N_1, L_1 = \lfloor N_1/2 \rfloor \pm c_1 \end{cases},$$

where L_0, L_1 are non-zero integers and ϵ_{LP}, ϵ_{HP} are small positive real valued parameters; N_0, N_1 denotes the low-pass $\mathbf{h}$ and high-pass $\mathbf{h_{q-1}}$ filters' lengths, respectively; $k, c_0, c_1 \in \mathbb{N}, k \neq 0$. Optimising $f(\mathbf{h}, \mathbf{h}_{q-1})$ in (3.27) subject to such polyphase bound constraints lead to global solutions of $(\mathbf{P}_0)$ such that $H(z)$, $H_{q-1}(z)$ have nearly flat pass-bands in $[0, \frac{\pi}{q}]$, $[\frac{(q-1)\pi}{q}, \pi]$, respectively. The relationship between polyphase component flatness and filters' pass-band flatness is discussed in appendix A.2.

Claim 3.3.1. *Consider $H(z)$ to be a low-pass filter of the FB structure in Fig. 3.1 having flat pass-bands in $[0, \frac{\pi}{q}]$, if the resulting synthesis filter $F_{q-1}(z)$ filter is defined by (3.13) as $F_{q-1}(z) = (-1)^{q-1} \det \mathbf{A}_{-(0,q-1)}(z)$, then $F_{q-1}(z)$ is a high-pass filter with flat pass-band response in $[\frac{(q-1)\pi}{q}, \pi]$.*

Proof. The low-pass filter $H(z)$ having flat pass-band in $[0, \frac{\pi}{q}]$ results in its $q-1$ polyphase components $H_0, \cdots, H_{q-2}$ having flat pass-band in $[0, \frac{(q-1)\pi}{q}]$; $F_{q-1}(z) = (-1)^m \times \det \mathbf{A}_{-(0,q-1)}(z)$ where $\mathbf{A}(z)$ is defined in (3.15) suggests that $F_{q-1}(z)$ is dependent on the modulated polyphases $H_0(zW^{n_0}), \cdots, H_{q-2}(zW^{n_{q-2}})$, $n_0, \cdots, n_{q-2} = 1, \cdots, q-1$. If we apply Laplace expansion on $\det \mathbf{A}_{-(0,q-1)}(z)$, we attain a sum of $(q-1)!$ product components, each of which can be defined as:

$$p_k(z) = \left[H_0(zW^{n_0}) \times \ldots \times H_{q-2}(zW^{n_{q-2}})\right] \tag{3.31}$$

for any index $k = 1, \cdots, (q-1)!$ corresponding to a choice of the combination of $n_0, \cdots, n_{q-2} = 1, \ldots, q-1$ such that $n_0 \neq n_1 \neq \cdots \neq n_{q-2}$. In the following we show that each of the product term in (3.31) has its magnitude $|p_k(\omega)|$ being flat in its pass-band response in $[\frac{(q-1)\pi}{q}, \pi]$ as a result of the assumption that $H_0, \ldots, H_{q-2}$ all have flat pass-band response in $[0, \frac{(q-1)\pi}{q}]$. Let $|H_i(z)|, i = 0, \cdots, q-2$ and $|H_i(zW)|$ have frequency response as shown in Fig. 3.3. By induction, we can verify that for any $|H_i(zW^n)|, n = 1, \cdots, q-1$, the corresponding stop-band region varies across all frequencies except for $\omega \in [\frac{q-1}{q}\pi, \frac{q+1}{q}\pi]$. Hence the product filter $|p_k(\omega)|$ is a high-pass filter with flat pass-band response in the frequency region of $\omega \in [\frac{q-1}{q}\pi, \frac{q+1}{q}\pi]$.

The phase response in the pass-band region of the product term $p_k(\omega)$ is the sum of all the phases of $H_0, \ldots, H_{q-2}$ in their pass-band regions. Thus the filter's phase is approximately constant as k varies. This results in $F_{q-1}(z)$ having flat pass-band response in $[\frac{q-1}{q}\pi, \frac{q+1}{q}\pi]$ or $\pm[\frac{q-1}{q}\pi, \pi]$ as $F_{q-1}(z)$ is a real coefficient FIR filter. □

As a result, the synthesis high-pass response is greatly dependent on the analysis low-pass response. Even though the proof is shown for ideal brick wall filter, its use is only to illustrate the approach and the property also applies for non-ideal filters. Thus, if the analysis low-pass filter $H(z)$ is a real non-ideal filter with good stop band, transition band and nearly flat pass-band responses, then similar property can be attained for the resultant synthesis high-pass filter $F_{q-1}(z)$. Hence, the global solution of problem $(\mathbf{P}_0)$ results in the high-pass filters $H_{q-1}(z)$, $F_{q-1}(z)$ with good flatness in their pass-band. Also, since two of their q-polyphase components are approximate delays as a result of (3.30), the product filter $R_{q-1}(z) = H_{q-1}(z)F_{q-1}(z)$ has a good flatness in its pass-band region, that is, approximates a q^{th}-band filter with pass-band response in $[\frac{(q-1)\pi}{q}, \pi]$.

The design of q^{th}-band filters based on least square criterion and subject to linear constraints has been studied in (Wisutmethangoon and Nguyen 1999). The filters obtained

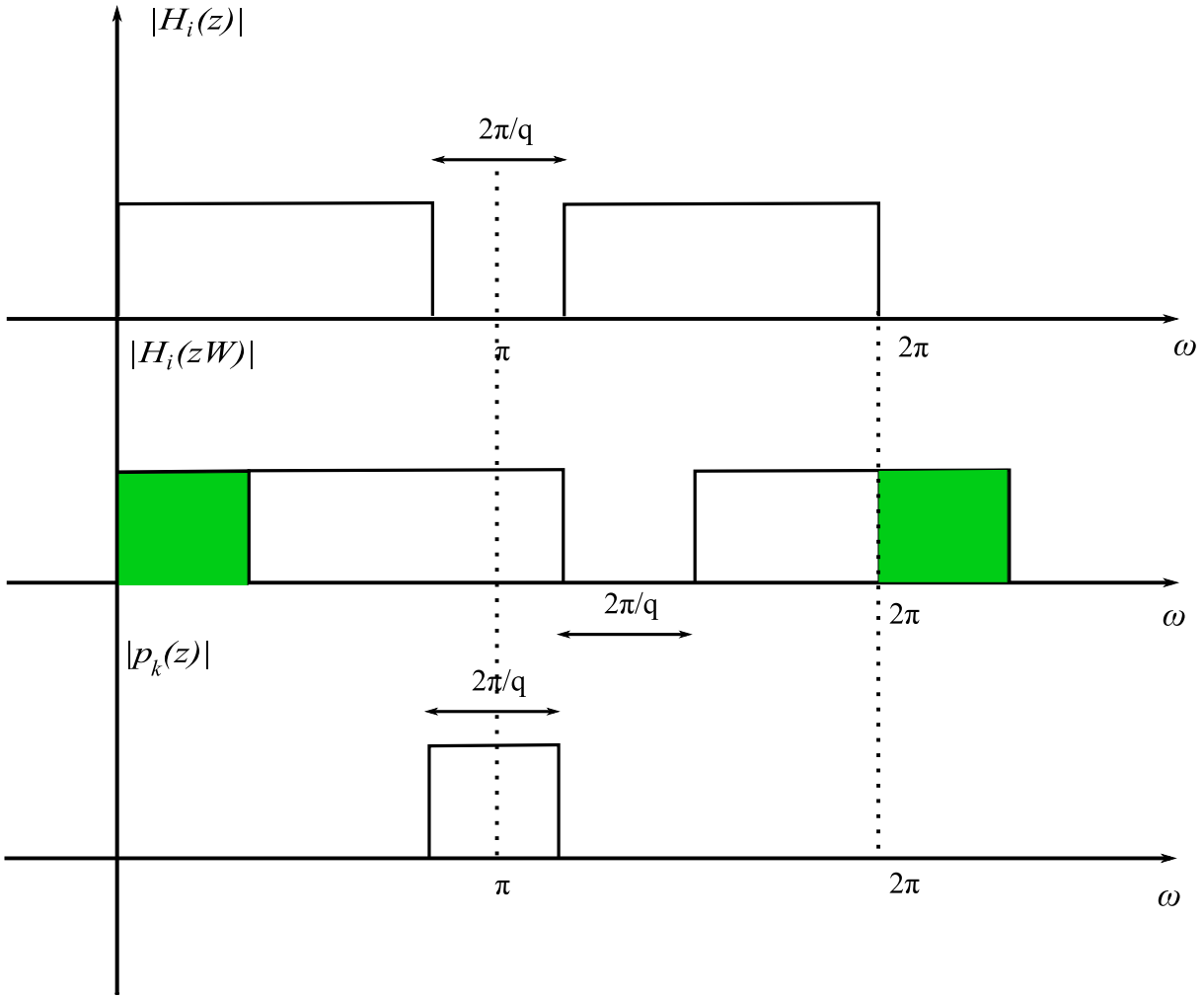

Figure 3.3. Top: Frequency response of the polyphase components of $H(z)$ assuming that they approximate brick-wall response. Middle: Frequency response of $|H_i(zW)|, i = 0, \cdots, q-2$, $W = e^{-2\pi/q}$. Bottom: Frequency response of $|p_k(\omega)|$.

in that study have good least square error as the symmetry index[6] is close to the centre tap of the filter impulse response. In our design, this result means that we should choose the parameters L_0, L_1 to be near the centre taps of $\mathbf{h}$ and $\mathbf{h}_{q-1}$, respectively to obtain filters with good frequency responses. Fig. 3.4 demonstrates the approximate delay polyphase component and the frequency response of $R_{q-1}(z)$ as a result of $(\mathbf{P}_0)$ corresponding to the design example 2a in the next section (i.e. RFB of $(\frac{4}{5}, \frac{1}{5})$) re-sampling ratio.

[6] symmetry index of an q^{th}-band filter denotes the filter's impulse response's index in which the corresponding q-polyphase component is pure delay and the coefficient at such index is non-zero

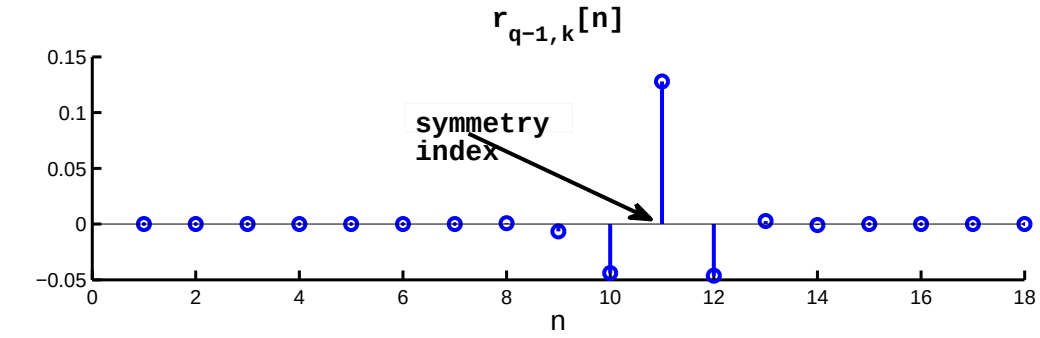

(a) approximate pure delay of the $r_{q-1,k}$ polyphase component

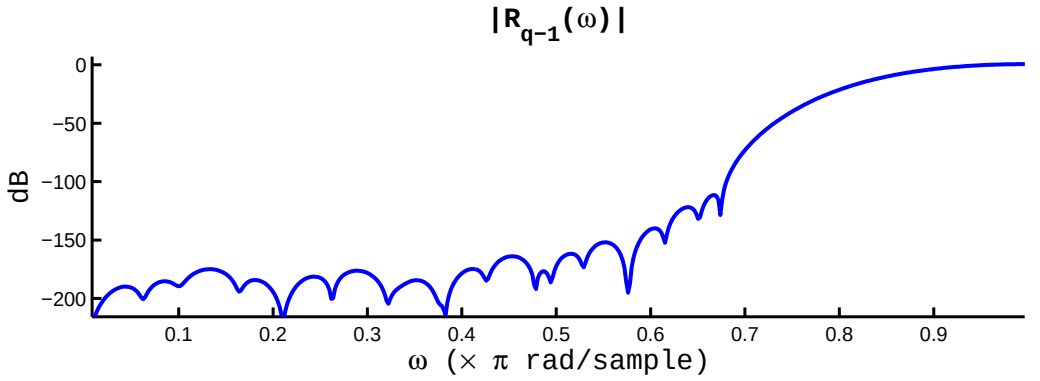

(b) $|R_{q-1}(\omega)|$

Figure 3.4. A $(4/5, 1/5)$ RFB design from the nonlinear optimisation approach. (a) the k^{th} $5-$poylyphase component of $R_4(z)$ filter and (b) the approximate 5^{th}-band response of $R_4(\omega)$.

3.3.2 Linearisation of the non-linear constraints

In this approach, the q order nonlinear PR conditions (3.16) are linearised by pre-designing the analysis low-pass filter. The filter bank design problem is separated into two halves. We first design the low-pass analysis filter subject to only linear constraints arising from the regularity conditions. The filter is required to exhibit good frequency selectivity in addition to having vanishing moments, and we label this sub-problem $(\mathbf{P}_{LP})$. In the next step, the high-pass analysis filter is designed such that the overall RFB satisfies perfect reconstruction; we label this sub-problem $(\mathbf{P}_{HP})$. In this latter sub-problem, the PR condition is *linear* since the analysis low-pass filter is known, and so $(\mathbf{P}_{HP})$ becomes a convex sub-problem. The design challenge becomes a question of

how to design $H(z)$ such that $H_{q-1}(z)$ has the shortest possible length while satisfying all desired properties.

The design problem is decomposed into two sub-problems as follows:

Problem $(\mathbf{P}_{LP})$: Designing low-pass filter by minimisation

$$\begin{aligned} \min_{\mathbf{h}} \quad & f(\mathbf{h}) = \mathbf{h}^t \mathbf{M_{LP}} \mathbf{h}, \qquad \text{subject to} \\ & \mathbf{T_{LP}} \mathbf{h} = \begin{bmatrix} \mathbf{0}^t & \sqrt{q-1} \end{bmatrix}^t, \qquad (3.32) \\ & |\mathbf{h}(m_0)| \leq \epsilon_{LP}, \qquad (3.33) \end{aligned}$$

where $\mathbf{M_{LP}}$ is the positive semi-definite matrix described in Section 3.2.3, $\mathbf{T_{LP}}$ is constructed based on regularity conditions imposed on the analysis low-pass filter as in (3.17). When $H(z)$ is known, then so is $F_{q-1}(z)$. The product $R_{q-1}(z) = F_{q-1}(z)H_{q-1}(z)$ can be written in matrix form as $\mathbf{r}_{q-1} = \mathbf{F}\mathbf{h}$; where $\mathbf{r}_{q-1}$ is a column vector representing the impulse response of the filter $R_{q-1}(z)$, $\mathbf{F}$ is a $N_f \times N_1$ Toeplitz matrix containing the coefficients of the filter F_{q-1} and N_f is the filter's length.

Problem $(\mathbf{P}_{HP})$: Designing a matching PR high pass filter by minimisation

$$\begin{aligned} \min_{\mathbf{h}_{q-1}} \quad & f(\mathbf{h}_{q-1}) = \mathbf{h}_{q-1}^t \mathbf{M_{HP}} \mathbf{h}_{q-1}, \quad \text{subject to} \\ & \mathbf{T_{HP}} \mathbf{h}_{q-1} = \begin{bmatrix} \mathbf{0}^t & 1 \end{bmatrix}^t, \\ & r_{q-1}(\mathbf{h}_{q-1}) = \mathbf{F_{q-1}} \mathbf{h}_{q-1} \equiv \begin{bmatrix} \mathbf{0}^t & \alpha & \mathbf{0}^t \end{bmatrix}^t, \qquad (3.34) \end{aligned}$$

where $\mathbf{F_{q-1}}$ is a $\frac{N_f}{q} \times N_1$ matrix obtained by choosing rows corresponding to zero coefficient index from matrix $\mathbf{F}$, N_1 is the length of the vector $\mathbf{h}_{q-1}$; $\mathbf{T_{HP}}$ is the regularity matrix derived from (3.17). We choose $m_0 = L_0 \pm kq$ of subproblem $(\mathbf{P}_{LP})$ such that L_0 approximates $N_0/2$ since it is desirable for the overall system delay n_0 to be close to the mid-point index of $\mathbf{r}_{q-1}$.

Fixing the analysis low-pass filter simplifies the PR constraints order to one and at the same time significantly reduces the variables of the optimisation. The advantage of this method is that our PR conditions are always kept linear regardless of the rate changing parameter q, which is most useful for large q.

Table 3.1. The filter design parameters

(a) Local optimisation parameters

Local optimisation method				
	Example 1a: $(2/3, 1/3)$, $K = 1$	Example 1b: $(2/3, 1/3)$, $K = 3$	Example 2a: $(4/5, 1/5)$, $K = 1$	Example 2b: $(4/5, 1/5)$, $K = 3$
n_0, L_0, N_0	$31, 18, 35$	$31, 20, 38$	$46, 26, 50$	$51, 28, 50$
L_1, N_1	$10, 20$	$10, 20$	$14, 28$	$18, 35$
ω_{sLP}	$\frac{\pi}{3} + 0.07\pi$	$\frac{\pi}{3} + 0.07\pi$	$\frac{\pi}{5} + 0.07\pi$	$\frac{\pi}{5} + 0.07\pi$
ω_{sHP}	$\frac{2\pi}{3} - 0.1\pi$	$\frac{2\pi}{3} - 0.1\pi$	$\frac{4\pi}{5} - 0.1\pi$	$\frac{4\pi}{5} - 0.1\pi$

(b) Linearised parameters

Linearised method					
	Example 3a: $(2/3, 1/3)$, $K = 1$	Example 3b: $(2/3, 1/3)$, $K = 3$	Example 4a: $(4/5, 1/5)$, $K = 1$	Example 4b: $(4/5, 1/5)$, $K = 3$	Example 5: $(5/6, 1/6)$, $K = 3$
n_0, L_0, N_0	$31, 16, 30$	$31, 16, 30$	$46, 20, 38$	$51, 22, 42$	$64, 33, 65$
N_1	28	28	40	43	35
ω_{sLP}	$\frac{\pi}{3} + 0.07\pi$	$\frac{\pi}{3} + 0.07\pi$	$\frac{\pi}{5} + 0.06\pi$	$\frac{\pi}{5} + 0.06\pi$	$\frac{\pi}{6} + 0.032\pi$
ω_{sHP}	$\frac{2\pi}{3} - 0.11\pi$	$\frac{2\pi}{3} - 0.11\pi$	$\frac{4\pi}{5} - 0.11\pi$	$\frac{4\pi}{5} - 0.1\pi$	$\frac{5\pi}{6} - 0.08\pi$

3.4 Filter design results

In this section, four design examples based on local optimisation and five examples based on the linearised approach are presented. The designs' parameters are summarised in Table 3.1 (a), (b). The obtained RFB all satisfy PR with reconstruction error in the order of 10^{-10}. Most of the frequency response comparisons are made with respect to the designs described in (Blu 1998) since that is the only reported FIR critically sampled structure which satisfies PR condition and possesses one regularity order. Note that for Blu's approach, higher regularity orders cannot be attained. In (Bayram and Selesnick 2009b)'s approach, it is capable of producing arbitrary number of regularity orders, but the RFB design does not satisfy PR condition. Instead only near PR is obtained in such design. To complete the comparison, we also compare against Bayram and Selesnick's design in one example. The filters' lengths are shown in table 3.2.

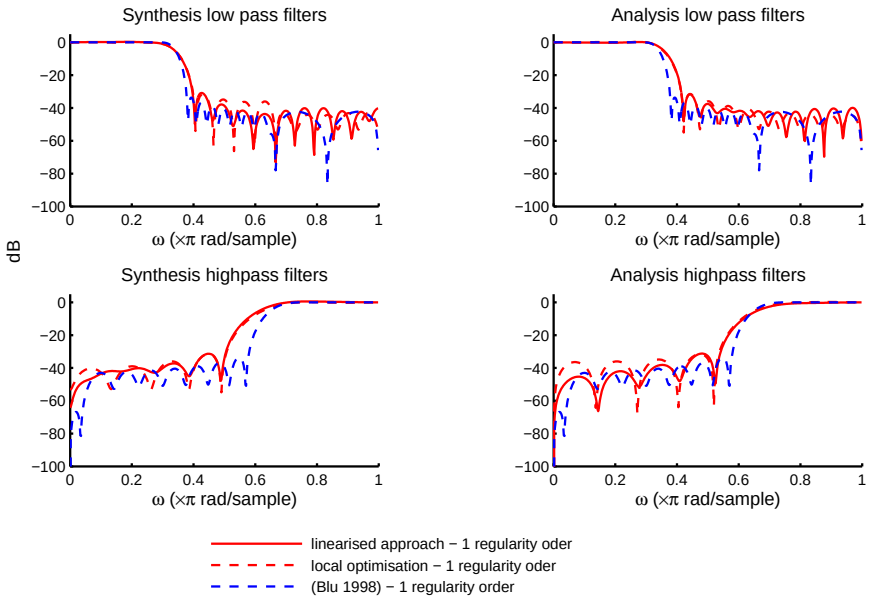

(a) $(2/3, 1/3)$ RFB filters' responses - one regularity order

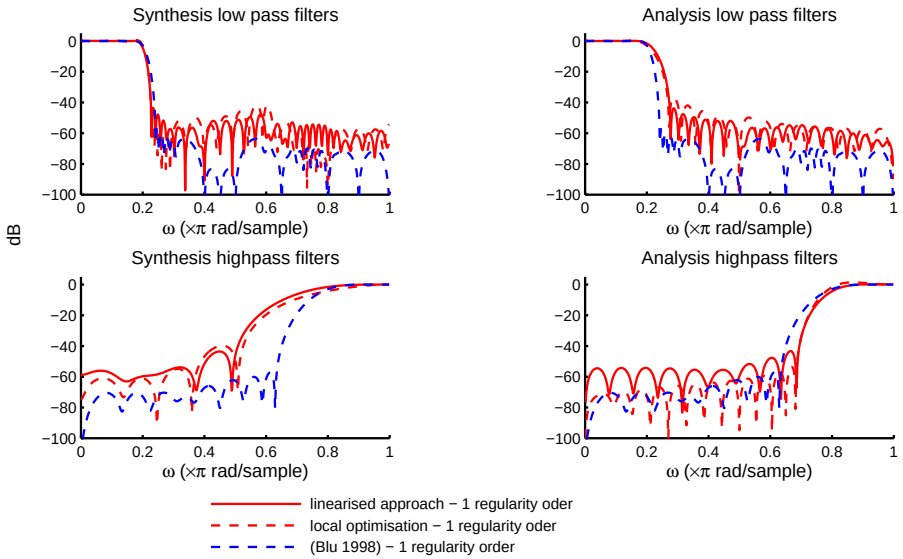

(b) $(4/5, 1/5)$ RFB filters' responses - one regularity order

Figure 3.5. Comparisons between the proposed approaches of RFBs $(2/3, 1/3)$ (a), $(4/5, 1/5)$ (b) with one regularity order versus literature (Blu 1998) of the same re-sampling rates and regularity order. From left to right: Top panels show the low-pass synthesis and analysis filters' frequency responses, respectively; bottom panels show the high-pass synthesis and analysis filters' frequency responses, respectively. Red solid and dashed traces represent linearised and local optimisation designs, respectively while blue dash illustrates literature (Blu 1998) design.

Fig. 3.5 illustrates the filters' frequency responses of *example 1a, 3a* (a) and *example 2a, 4a* (b) comparing to (Blu 1998) of the same re-sampling rates and regularity order, respectively. The filters' lengths are selected such that for each design, the total number of taps are approximately equal between the design methods. It can be seen that for one regularity order, both proposed methods result in wider transition band width as compared to the literature (Blu 1998). However, it should be noted that (Blu 1998) does not lead to RFB with high regularity while the proposed bi-orthogonal structure does. With the orthogonality property relaxed for our designs, we are free to impose higher regularity order than the design in (Blu 1998), which has the effect of increasing the smoothness of the scaling functions (Bayram and Selesnick 2007). This underlines the greatest improvement as compared to the existing literature (Blu 1998). In Fig. 3.6 frequency responses of RFB with three regularity orders designed based on the two proposed methods are plotted against each other. In Fig. 3.6 (a), both the proposed methods illustrate similar filters' frequency responses for re-sampling rates $(2/3, 1/3)$ design. In Fig. 3.6 (b), the local optimisation method results in better frequency responses in analysis low-pass and synthesis high-pass filters while it is inferior in the analysis high-pass response. It should be noted that linearised method is better used in cases of high value parameter q since such parameter corresponds to the highest order of the non-linear constraints in the local optimisation method, which significantly increase the design complexity. For example the $(5/6, 1/6)$ RFB with three regularity orders in example 5, is designed using the linearised approach. The designed filters are plotted against (Blu 1998) in Fig. 3.7 (a), (b). In Fig. 3.8 the father wavelet functions are illustrated. In appendix B.1.3, B.1.4, filter designs based on linearised method of higher q parameters are shown (for $q = 7, 10$). Note that only linearised method should be used for such high values of q since the complexity of solving high order nonlinear constraints of the local optimisation method increases significantly in those cases, which can lead to impractically long running time. To complete the comparison, filters' frequency responses of the RFB $(4/5, 1/5)$ structure with three regularity orders are plotted against the literature (Bayram and Selesnick 2009b) of the same regularity orders and shown in Fig. 3.7 (c), (d). In the comparison with Bayram's design (Bayram and Selesnick 2009b), the transition band and stop band performance have improved with the same number of regularity orders imposed. This is illustrated in Fig. 3.7 (c), (d). Most importantly, our proposed design results in PR FBs, where reconstruction error is in the order of 10^{-10}, with arbitrary K orders of regularity while the literature

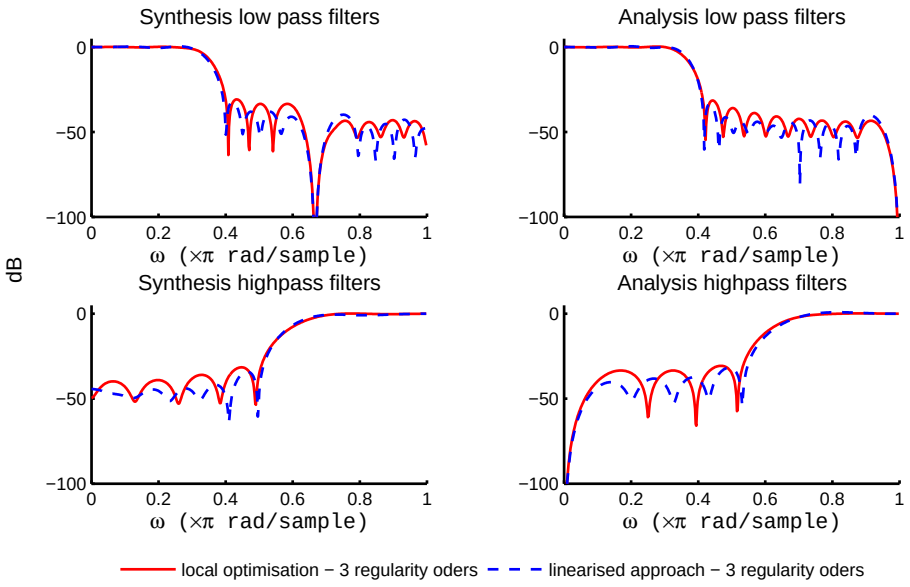

(a) $(2/3, 1/3)$ RFB filters' responses - three regularity orders

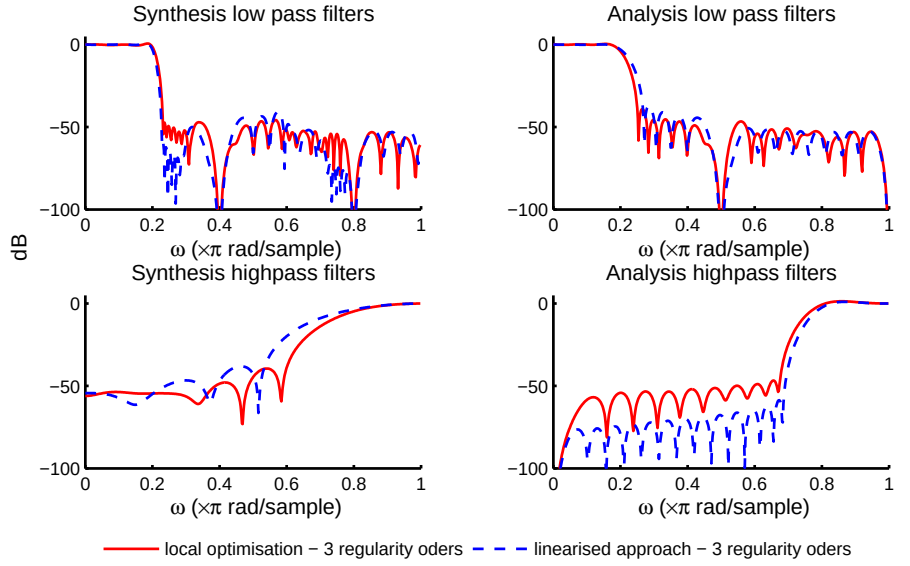

(b) $(4/5, 1/5)$ RFB filters' responses - three regularity orders

Figure 3.6. Comparison between proposed methods for $(2/3, 1/3)$ (a) and $(4/5, 1/5)$ (b) RFBs with three regularity orders. From left to right: Top panels show the low-pass synthesis and analysis filters' frequency responses, respectively; bottom panels show the high-pass synthesis and analysis filters' frequency responses, respectively. Red solid traces represents local optimisation filters while dashed blue represents linearised filters.

counterpart (Bayram and Selesnick 2009b) only attains near PR FBs (reconstruction error is approximately 10^{-4}).

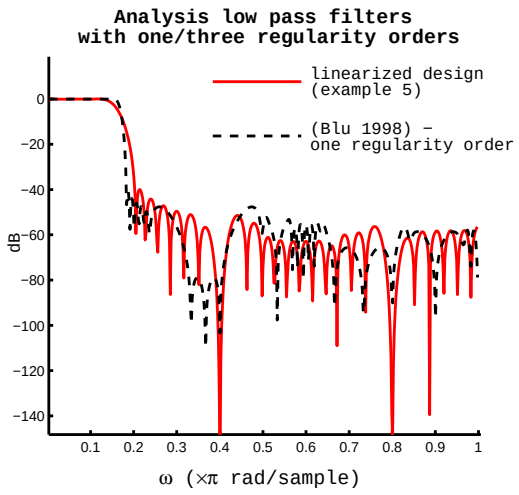

(a) $(5/6, 1/6)$ RFB analysis filters

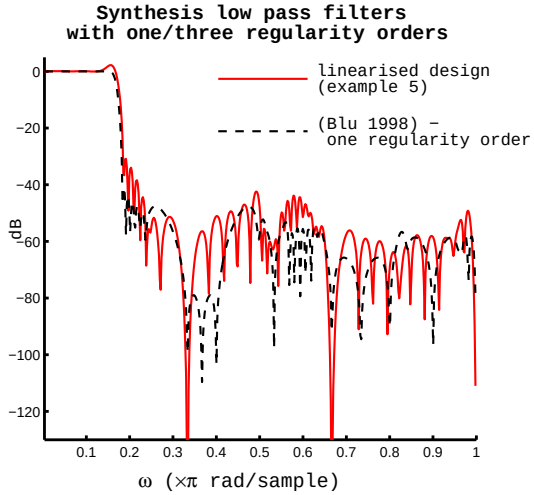

(b) $(5/6, 1/6)$ RFB synthesis filters

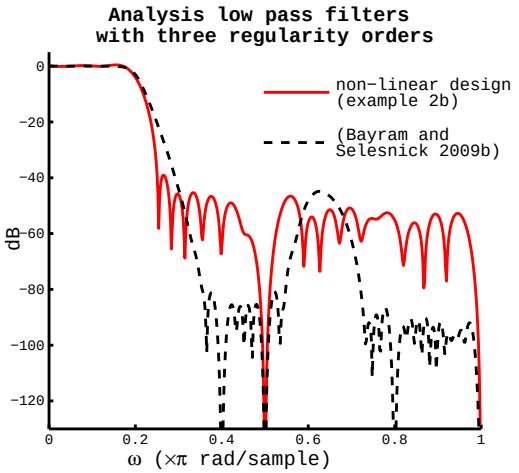

(c) $(4/5, 1/5)$ RFB analysis filters

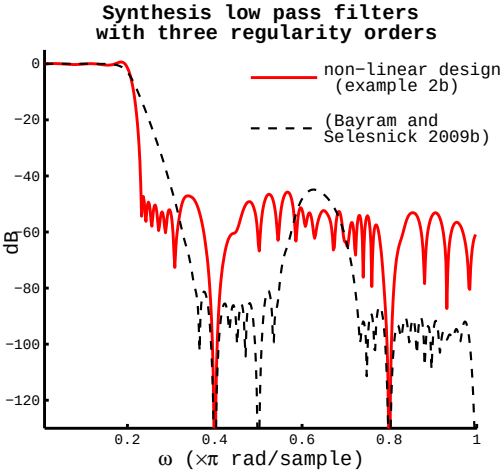

(d) $(4/5, 1/5)$ RFB synthesis filters

Figure 3.7. (a), (b) are the analysis and synthesis low-pass filters' responses, respectively. Solid traces are the responses of $(5/6, 1/6)$ RFB (example 5) while dashed traces show the frequency response of (Blu 1998) with three and one regularity orders, respectively. Solid traces of (c), (d) represent low-pass filters of $(4/5, 1/5)$ RFB (example 2b) while dashed traces show the frequency response of (Bayram and Selesnick 2009b), both with three regularity orders.

3.5 Shift error and computational complexity

Fig. 3.8 illustrate the father wavelet functions and their shifted version overlaying in the same interval. The functions are obtained by iterating the low-pass filters from example 5 (3.8 (a), (b)) and example 2b (3.8 (c), (d)) with three regularity orders. The

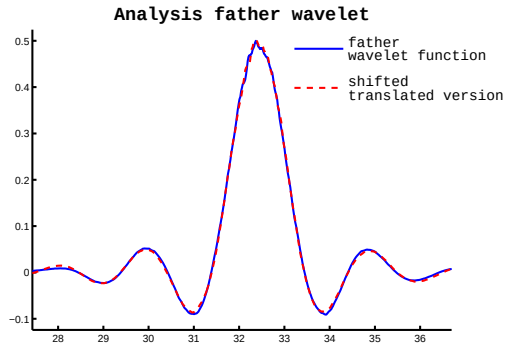

(a) Linearised design $(5/6, 1/6)$ RFB analysis father wavelet

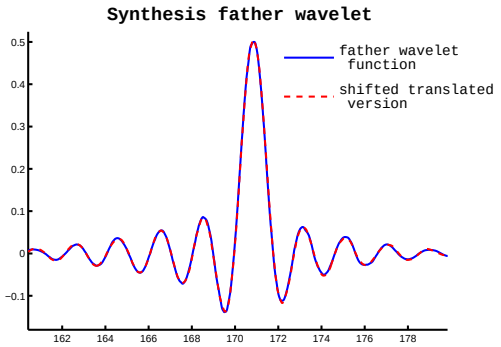

(b) Linearised design $(5/6, 1/6)$ RFB synthesis father wavelet

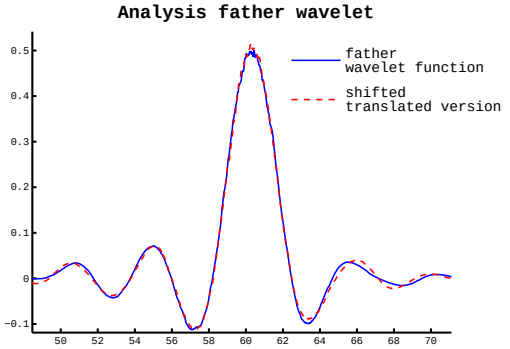

(c) Local optimisation design $(4/5, 1/5)$ RFB analysis father wavelet

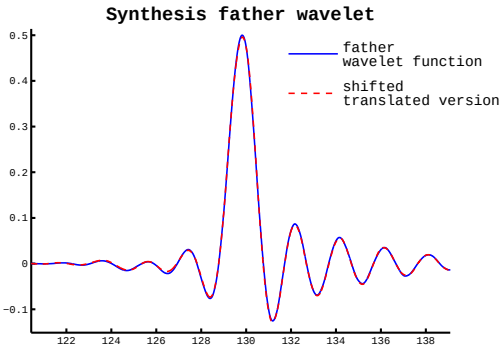

(d) Local optimisation design $(4/5, 1/5)$ RFB synthesis father wavelet

Figure 3.8. Father wavelet functions of example 5 (a), (b) and example 2b (c), (d). Red traces of (a), (b) are the analysis/synthesis father wavelet functions obtained from iterating the low-pass filters of example 5 ($(5/6, 1/6)$ RFB) and (c), (d) are the functions of example 2b ($(4/5, 1/5)$ RFB), both with three regularity orders. The blue traces in all plots represent the translated version of he functions being shifted to the same interval.

maximum shift error, defined as maximum error between any two limit functions being shifted on the same interval (Blu 1993), is used to measure the shift variance of our designs. With scaling functions obtained from iterating the synthesis and analysis scaling filters 25 times, the maximum shift errors are measured to be approximately 0.02 and 0.008 for example 2b and 5, respectively.

To demonstrate the difference of computations between the cases of $(5/6, 1/6)$, if we consider the multiply-add operation as a measure for computation, for the filters' length as illustrated in Table 3.1(b) the total number of multiply-add operations in our

design is approximately $75L_x$, compared to Blu's design of $78L_x$, where L_x is the input signal's length. It should be noted that as different to orthogonal method in (Blu 1998), in which the analysis filters have the same lengths as the synthesis filters, the proposed methods are bi-orthogonal and the synthesis low-pass filters are determined by $(q-2)N_0 + (q-1)N_1 - A$. The parameters N_0, N_1 represent the analysis low-pass and high-pass filters' lengths, respectively; q determines the re-sampling ratio of the RFB structure and A is a constant which varies with re-sampling ratio parameter q. This results in lengthy synthesis low-pass filter compared with the analysis filters. In the proposed RFB design, PR conditions are imposed by forcing $R_{q-1}(z)$ filter to be a q^{th}-band filter. The number of PR conditions will always be approximately $\frac{N_0+N_1}{q}$, where $N_0 + N_1$ represents the total number of variables of the optimisation. It differs from the orthogonal case in which the number of orthogonal conditions is in the order of $N/2 + C$, where C is some constant depending on rate changing parameters p, q and N is a total number of variables. For example, in Blu's $(5/6, 1/6)$ design (Blu 1998), there are 168 conditions for 199 unknowns, while in our example 5, $N_0 = 65, N_1 = 35$ leads to 15 PR conditions for 100 unknowns. The proposed design approach in this thesis thus provides greater degrees of freedom (fewer constraints) in filter design despite having to deal with high order (q) polynomials as PR conditions. In orthogonal FBs, the orthogonal conditions are always quadratic regardless of the values of p and q.

3.6 Chapter summary

In this chapter, we have presented a method of designing a $(q-1/q, 1/q)$ rational filter bank with general K regularity orders together with two approaches to solve the nonlinear optimisation problem which improves the robustness against initialisations. The filters' frequency selectivity are optimised to enable the designs to approximate rational DWTs. The design method is potentially useful for filter bank designs with more general $(p/q, (q-p)/q)$ since the relationship between the regularity factors of analysis and synthesis filters is valid for more general cases of $q - p > 1$. However, for such regimes, the linearized method described here cannot be used. In the next chapter, we address the design of more general p, q pairs, which lead to more flexible Q factor rational DWTs.

Table 3.2. Filters' lengths comparison

	Analysis low-pass	Synthesis low-pass	Analysis high-pass	Synthesis high-pass	Regularity K
Local optimisation approach					
Example 1a $(\frac{2}{3}, \frac{1}{3})$	35	76	20	34	$K = 1$
Example 1b $(\frac{2}{3}, \frac{1}{3})$	38	75	280	37	$K = 3$
Example 2a $(\frac{4}{5}, \frac{1}{5})$	50	212	28	44	$K = 1$
Example 2b $(\frac{4}{5}, \frac{1}{5})$	50	244	35	45	$K = 3$
Linearised approach					
Example 3a $(\frac{2}{3}, \frac{1}{3})$	30	76	28	34	$K = 1$
Example 3b $(\frac{2}{3}, \frac{1}{3})$	30	75	28	37	$K = 3$
Example 4a $(\frac{4}{5}, \frac{1}{5})$	38	212	40	44	$K = 1$
Example 4b $(\frac{4}{5}, \frac{1}{5})$	42	244	43	45	$K = 3$
Example 5 $(\frac{5}{6}, \frac{1}{6})$	65	320	35	47	$K = 3$
Literature (Blu 1998)					
$(\frac{2}{3}, \frac{1}{3})$	55	55	28	28	$K = 1$
$(\frac{4}{5}, \frac{1}{5})$	116	116	32	32	$K = 1$
$(\frac{5}{6}, \frac{1}{6})$	199	199	44	44	$K = 1$
$(q - 1/q, 1/q)$	No solution				$K \geq 2$
Literature (Bayram and Selesnick 2009b)					
$(\frac{5}{6}, \frac{1}{6})$	208	208			$K = 3$
$(\frac{4}{5}, \frac{1}{5})$	123	123			$K = 3$

Chapter 4

Bi-orthgonal RFB structure of $\left(\frac{p}{q}, \frac{q-p}{q}\right)$ - flexible Q factor transforms

AN approach for designing a general two-band, FIR, critically sampled, rational rate filter bank (RFB) with perfect reconstruction (PR) and regularity factors is proposed in this chapter. Designs obtained from this approach, when iterated, lead to rational discrete wavelet transform (RADWT) with *adjustable dilation factor*. The RFB design is based on solving a nonlinear constrained optimisation problem in which the nonlinear constraints come from the perfect reconstruction conditions. An *iterative algorithm*, which solves a convex quadratic problem with linear constraints at each iteration step, is proposed to solve the original nonlinear optimisation. The necessity for the iterative algorithm to solve the non-linear constrained optimisation problem is discussed in details throughout the chapter. The resultant RFB designs are robust against the algorithm's initialisation. This RFB structure is a generalisation of the work presented in chapter 3, differentiated by the *adjustibility* of the resulting RADWTs' dilation factor and the solving algorithm.

4.1 Introduction and motivation

In exploiting the sparsity representation of oscillatory signals, Selesnick (Selesnick 2011c) decomposed signals into high and low oscillatory pulses using a procedure similar to the basis pursuit (BP) principle (Chen *et al.* 2001) with a dictionary consisting of frames generated by over-complete rational discrete wavelets (Bayram and Selesnick 2009a). The principle for separating these signals relies on the incoherence between the frames of the high and low Q (quality factor) rational discrete wavelets (Selesnick 2011b), which demonstrates the demand for for flexible Q rational decompositions. In the existing literature for flexible Q transforms (Bayram and Selesnick 2009a, Selesnick 2011a), over-complete designs are more prevalent and these are usually designed in the Fourier domain which means compact support is theoretically not possible (i.e. non-FIR filters). Note however that such designs typically exhibit fast-time domain decay and so are nearly compact for practical purposes.

In this chapter, we propose a method to design two channel FIR rational FBs (RFBs) satisfying regularity and PR conditions. Such filter banks lead to non-expansive constant-Q representations with a *flexible quality factor* Q. Hence, they provide similar representative advantages as the over-complete schemes but without the burden incurred by redundancy. The designs we seek are bi-orthogonal and obtained in the time domain. The re-sampling ratios between the two channels can be arbitrary rational numbers, as long as it remains permissible as discussed in chapter 2 (Kovacevic and Vetterli 1993) though re-sampling ratios with large denominators will result in high computational complexity in the design process. Together with the regularity conditions, this allows the associated rational wavelets to have an adjustable Q factor. This differs from the work in chapter 3 where the re-sampling ratios are strictly limited to $(\frac{q-1}{q}, \frac{1}{q}), q \geq 2$. The central result of chapter 3 is generalised into one that connects the regularity factors between the analysis and synthesis banks of the generalised re-sampling rate bi-orthogonal RFB. An iterative routine, consisting of a sequence of quadratic optimisation problems subjected to linear constraints, is proposed to solve the original non-linear constrained design problem.

In section 4.2, we discuss the PR conditions together with regularity requirements of the NUFBs. In section 4.3, we present the algorithm to solve the design problem, which is followed by the design examples in section 4.4. In section 4.5, discussions on the algorithm's convergence is presented while section 4.6 is the chapter summary.

4.2 Regular perfect reconstruction rational FBs

In this chapter, we restrict our attention to the cases of two-channel FBs with re-sampling ratios $(\frac{p_0}{q}, \frac{p_1}{q})$, $p_0 + p_1 = q$ which satisfy the conditions described in (Kovacevic and Vetterli 1993) and summarised in (2.1), (2.2), (2.3) of chapter 2. Fig. 4.1(a) shows the FB structure. Here, we re-summarise the feasible condition of a rational FB for design completeness. It is possible for a critically-sampled M-channel RFB structure with *real filters*, to extract in the following frequency bands of input signal for any channel $i = 0 \ldots, M-1$:

$$X_i : \left[\frac{k}{q}\pi, \frac{k+p}{q}\pi\right] \tag{4.1}$$

if there exist l, s such that one of the following pairs of conditions is satisfied,

$$k = sp - lq, \qquad l = 2t, \tag{4.2}$$

$$k - q = lq - sp, \qquad l = 2t + 1, \tag{4.3}$$

where $l = 0, \ldots, p-1; s = 0, \ldots, q-1$; and $k = 0, \ldots, q-p$. If the solution exists for (2.2) or (2.3), then the filters are required to have pass-bands

$$N_i, S_i : \left[\frac{s}{q}, \frac{s+1}{q}\right]. \tag{4.4}$$

In this chapter the number of channel M of the rational filter bank is restricted to 2.

4.2.1 Perfect reconstruction (PR) FBs

In what follows, we summarise the expressions for PR conditions for a rational bi-orthogonal FB of Fig. 4.1 (a), for the case $p_1 \geq 1$. From lemma 3.2.1, it is possible to decompose the rational FB structure in Fig. 4.1(a) to an equivalent q-channel in Fig. 4.1(b), as long as the following conditions are satisfied:

$$H_{LP}(z) = \sum_{n=0}^{p_0-1} z^{qn} H_n(z^{p_0}), \qquad F_{LP}(z) = \sum_{n=0}^{p_0-1} z^{-qn} F_n(z^{p_0}) \tag{4.5}$$

$$H_{HP}(z) = \sum_{n=0}^{p_1-1} z^{qn} H_{n+p_0}(z^{p_1}), \qquad F_{HP}(z) = \sum_{n=0}^{p_1-1} z^{-qn} F_{n+p_0}(z^{p_1}) \tag{4.6}$$

The equivalence of the two structures in Fig. 4.1(a) and Fig. 4.1(b) suggests that every PR non-uniform (i.e. rational) two-channel FB is equivalent to a PR uniform q-channel

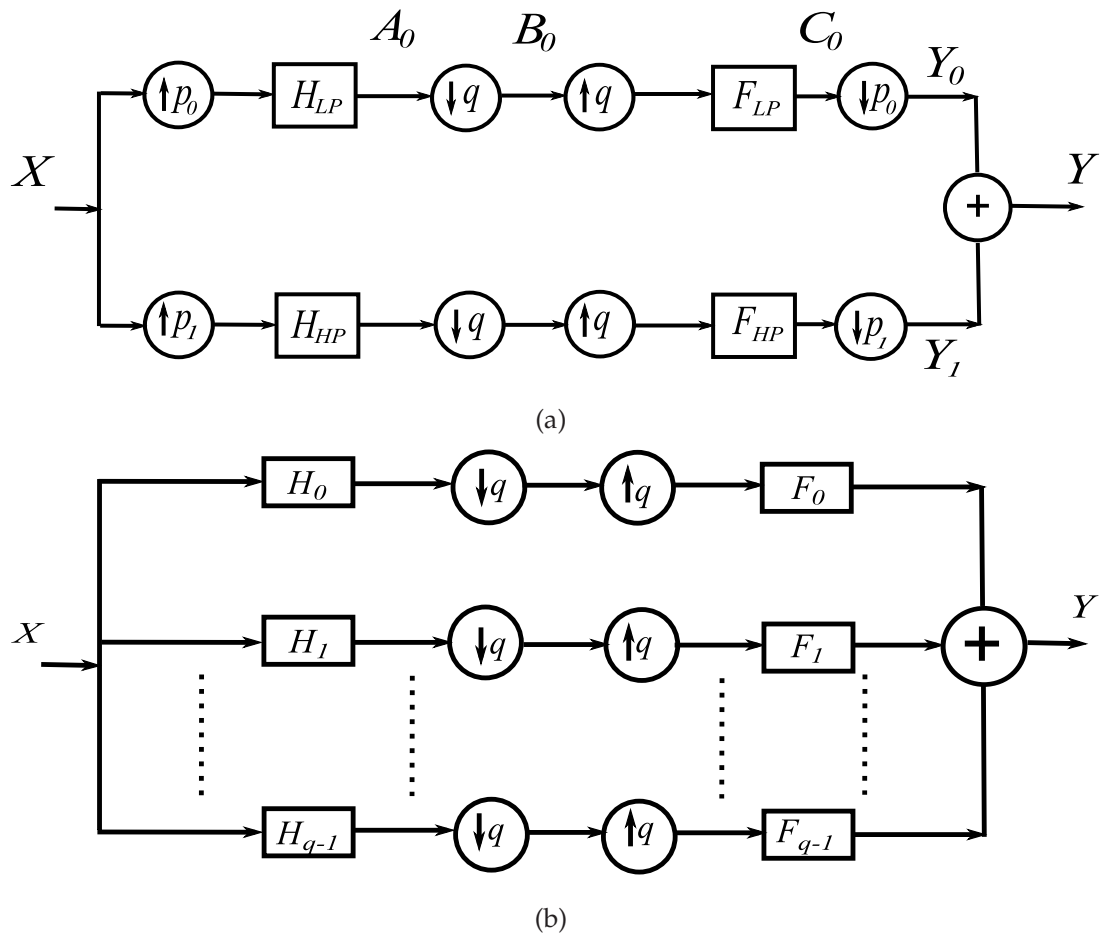

Figure 4.1. Rational rate filter bank with rate changing of $(\frac{p_0}{q}, \frac{p_1}{q})$ for coprime pairs (p_0, q) and (p_1, q) (a) and the equivalent uniform q-channel FB (b).

FB. The design problem is thus transformed to designing a uniform q-channel FB which satisfies PR condition. Similar discussion though has been described in section 3.2 of chapter 3, which re-summarise here for completeness.

Denote the alias component (AC) matrix of the uniform q-channel FB by $\mathbf{A}(z)$ as formulated in (3.15). The condition for PR is expressed by

$$\mathbf{A}(z)\mathbf{F}(z) = \begin{bmatrix} \alpha z^{-n_0} & \mathbf{0}^t \end{bmatrix}^t, \tag{4.7}$$

where $\mathbf{F}(z) = \begin{bmatrix} F_0(z) & F_1(z) & \dots & F_{q-1}(z) \end{bmatrix}^t$. If the set of analysis filters are FIR, then the synthesis filters are also FIR if

$$F_m(z) = (-1)^m \det \mathbf{A}_{-0m}(z), \qquad \text{for } m = 0, \cdots, q-1, \tag{4.8}$$

where $\mathbf{A}_{-0m}(z)$ is the matrix $\mathbf{A}$ with row 0 and column m deleted. Let $Q_m(z) = F_m(z)H_m(z)$. The PR condition in (4.7) requires $Q_m(z)$ be an q^{th}-band filter (Saghizadeh

and Willson 1998), or equivalently, that one of its q polyphase components be a pure delay. Thus, if $\mathbf{q}_m$ is the column vector representing the impulse response of $Q_m(z)$, re-written as $Q_m(z) = (-1)^m \det \mathbf{A}_{-0m}(z) H_m(z)$, its *k-th q-polyphase component*, for $k = q(\frac{q-1}{2} - \left\lfloor \frac{q-1}{2} \right\rfloor)$, is required to satisfy

$$\mathbf{q}_{m,k} = \begin{bmatrix} \mathbf{0}^t & \alpha & \mathbf{0}^t \end{bmatrix}^t, \quad \alpha \neq 0, \tag{4.9}$$

where $\lfloor . \rfloor$ is the rounding operation to the nearest integer less than or equal to its argument.

4.2.2 Regularity

Regularity conditions of RFB with re-sampling parameters p_0, p_1, q as illustrated in Fig. 4.1 (a) are established in (Bayram and Selesnick 2009c). A rational FB as in Fig. 4.1 (a) possesses K regularity factors if the analysis and synthesis low-pass filters are divisible by $(1 + z^{-1} + \cdots + z^{-(p_0-1)})^K$ and $(1 + z^{-1} + \cdots + z^{-(q-1)})^K$, respectively, and the high-pass analysis filter is divisible by $(1 - z^{-1})^K$. [7] Such regularity conditions are generalised versions of those described in section 3.2.2 of chapter 3, in which $q = p_0 + 1$, $p_1 = 1$. We thus formulate the regularity conditions, corresponding to the analysis low-pass and high-pass filters $\mathbf{h}_{LP}, \mathbf{h}_{HP}$, in vector form as:

$$\mathbf{T}_{LP} \mathbf{h}_{LP} = \mathbf{0}, \tag{4.10}$$

$$\mathbf{T}_{HP} \mathbf{h}_{HP} = \mathbf{0}, \tag{4.11}$$

where $\mathbf{T}_{LP}, \mathbf{T}_{HP}$, described in (Blu 1998), are rectangular matrices of size $(p_0 - 1)K \times N_L$ and $K \times N_H$, respectively; $\mathbf{h}_{LP}$, $\mathbf{h}_{HP}$ are column vectors representing the impulse responses of the analysis low-pass filter $H_{LP}(z)$ and high-pass filter $H_{HP}(z)$, respectively. While regularity conditions for the analysis low-pass and high-pass filters can be imposed through linear conditions (4.10)–(4.11) on the filters' coefficients, the regularity conditions for the synthesis low-pass filter requires imposing extra conditions on $\mathbf{h}_{HP}$ for a general parameters $\{p_0, p_1, q\}$ in the RFB structure. The following result generalises the regularity condition for the proposed bi-orthogonal RFB in the thesis.

[7] The low-pass filters of the FB in Fig. 4.1(a) satisfying the described regularity condition can be considered as fractional rate changers which preserve the set of discrete time polynomial signals of degree $K - 1$, and such signals are annihilated by the corresponding analysis high-pass filter with regularity factor (Bayram and Selesnick 2009c).

Lemma 4.2.1. *If the analysis and synthesis filters, as described in (4.5)–(4.8), both satisfy the regularity conditions (4.10)–(4.11) and each of the (p_1)-polyphase components of the analysis high-pass filter is divisible by $(1-z^{-1})^K$, then the synthesis low-pass filter satisfies the required regularity conditions.*

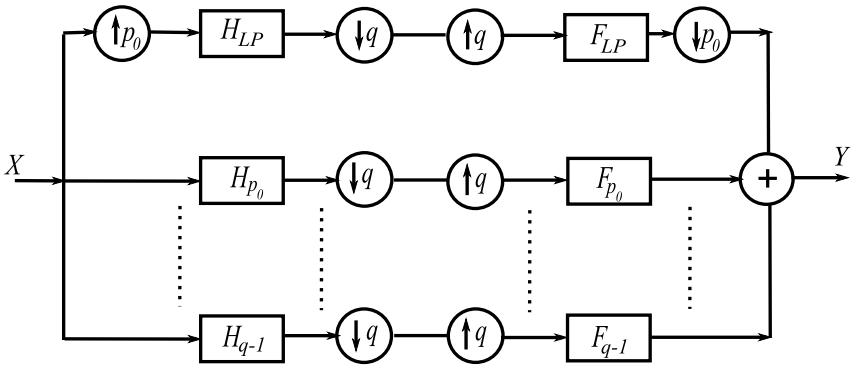

Figure 4.2. The equivalent rational FB structure with the two-channel RFB structure in Fig. 4.1 (a), with only high pass channel being decomposed into their polyphase components

Proof. Let $\mathbf{C}$ be the alias component matrix of the structure in Fig. 4.2; it is merely a "merged" re-drawing of the FBs in Fig. 4.1(a) and (b). The PR conditions for Fig. 4.2 can be written as:

$$H_{LP}(zW^k)F_{LP}(z) + H_{LP}(zW^kW_{p_0})F_{LP}(zW_{p_0}) + \ldots + H_{LP}(zW^kW_{p_0}^{p_0-1})\times$$
$$F_{LP}(zW_{p_0}^{p_0-1}) + \sum_{i=0}^{q-p_0-1} H_{p_0+i}(z^{p_0}W^{kp_0})F_{p_0+i}(z^{p_0}) = \alpha\delta[k]z^{-n_0p_0}, \qquad (4.12)$$

where $k = 0,\cdots,q-1$, W, W_{p_0} are the fundamental q^{th} and $p_0{}^{\text{th}}$ roots of unity, respectively and $\delta[k]$ is the Kronecker delta. For presentation purpose, $q \times q$ matrix $\mathbf{C}$ is decomposed to $\begin{bmatrix}\mathbf{C_{LP}} & \mathbf{C_{HP}}\end{bmatrix}$, for which $\mathbf{C_{LP}}, \mathbf{C_{HP}}$ are $q \times p_0$, $q \times (q-p_0)$ matrices and represented as in (4.13)

$$\mathbf{C_{LP}} = \begin{bmatrix} H_{LP}(z) & H_{LP}(zW_{p_0}) & \cdots & H_{LP}(zW_{p_0}^{p_0-1}) \\ \vdots & \vdots & \vdots & \vdots \\ H_{LP}(zW^{q-1}) & H_{LP}(zW^{q-1}W_{p_0}) & \cdots & H_{LP}(zW^{q-1}W_{p_0}^{p_0-1}) \end{bmatrix},$$
$$\mathbf{C_{HP}} = \begin{bmatrix} H_{p_0}(z^{p_0}W^{0\times p_0}) & \cdots & H_{q-1}(z^{p_0}W^{0\times p_0}) \\ \vdots & \vdots & \vdots \\ H_{p_0}(z^{p_0}W^{(q-1)p_0}) & \cdots & H_{q-1}(z^{p_0}W^{(q-1)p_0}) \end{bmatrix}. \qquad (4.13)$$

The conditions in (4.12) can be expressed in matrix form as

$$\mathbf{C}\begin{bmatrix} F_{LP}(z) & \cdots & F_{LP}(zW_{p_0}^{p_0-1}) & F_{p_0}(z^{p_0}) & \cdots & F_{q-1}(z^{p_0}) \end{bmatrix}^t = \begin{bmatrix} \alpha z^{-n_0 p_0} \\ \mathbf{0_{q-1}} \end{bmatrix}, \tag{4.14}$$

where $\mathbf{0_{q-1}}$ is the $(q-1)\times 1$ zero vector. Now, $F_{LP}(z)$ in condition (4.14) can be written as

$$F_{LP}(z) = \alpha z^{-n_0 p_0} \frac{\det \mathbf{C}_{-00}}{\det \mathbf{C}}, \tag{4.15}$$

where $\mathbf{C}_{-00}$ represents matrix $\mathbf{C}$ with 0 row and column removed. Condition (4.14) can be rewritten as:

$$\mathbf{CF} = \mathbf{D}, \tag{4.16}$$

where $\mathbf{F}$ is $q \times q$ matrix such that $[\mathbf{F}]_{i,j} = F_{LP}(zW^j W_{p_0}^i)$ for $i = 0, \cdots, p_0 - 1$, $j = 0, \cdots, q-1$ and $[\mathbf{F}]_{i,j} = F_i((zW^j)^{p_0})$ for $i = p_0, \cdots, q-1$, $j = 0, \cdots, q-1$; $\mathbf{D}$ is a diagonal matrix whose main diagonal entries are $[\mathbf{D}]_{i,i} = \alpha_i z^{-n_0 p_0}$.

From (4.16), we have $\det \mathbf{C} \times \det \mathbf{F} = \det \mathbf{D}$ or $\det \mathbf{C} \times \det \mathbf{F} = \alpha z^{-L}$ for some integer L. Since the filters are FIR, $\det \mathbf{C}$, $\det \mathbf{F}$ are polynomials of z. If the product $\det \mathbf{C} \times \det \mathbf{F}$ is equal to a pure delay, it implies that $\det \mathbf{C}$, $\det \mathbf{F}$ are themselves pure delays. To show this result, assume they are not pure delays, then there exist non-zero coefficients a_m, b_m such that $a_m z^{k_{min}}, b_m z^{k_{max}}$ are the lowest and highest order components of $\det \mathbf{C}$, respectively; similarly $c_m z^{l_{min}}, d_m z^{l_{max}}$ are the lowest and highest order components of $\det \mathbf{F}$, respectively. The product will then have at least two components $a_m c_m z^{k_{min}+l_{min}}, b_m d_m z^{k_{max}+l_{max}}$, and so cannot be a pure delay thus contradicting to the initial assumption. Thus, (4.15) becomes:

$$F_{LP}(z) = \zeta z^{-a} \det \mathbf{C}_{-00} \tag{4.17}$$

for some $\zeta \in \mathbb{R}$, $a \in \mathbb{N}$; note that (4.17) expresses F_{LP} in terms of analysis low-pass and high-pass filters.

We now show that if the analysis low-pass and high-pass filters possess regularity factors as described in (4.10) and (4.11), then the synthesis low-pass filter F_{LP} possesses the same number of regularity factors (therefore divisible by $(1 + z^{-1} + \cdots + z^{-(q-1)})^K$), providing PR is satisfied. If the analysis low-pass filter possesses regularity conditions and each of the (p_1)-polyphase components of the analysis high-pass filter is divisible by $(1 - z^{-1})^K$, the following can be deduced:

$$H_{LP}(z) = [(z - W_{p_0}) \ldots (z - W_{p_0}^{(p_0-1)})]^K P(z), \tag{4.18}$$

$$H_i(z) = (z-1)^K Q(z), \qquad i = p_0, \cdots, q-1, \tag{4.19}$$

where $P(z), Q(z)$ are polynomials of z and $p_0 + p_1 = q$. Consider the $(q-1)^{\text{th}}$ row of matrix $\mathbf{C}_{-00}(z)$, namely $\mathbf{r}_{q-1}$, which is also row q of the matrix $\mathbf{C}$ excluding the first element $H_{LP}(zW^{q-1})$. Thus, we have

$$\mathbf{r}_{q-1}[k] = \begin{cases} H_{LP}(zW^{q-1}W_{p_0}^{k}) & \text{for} \quad k = 1, \ldots, p_0 - 1 \\ H_k(z^{p_0}W^{p_0(q-1)}) & \text{for} \quad k = p_0, \ldots, q-1 \end{cases} . \tag{4.20}$$

For each element $\mathbf{r}_{q-1}[k], k = 1, \ldots, p_0 - 1$, we can obtain a common factor $(z - W)^K$. For example, if we substitute (4.18) into the first element $\mathbf{r}_{q-1}[0] = H_{LP}(zW^{q-1}W_{p_0})$, the first factor of (4.18), $(z - W_{p_0})^K$ becomes $(zW^{q-1}W_{p_0} - W_{p_0})^K = [\frac{1}{W^{q-1}W_{p_0}}(z - W)]^K$. Similarly, for other elements of $\mathbf{r}_{q-1}[k], k = 0, \ldots, p_0 - 2$, we can always find a factor of $H_{LP}(z)$, $(z - W_{p_0}^m)^K, m = 1, \ldots, p_0 - 1$ as defined in (4.18) that leads to the common factor $(z - W)^K$.

If we substitute (4.19) into other elements of $\mathbf{r}_{q-1}[k], k = p_0, \ldots, q-1$, we can also find common $(z - W)^K$ as a result of the factor $(z-1)^K$ of $H_i(z)$ defined in (4.19). Hence, all the elements in row $(q-1)$ of $\mathbf{C}_{-00}(z)$ have common factor $(z - W)^K$ and so $\det \mathbf{C}_{-00}(z)$ also has factor $(z - W)^K$. Similarly if we consider row $(q-n)$ of $\mathbf{C}_{-00}(z)$, we can find common fators $(z - W^n)^K, n = 1, \cdots, q-1$ as a result of (4.18), (4.19). Thus, synthesis low-pass filter $F_{LP}(z)$ possesses the regularity factor of $[(z - W) \ldots (z - W^{(q-1)})]^K$ or equivalently, it is divisible by $(1 + z^{-1} + \cdots + z^{-(q-1)})^K$. This proves the lemma. □

The additional regularity condition on $\mathbf{h}_{HP}$ can be formulated as:

$$\mathbf{T}_{HP_{poly}}\mathbf{h}_{HP} = \mathbf{0}, \tag{4.21}$$

where $\mathbf{T}_{HP_{poly}}$ is an $Kp_1 \times N_H$ rectangular matrix representing regularity conditions imposed on the polyphase components of the analysis high-pass filters. This is constructed based on the conditions in (4.19). Note this can easily be concatenated with $\mathbf{T}_{HP}$ in (4.11) to form a larger set of linear constraints on h_{HP}.

In designing PR rational FBs with regularity factors, we formulate the problem as follows: Find the most frequency selective H_{LP}, H_{HP} filters whose impulse responses are decomposed into p_0, p_1 polyphase components as in (4.5)–(4.6) to form the uniform q-channel FB as shown in Fig. 4.1(b). The filters' frequency selectivity is crucial in reducing *shift error* between the resulting discrete rational wavelets (Blu 1993, Blu 1998). The filters' polyphase components need to satisfy (4.7)–(4.9) and the additional linear

conditions arising from regularity conditions (4.10), (4.11), (4.21). To qualify as genuine low-pass and high-pass filters, we optimise the magnitude responses of H_{LP}, H_{HP}, based on a least square error objective function:

$$\begin{aligned} f &= \alpha_0 \int_0^{\omega_{plp}} |H_{LP}(\omega) - H_{LP}(0)|^2 d\omega + \alpha_1 \int_{\omega_{slp}}^{\pi} |H_{LP}(\omega)|^2 d\omega \\ &+ \alpha_2 \int_{\omega_{php}}^{\pi} |H_{HP}(\omega) - H_{HP}(\pi)|^2 d\omega + \alpha_3 \int_0^{\omega_{shp}} |H_{HP}(\omega)|^2 d\omega \\ &= \underbrace{\mathbf{h}_{LP}^t \left(\alpha_0 \mathbf{P}_{P_{LP}} + \alpha_1 \mathbf{P}_{S_{LP}}\right) \mathbf{h}_{LP}}_{f_1(\mathbf{h}_{LP})} + \underbrace{\mathbf{h}_{HP}^t \left(\alpha_2 \mathbf{P}_{P_{HP}} + \alpha_3 \mathbf{P}_{S_{HP}}\right) \mathbf{h}_{HP}}_{f_2(\mathbf{h}_{HP})}, \end{aligned} \tag{4.22}$$

where $\mathbf{h}_{LP}, \mathbf{h}_{HP}$ are the $N_L \times 1, N_H \times 1$ column vectors representing impulse responses of the analysis low-pass and high-pass filters, respectively; $\omega_{slp} = \frac{\pi}{q} + \Delta\omega_{LP}$, $\omega_{plp} = \frac{\pi}{q} - \Delta\omega_{LP}$ and $\omega_{shp} = \frac{(q-1)\pi}{q} - \Delta\omega_{HP}$, $\omega_{php} = \frac{(q-1)\pi}{q} + \Delta\omega_{HP}$ are the low-pass/high-pass filter's stop-band and pass-band edges, respectively; $\alpha_i \geq 0$ for $i = 0, \cdots, 3$ are the weights; $\mathbf{P}_{S_{LP}}$, $\mathbf{P}_{S_{HP}}$, $\mathbf{P}_{P_{LP}}$, $\mathbf{P}_{P_{HP}}$ are real symmetric positive semidefinite matrices. $\mathbf{P}_{S_{LP}}$, $\mathbf{P}_{S_{HP}}$, are defined as in (3.28),(3.29) while $\mathbf{P}_{P_{LP}}$, $\mathbf{P}_{P_{HP}}$ can be obtained as

$$\left[\mathbf{P}_{P_{LP}}\right]_{m,n} = \begin{cases} \frac{2}{\pi}\left[\omega_{plp} - \frac{\sin(m\omega_{plp})}{m} - \frac{\sin(n\omega_{plp})}{n} + \frac{\sin((m-n)\omega_{plp})}{m-n}\right] & m \neq n \\ \frac{2}{\pi}\left[2\omega_{plp} - \frac{2\sin(m\omega_{plp})}{m}\right] & m = n \end{cases} \tag{4.23}$$

$$\left[\mathbf{P}_{P_{HP}}\right]_{m,n} = \begin{cases} \frac{2}{\pi}\left[\frac{(\pi-\omega_{php})}{(-1)^{m+n}} + \frac{\sin(m\omega_{php})}{m\times(-1)^m} + \frac{\sin(n\omega_{php})}{n\times(-1)^n} - \frac{\sin((m-n)\omega_{php})}{m-n}\right] & m \neq n \\ \frac{2}{\pi}\left[2(\pi - \omega_{php}) + \frac{2\sin(m\omega_{php})}{m\times(-1)^m}\right] & m = n \end{cases}, \tag{4.24}$$

where $\mathbf{P}_{P_{LP}}$, $\mathbf{P}_{P_{HP}}$ are $N_L \times N_L$, $N_H \times N_H$ matrices, respectively.

4.3 Design algorithm

The discussion in Sec. 4.2 leads to a formulation of the FB design problem as a constrained optimisation problem, where the cost function is defined in (4.22) and the constraints are given in (4.8), (4.10)–(4.11), (4.21). The key features of this formulation are:

- The cost function $f(\mathbf{h}_{LP}, \mathbf{h}_{HP})$ is quadratic in $\mathbf{h}_{LP}$ and $\mathbf{h}_{HP}$ since $f_1(\mathbf{h}_{LP})$ and $f_2(\mathbf{h}_{HP})$ in (4.22) are quadratic.
- If $\{\mathbf{h}_i : i = 0, \cdots, q-1\}$ are defined as the polyphase components of $\mathbf{h}_{LP}$, $\mathbf{h}_{HP}$ such that $\mathbf{h}_i[n] = \mathbf{h}_{LP}[i + np_0]$ for $i = 0, \cdots, p_0 - 1$ and $\mathbf{h}_i[n] = \mathbf{h}_{HP}[i - p_0 + np_1]$

for $i = p_0, \cdots, q-1; p_0 + p_1 = q$, then $\{\mathbf{h}_i\}_{i=0}^{q-1}$ are the impulse responses of the analysis filters of the uniform q-channel FB in Fig. 4.1(b). Thus, the PR condition (4.8) represents q^{th} order constraints since $\mathbf{q}_{m,k}$ of (4.9) is derived from the determinant of the alias component matrix of the uniform q-channel FB. The coefficient $\mathbf{q}_{m,k}[n]$ can therefore be expressed as the sum of products of the coefficients of filters $\{\mathbf{h}_i\}_{i=0}^{q-1}$,

$$\mathbf{q}_{m,k}[n] = \sum_{n_i \in K_n = \{K_n^r\}_{r \in \mathbb{N}}} a_r \prod_{i=0}^{q-1} \mathbf{h}_i[n_i], \tag{4.25}$$

where K_n^r is a subset of indices $\{n_i, i = 0, \ldots, q-1 : n_i \in \mathbb{N}, \sum_{i=0}^{q-1} n_i = n\}$; K_n is the union of the sets K_n^r for all values of r. The real valued constants a_r are determined by indices n_i corresponding to the subset K_n^r, defined in section III of (Saghizadeh and Willson 1998). The PR condition requires $\mathbf{q}_{m,k}[n] = 0$ for $n = 0, \cdots, N_{\mathbf{q}} - 1, n \neq n_0$; n_0 determines the FB system delay while N_q is the length of vector $\mathbf{q}_{m,k}$.

- All other constraints of the optimisation problem are linear.

The filter bank design problem is formulated as a nonlinear constrained optimisation problem with respect to unknowns $\mathbf{h}_{LP}, \mathbf{h}_{HP}$. The highest order nonlinear constraints arise from PR conditions (4.25). In chapter 3, we have proposed two methods to solve such problem, namely local optimisation and linearised methods. The first method, which still works for this problem, is based on a line-search algorithm to find a near optimal solution[8] once a suitable initialisation is found. However, such method, as discussed in chapter 3, results in impractically long running time when the parameter q is large due to its high computational complexity for solving a high order nonlinear constraint. The second method cannot be applied for this problem as $p_1 > 1$. We thus propose an iterative procedure, where each iteration solves a quadratic problem with linear constraints, to solve the original non-linear problem for the parameters $p_1 > 1$. This leads to an effective mean of finding a solution for a high order constraint optimisation problem. Even though a global solution is not guaranteed, the procedure has low computational complexity, since each iteration step solves a quadratic problem with linear constraints, and it is robust against the algorithm initialisations. A discussion on this algorithm behavior is contained in section 4.5.

[8] Matlab toolbox function `fmincon` and the active-set (line search) sub-algorithm was used for such purpose

4.3.1 Iterative algorithm

The cost function (4.22) consists of two separate quadratic functions of variable vectors $\mathbf{h}_{LP}$, $\mathbf{h}_{HP}$, which suggests that the design problem can be split into two steps: (i) design the analysis low-pass filter $\mathbf{h}_{LP}$ by optimising quadratic function $f_1(\mathbf{h}_{LP})$ satisfying regularity condition (4.10) and (ii) design the analysis high-pass filter $\mathbf{h}_{HP}$ by optimising $f_2(\mathbf{h}_{HP})$ subject to PR condition (4.25) and regularity conditions (4.11), (4.21). Completing step one will reduce the order of the PR constraints (4.25) in step two, from q to p_1, since $\{\mathbf{h}_i\}_{i=0}^{p_0-1}$ (polyphase components of $\mathbf{h}_{LP}$) are already determined in step one. In case of $p_1 = 1$ we have a simple quadratic problem with linear constraints. When $p_1 \neq 1$, a recursive procedure is proposed is to compute a sequence of solutions $\{\mathbf{h}_{HP}^l\}_{l\in\mathbb{N}}$, such that $\mathbf{h}_{HP}^{\infty} \to \mathbf{h}_{HP}$.

To avoid having too many subscripts, we substitute $\mathbf{q}_{m,k}[n]$ with $\Gamma[n]$. At iteration l, $\mathbf{h}_{HP}^{l-1}$ is known, and $f_2(\mathbf{h}_{HP})$ is minimised subject to (4.26), which can be written as

$$\Gamma^l[n] = \sum_{j=p_0}^{q-1} \Gamma_j^l[n] = 0, \tag{4.26}$$

where $\Gamma_j^l[n]$ is defined as

$$\Gamma_j^l[n] = \sum_{n_i \in K_n = \{K_n^r\}_{r\in\mathbb{N}}} a_r \Big\{ \prod_{i=0}^{p_0-1} \mathbf{h}_i[n_i] \Big\} \prod_{i=p_0, i\neq j}^{q-1} \mathbf{h}_i^{l-1}[n_i]\mathbf{h}_j[n_j], \tag{4.27}$$

for $n = 0, \cdots, N_{\mathbf{q}} - 1, n \neq n_0$. Note that $\Gamma_j^l[n]$ is formulated based on (4.25) with low-pass filter's polyphase components $\{\mathbf{h}_i\}_{i=0}^{p_0-1}$ known from step one. In other words, the bracketed $\Big\{ \prod_{i=0}^{p_0-1} \mathbf{h}_i[n_i] \Big\}$ in (4.27) is known, as are $\{\mathbf{h}_i^{l-1}\}_{i=p_0, i\neq j}^{q-1}$ from the previous iteration (i.e. analysis high-pass filter's polyphase components of step $l-1$). As a result, $\Gamma_j^l[n]$ is linear with respect to $\mathbf{h}_j$ for $j = p_0, \cdots, q-1$. Hence, the optimisation problem for each iteration is a quadratic problem in $\mathbf{h}_{HP}$ with linear constraints defined in (4.11), (4.21) and (4.26). If $\mathbf{h}_{HPmin}$ is the solution at iteration l, we let

$$\mathbf{h}_{HP}^l = \frac{\mathbf{h}_{HPmin} + \mathbf{h}_{HP}^{l-1}}{2}. \tag{4.28}$$

At convergence ($l = N$), we have $\mathbf{h}_{HP}^{N-1} \to \mathbf{h}_{HP}^N$ which leads to $\mathbf{h}_{HP}^{N-1} \to \mathbf{h}_{HPmin}$ (for $\mathbf{h}_{HPmin}$ denotes optimal solution of $\mathbf{h}_{HP}$ at current iteration N). Hence, $\Gamma^N[n]$ of (4.26)

becomes

$$\sum_{j=p_0}^{q-1}\Big\{\sum_{n_i\in K_n=\{K_n^r\}_{r\in\mathbb{N}}} a_r\Big\{\prod_{i=0}^{p_0-1}\mathbf{h}_i[n_i]\Big\}\prod_{i=p_0,i\neq j}^{q-1}\mathbf{h}_i^N[n_i]\mathbf{h}_j^N[n_j]\Big\}$$
$$= p_1\sum_{n_i\in K_n=\{K_n^r\}_{r\in\mathbb{N}}} a_r\Big\{\prod_{i=0}^{p_0-1}\mathbf{h}_i[n_i]\Big\}\prod_{i=p_0}^{q-1}\mathbf{h}_i^N[n_i]. \tag{4.29}$$

Since RHS of (4.29) is independent of j, equating $\Gamma^N[n]=0$ (see (4.26)) gives

$$\sum_{n_i\in K_n=\{K_n^r\}_{r\in\mathbb{N}}} a_r\prod_{i=0}^{p_0-1}\mathbf{h}_i[n_i]\prod_{i=p_0}^{q-1}\mathbf{h}_i^N[n_i]=0, \tag{4.30}$$

which is the PR condition of the FB, whose solutions are the filters $\mathbf{h}_{LP}$ and $\mathbf{h}_{HP}^N$. Overall, our iterative algorithm turns an nonlinear constraint optimisation problem with nonlinear constraints into a sequence of recursive quadratic problems with linear constraints, with the PR condition of the original problem being satisfied at convergence. The design algorithm steps can be summarised as:

- Design analysis low-pass filter by minimising $f_1(\mathbf{h}_{LP})$ in (4.22) subject to (4.10). We set $H_{LP}(0)=\sqrt{p_0}$ to avoid trivial solutions.
- Randomly choose an initial filter $\mathbf{h}_{HP}^0$. Empirically, the performance of the algorithm is not sensitive to this initialisation (see Sec. 4.5 for discussion).
- At iteration step l, $\mathbf{h}_{LP}, \mathbf{h}_{HP}^{l-1}$ are known, we can attain $\mathbf{h}_{HPmin}=\underset{\mathbf{h}_{HP}}{\operatorname{argmin}} f_2(\mathbf{h}_{HP})$ subject to (4.11), (4.21), (4.26). To avoid a trivial solution, we set $H_{HP}(\pi)=\sqrt{p_1}$; $\mathbf{h}_{HP}^l$ is computed as in (4.28).
- The iteration is terminated if reconstruction error ϵ_r, computed as we substitute $\mathbf{h}_{LP}, \mathbf{h}_{HP}^l$ into expression (4.25), is less than a given threshold being used as 10^{-10} in our designs.

4.4 Design Results

To demonstrate the gradual change in dilation factor of the RADWTs, four example designs are illustrated in Figs. 4.3 and 4.4. The design examples are selected to illustrate the variation in dilation factor with respect to low to high resonance wavelet functions as defined in (Selesnick 2010)[9]. All analysis filters are designed to be q^{th}-band filters.

[9]The high resonance corresponds to sustained oscillatory signals and high Q factor (Selesnick 2011c).

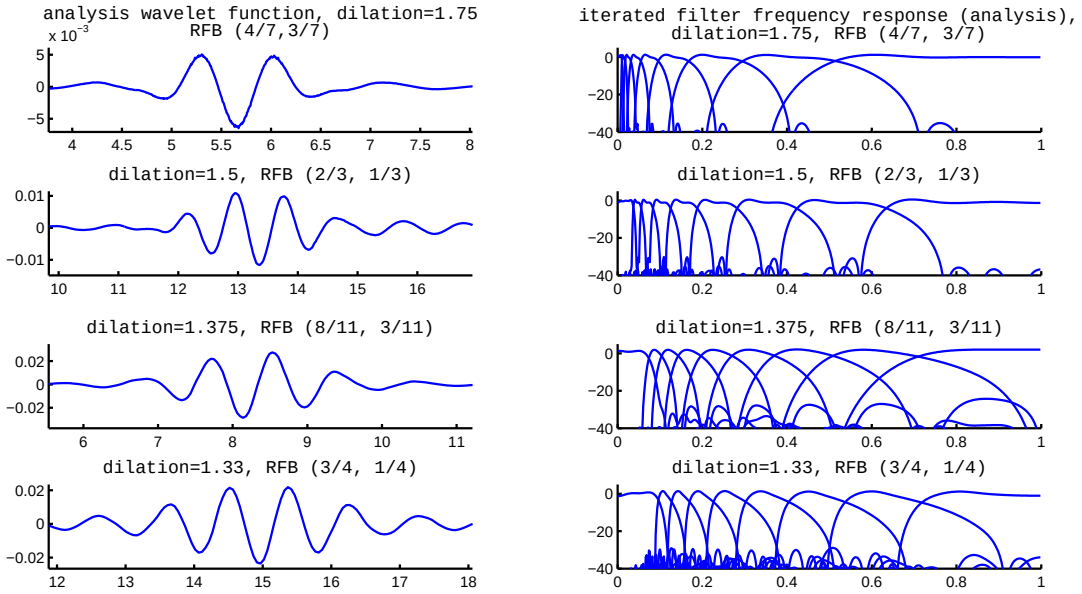

Figure 4.3. Left panels: Analysis wavelet functions of rational FBs. Right panels show the corresponding frequency response of the filters being iterated.

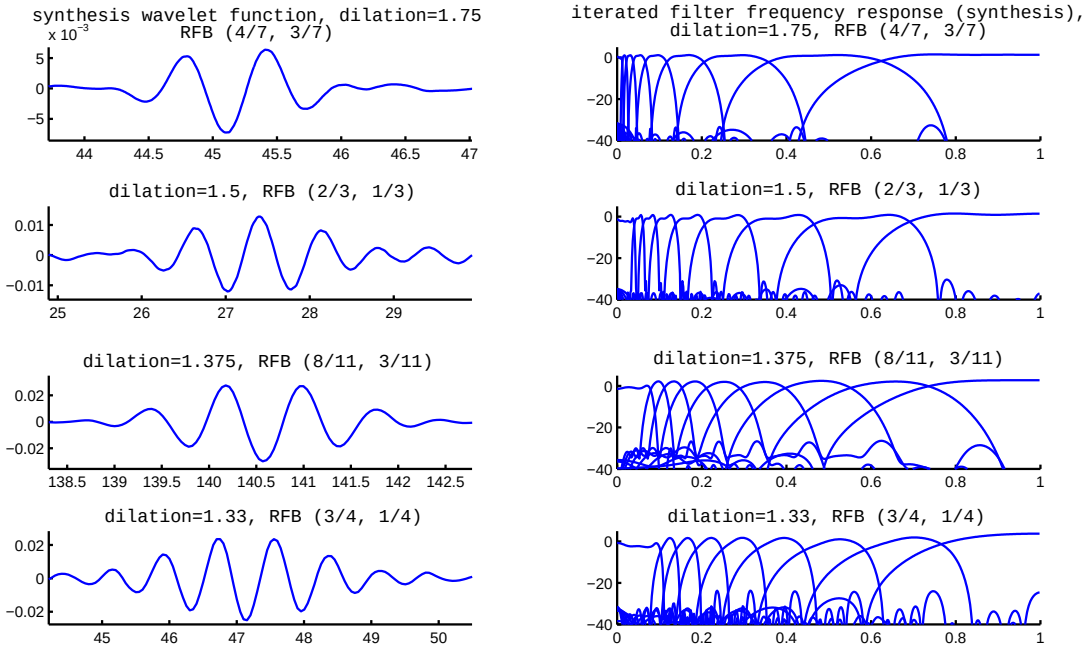

Figure 4.4. Left panels: Synthesis wavelet functions of rational FBs. Right panels show the corresponding frequency response of the filters being iterated.

The topic of designing FIR q^{th}-band filters with regularity factors has been addressed in (Wisutmethangoon and Nguyen 1999), we discuss here shortly for completeness.

If the low-pass filter $\mathbf{h}_{LP}$ has length N_L, then the index $L_0 = \lfloor N_L/2 \rfloor$ will determine the q-polyphase component $\mathbf{h}_{L_0}[n] = \mathbf{h}_{LP}[L_0 + nq]$, for $n \in \mathbb{Z}$ such that $L_0 + nq > 0$, which is chosen to be pure delay. According to (Wisutmethangoon and Nguyen 1999), the regular FIR q^{th}-band filter has optimal frequency response if $\mathbf{h}_{L_0}$ is chosen to be the pure delay polyphase component and the non-zero coefficient is at index L_0. We define the subset of indices K_p as $\{n_p : n_p = L_0 + nq, n \in \mathbb{Z}, 0 < n_p < N_L, n_p \neq L_0\}$ and the $N_L \times N_L$ matrices $\mathbf{P}_{P_{LP}}$, $\mathbf{P}_{S_{LP}}$ as in (4.23), (3.28). The matrices $\mathbf{P}_{P_{-K_p}}$, $\mathbf{P}_{S_{-K_p}}$ are $\mathbf{P}_{P_{LP}}$, $\mathbf{P}_{S_{LP}}$ with rows and columns at indices K_p removed. The q^{th}-band filter design with regularity factors can be formulated as

Problem $(\mathbf{P}_{q^{th}-band})$: Designing low-pass regular q^{th}-band filter by minimisation

$$\min_{\mathbf{h}} \quad \mathbf{h}^t \left(\alpha_0 \mathbf{P}_{P_{-K_p}} + \alpha_1 \mathbf{P}_{S_{-K_p}}\right) \mathbf{h}, \quad \text{subject to}$$
$$\mathbf{T}_{-K_p}\mathbf{h} \quad = \mathbf{0},$$

where $\mathbf{T}_{-K_p}$ is the regular matrix $\mathbf{T}_{LP}$, defined in (4.10) with columns at indices K_p removed.

The following examples result in RADWTs with dilation factors of decreasing order. The rate changes and analysis low-pass/high-pass filters' lengths are summarised as follows:

Example 4.4.1. $(4/7, 3/7)$ *FB with two regularity orders, the analysis low-pass and high-pass filter lengths are both* 60*, dilation factor of* $7/4 = 1.75$*; the corresponding synthesis low/high-pass filters lengths are* $276, 202$*, respectively.*

Example 4.4.2. $(2/3, 1/3)$ *FB with two regularity orders, the analysis low-pass and high-pass filter lengths are* $35, 50$*, dilation factor of* $3/2 = 1.5$*; the corresponding synthesis low/high-pass filters lengths are* $135, 35$*, respectively.*

Example 4.4.3. $(8/11, 3/11)$ *FB with two regularity orders, the analysis low-pass and high-pass filter lengths are* $70, 75$*, dilation factor of* $11/8 = 1.375$*; the corresponding synthesis low/high-pass filters lengths are* $505, 185$*, respectively.*

Example 4.4.4. $(3/4, 1/4)$ *FB with two regularity orders, the analysis low-pass and high-pass filter lengths are* $33, 52$*, dilation factor of* $4/3 = 1.33$*; the corresponding synthesis low/high-pass filters lengths are* $202, 30$*, respectively.*

It can be seen from Fig. 4.3 and 4.4 that the Q factors of the RADWTs gradually increases as the dilation factor decreases and the more sustained oscillation characteristic

they become. Examples 4.4.1 and 4.4.3 are designed based on the iterative algorithm described in section 4.3.1 and the filters' frequency responses are shown in Fig. 4.5 and 4.6, respectively. The examples 4.4.2 and 4.4.4 are designed based on *linearised method* described in section 3.3.2 and the filters' frequency responses are shown in appendices B.1.1, B.1.2, respectively. Note that the design filters containing re-sampling ratios of high integer values in the denominators (i.e. *example* 4.4.3) requires longer filter in the synthesis bank since their lengths are determined by the analysis filters' lengths multiplied by the denominator q.

Figures 4.5 and 4.6 show frequency responses of the analysis and synthesis filters of examples 4.4.1, 4.4.3 by iterative algorithm method proposed in section 4.3.1 corresponding to RFB designs of $(\frac{4}{7}, \frac{3}{7})$, $(\frac{8}{11}, \frac{3}{11})$, respectively. For the two examples, the

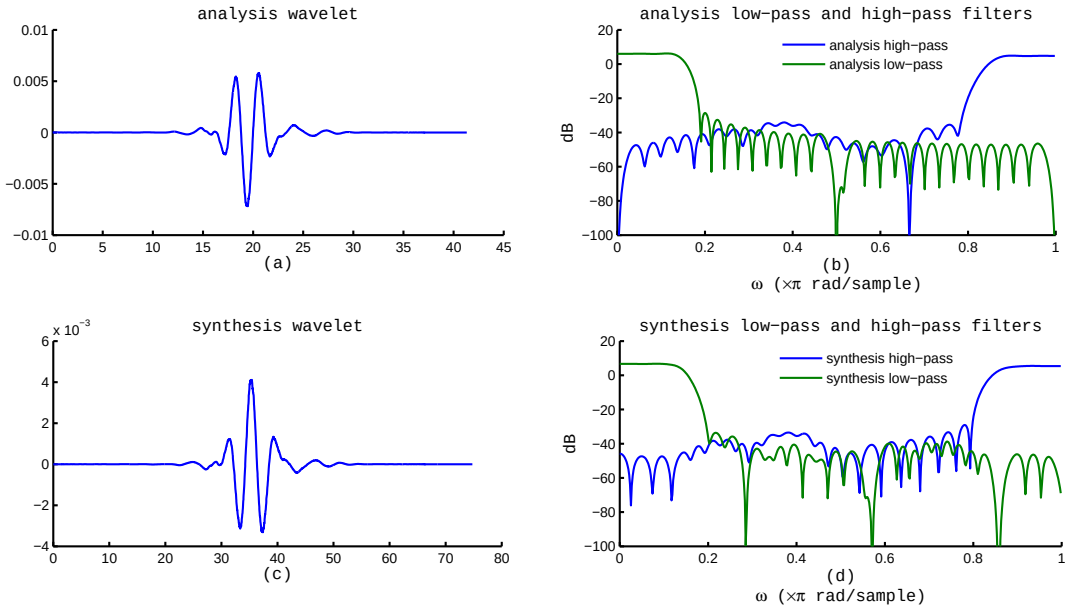

Figure 4.5. $(\frac{4}{7}, \frac{3}{7})$ RFB with two regularity orders. Left panels: Analysis (a) and Synthesis (c) wavelet functions, respectively. Right panels show the analysis (b) and synthesis (d) low-pass and high-pass filters' frequency response, respectively.

pass-band widths of the low-pass and high-pass filters are $\frac{\pi}{7}$ and $\frac{\pi}{11}$, respectively. Hence, the higher the q parameter, the narrower the pass-band width and transition band width for analysis filters are required, which is necessary for iterated filters to construct RADWTs. This equivalently requires longer filters. The responses shown in Fig. 4.5 and 4.6 clearly demonstrate that the filters of $(\frac{8}{11}, \frac{3}{11})$ structure have narrower

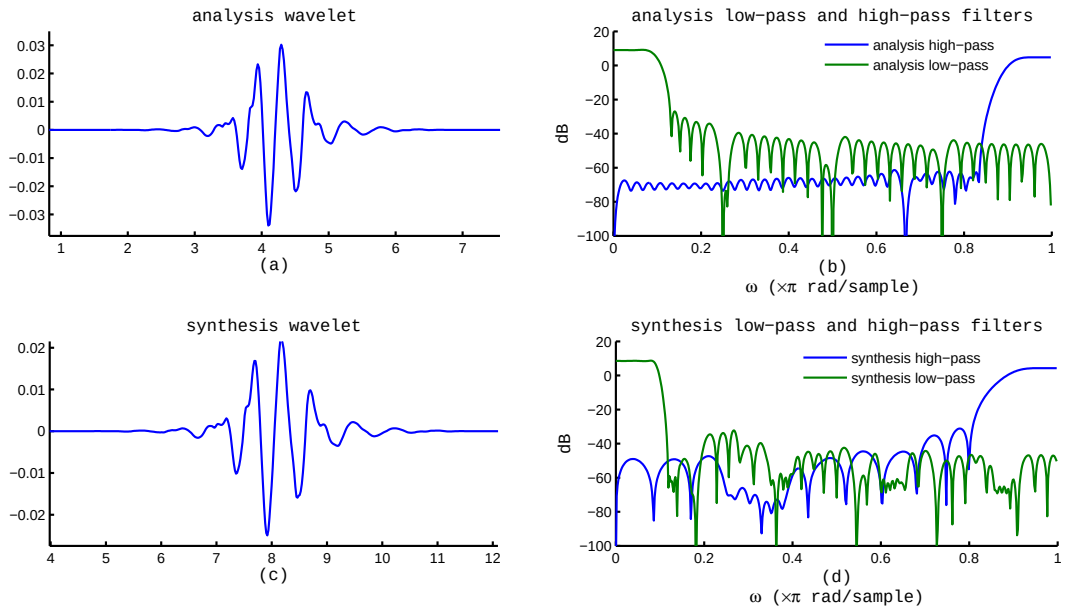

Figure 4.6. $(\frac{8}{11}, \frac{3}{11})$ RFB with two regularity orders. Left panels: Analysis (a) and Synthesis (c) wavelet functions, respectively. Right panels show the analysis (b) and synthesis (d) low-pass and high-pass filters' frequency response, respectively.

transition band compared to $(\frac{4}{7}, \frac{3}{7})$. Longer analysis filters are required for the former case, $70, 75$, as compared to $60, 60$ of the latter.

In verifying the iterative design method, other rates of RFB which are $(5/8, 3/8)$ and $(7/10, 3/10)$ with three regularity orders are considered. Fig. 4.7 and 4.8 illustrate frequency responses and the corresponding wavelet functions. The design parameters are shown in table 4.1.

Table 4.1. The filter design parameters for the examples.

	Iterative method				
	$(4/7, 3/7)$, $K = 2$	$(8/11, 3/11)$, $K = 2$	$(5/8, 3/8)$, $K = 3$	$(7/10, 3/10)$, $K = 3$	$(8/13, 5/13)$, $K = 1$
N_0, N_1	$60, 60$	$73, 78$	$63, 70$	$75, 85$	$65, 110$
ω_{sLP}	$\frac{\pi}{7} + .04\pi$	$\frac{\pi}{11} + .035\pi$	$\frac{\pi}{8} + .04\pi$	$\frac{\pi}{10} + .035\pi$	$\frac{\pi}{13} + .035\pi$
ω_{pLP}	$\frac{\pi}{7} - .01\pi$	$\frac{\pi}{11} - .01\pi$	$\frac{\pi}{8} - .01\pi$	$\frac{\pi}{10} - .01\pi$	$\frac{\pi}{13} - .01\pi$
ω_{sHP}	$\frac{6\pi}{7} - .06\pi$	$\frac{10\pi}{11} - .07\pi$	$\frac{7\pi}{8} - .055\pi$	$\frac{9\pi}{10} - .055\pi$	$\frac{12\pi}{13} - .045\pi$
ω_{pHP}	$\frac{6\pi}{7} + .02\pi$	$\frac{10\pi}{11} + .02\pi$	$\frac{7\pi}{8} + .03\pi$	$\frac{9\pi}{10} + .025\pi$	$\frac{12\pi}{13} + .02\pi$

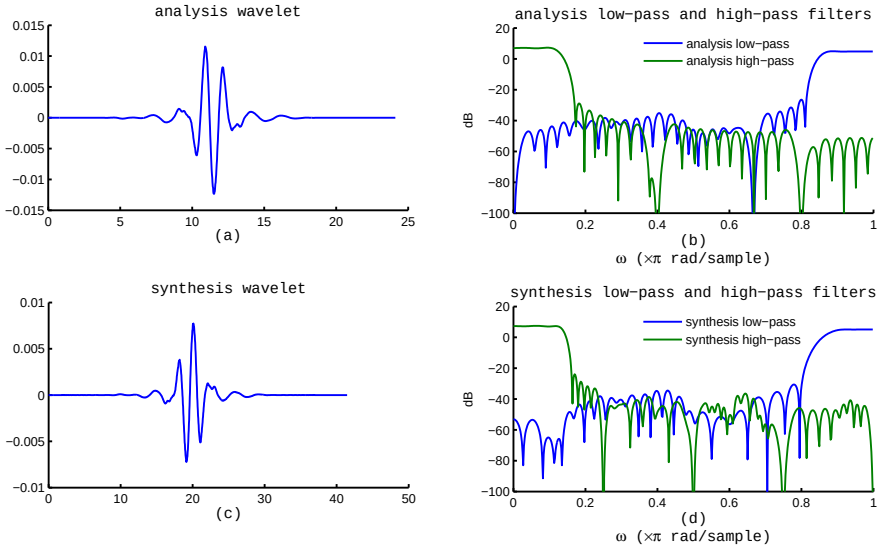

Figure 4.7. $(\frac{5}{8}, \frac{3}{8})$ RFB with three regularity orders. Left panels: Analysis (a) and Synthesis (c) wavelet functions, respectively. Right panels show the analysis (b) and synthesis (d) low-pass and high-pass filters' frequency response, respectively.

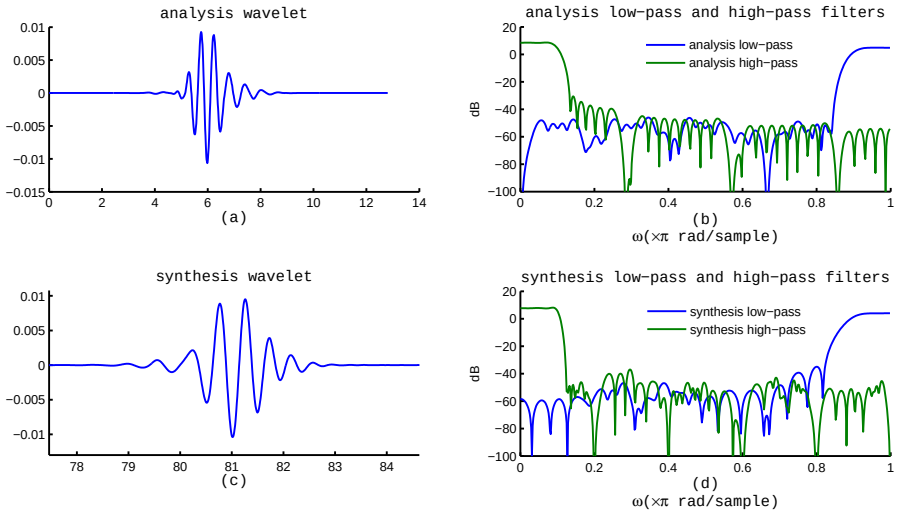

Figure 4.8. $(\frac{7}{10}, \frac{3}{10})$ RFB with three regularity orders. Left panels: Analysis (a) and Synthesis (c) wavelet functions, respectively. Right panels show the analysis (b) and synthesis (d) low-pass and high-pass filters' frequency response, respectively.

While designing RFB with higher regularity orders is possible, imposing such high regularity orders on long filters results in the coefficients of linear system of equations spanning a large dynamic range. For example, if the high-pass filter of N_1 taps are imposed with K regularity orders, the smallest coefficients for the resulting linear condition is 0 while the largest is $(N_1 - 1) \times (N_1 - 2) \ldots \times (N_1 - K - 1)$. Thus, if $N_1 = 91$

and $K = 5$, the largest coefficient is 61324560, which can potentially cause precision error during the optimisation.

In Fig. 4.9, the synthesis scaling functions of RFB $(\frac{5}{8}, \frac{3}{8})$ with one and four regularity orders are plotted. Note that the functions are obtained from two designs with the same filters' lengths. If we consider total variation measure (Gopinath and Burrus 1995), defined as

$$TV = \sum_i |\phi_J[i-1] - \phi_J[i]|, \tag{4.31}$$

where $\phi_J[i]$ is a discrete sequence representing the discrete scaling function, obtained from iterating the low-pass filter J times. The summation is computed over the support of the functions. The TV values, measured at $J = 12$ iterations, for RFB $(\frac{5}{8}, \frac{3}{8})$ with one and four regularity orders are 0.0082 and 0.0081, respectively, which shows smoother function from the four regularity order. Note that the same filter lengths, stop-band and pass-band edges parameters are used for both designs with the only difference is the number of regularity orders K. Fig. 4.9 illustrate the iterated low-pass filter being shifted on the same interval.

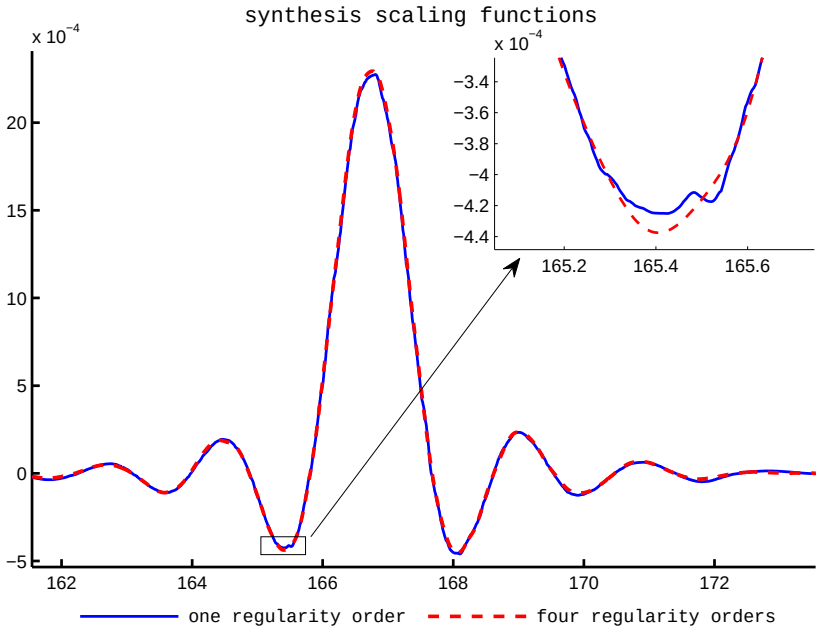

Figure 4.9. 12-time iterated synthesis low-pass filter of RFB $(\frac{5}{8}, \frac{3}{8})$ with one (solid blue) and four (dotted red) regularity orders, respectively.

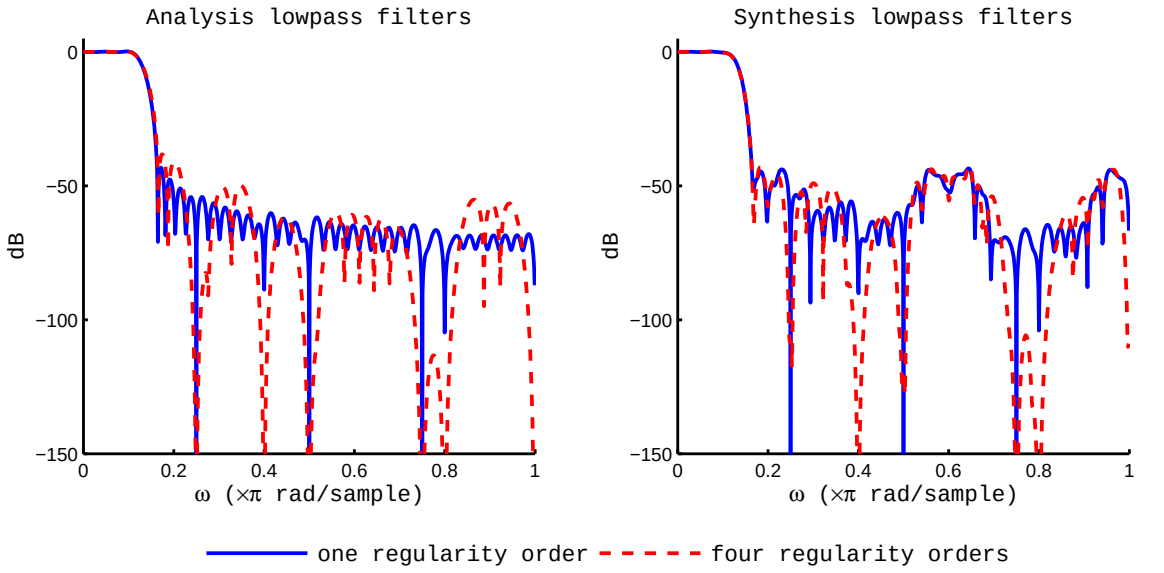

Figure 4.10. The analysis low-pass filters (left) and synthesis low-pass filters of RFB $(\frac{5}{8}, \frac{3}{8})$ with one (solid blue) and four (dotted red) regularity orders, respectively.

4.5 Convergence of the algorithm and remarks

The question of convergence of the design algorithm is an unsolved problem in this thesis even though extensive empirical observations suggest that the design algorithm always converges for the example cases presented in this chapter. The convergence occurs in less than 100 iterations in all experimental cases. We define the maximum error at each iteration step as

$$\max |\mathbf{h}_{HP}^{l-1} - \mathbf{h}_{HP}^{l}|, \tag{4.32}$$

where $\mathbf{h}_{HP}^{l-1}, \mathbf{h}_{HP}^{l}$ are the impulse responses of the analysis high-pass filter at step $l-1, l$, respectively. For each design experiment presented in this chapter, the iterative algorithm is randomly initialised for 100 times, at each time of trial the maximum absolute error at each iteration step (4.32) is recorded. The mean of such error for each iteration step is calculated and plotted in Fig. 4.11. The iterative algorithm converges when the error defined in (4.32) is less than 10^{-10}. The initialisation of the analysis low-pass and high-pass filters are generated with a Gaussian random generator with mean and variance being to $0, 1$, respectively.

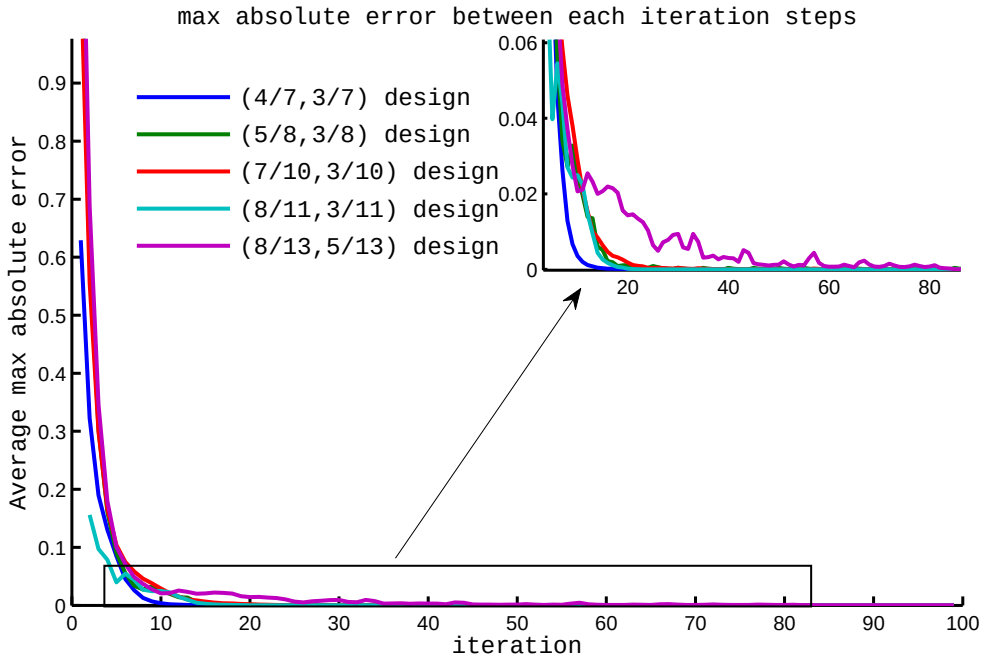

Figure 4.11. 100 run average of the maximum absolute error between two consecutive iterations.

The analysis low-pass and high-pass filters' lengths determine the number of linear constraints contributed to the PR condition. Hence the analysis high-pass filter is required to be long enough to satisfy all constraints, including PR contributed and to attain good stop band attenuation. For example, in examples 4.4.1 and 4.4.3, designing RFBs of $(4/7,3/7)$ and $(8/11,3/11)$ with two regularity orders require the analysis high-pass filters of 60 and 75 taps while the corresponding analysis low-pass filters are of 60 and 70 taps, respectively. The number of linear constraints resulted from PR condition for the two designs are approximately 17 and 13. This shows the number of degrees of freedom that are required for the analysis high-pass filters to attain good stop band attenuation and to drive the algorithm to convergence in the examples. In general, the number of linear constraints resulted from PR condition can be formulated as $\frac{N_0+N_1}{q} \pm C$ for N_0, N_1 being the analysis low-pass and high-pass filters' lengths; C represents some constant value. Hence, the total number of linear constraints for such optimisation is $\frac{N_0+N_1}{q} \pm C + R_{HP}$, with R_{HP} being the number of regularity conditions.

In this chapter, we pre-designed analysis low-pass filter to approximate q^{th}-band filters[10]. The PR condition (4.9) requires one of the q polyphase components of $Q_m(z) = F_m(z)H_m(z)$ to be a pure delay, which implies that it must be an q^{th}-band filter. By choosing the pre-designed analysis low-pass filter to be an approximate q^{th}-band filter, the resulting $Q_m(z)$ is also an approximate q^{th}-band filter for any analysis high-pass filter $\mathbf{h}_{HP}$ having a flat pass-band response in $[\frac{q-1}{q}\pi, \pi]$[11]. This increases the likelihood of convergence since at each iteration step, the obtained $\mathbf{h}_{HPmin}$ always approximates the algorithm solution, i.e. the corresponding $Q_m(z)$ being a q^{th}-band filter.

The iterative algorithm behaves similarly to the fixed point iteration method in which solutions of a high order polynomial are computed based on an iterative linear equations. The high order constraint in this problem, expressed in (4.25) and denoted as $f(\mathbf{h}_{HP}) = 0$ are rewritten as $g(\mathbf{h}_{HP}) = \mathbf{h}_{HP}$. The solution for the constraint is a fixed point of g.

The iterative algorithm discussed in this section fails to converge for the case $p_1 > 3$. In the proposed iterative approach, the high order p_1 constraints are relaxed to one (i.e. linear constraints). The relaxation is performed in (4.26), (4.27). In (4.27), each product term of the sum which results in p_1-order nonlinear constraints are linearised by setting $p_1 - 1$ polyphase components of the analysis high-pass filter to constant, i.e. equal to those of the previous iteration. Only one polyphase component is considered as unknowns, which leads to the constraints becoming linear for each iteration step. When $p_1 = 3$, the third order PR constraints were relaxed to sum of 3 sets of linear constraints with respect to the the three polyphase components of analysis high-pass filter $\mathbf{h}_{HP}$. Each set of the linear constraints corresponds to $\Gamma_j^l[n]$ as in (4.27) for $j = p_0, \ldots, q-1$ representing the index of the unknown polyphase component. Hence, for $p_1 > 3$, such relaxation from high order constraints to linear leads to failure in attaining the fixed point solution for the PR constraint of high order. For $p_1 > 3$ the error in (4.32) cannot be reduced sufficiently to satisfy the convergence condition. In all our empirical studies with $p_1 > 3$, the algorithm will find suitable filters (provided they are of sufficient lengths) with reconstruction error of 10^{-5}, despite not reaching convergence. The precise value varies with the design parameters such as the filter lengths and cut-off frequencies.

[10] q^{th}-band filter is defined as filters with pass-band response in the region of $[\frac{k_0\pi}{q}, \frac{k_1\pi}{q}]$ for intergers $k_0, k_1; k_0 < k_1 \leq q$ and one of its q-polyphase is a pure delay

[11] Such frequency response relationship is a result of the alias free condition (4.8).

We propose in cases of In such cases $p_1 > 3$ that only two polyphase components of $\mathbf{h}_{HP}$ out of p_1 polyphases should be used as unknowns in each iteration step in dealing with PR condition. Thus, (4.26) becomes:

$$\Gamma^l[n] = \sum_{j=p_0}^{p_0+1} \Gamma_j^l[n] = 0, \tag{4.33}$$

for

$$\Gamma_j^l[n] = \sum_{n_i \in K_n = \{K_n^r\}_{r\in\mathbb{N}}} a_r \Big\{ \prod_{i=0}^{p_0-1} \mathbf{h}_i[n_i] \Big\} \prod_{i=p_0, i\neq j}^{q-1} \mathbf{h}_i^{l-1}[n_i]\mathbf{h}_j[n_j], \tag{4.34}$$

$\Gamma_j^l[n]$ in this case only takes two values of $j = p_0, p_0+1$ which corresponds to the unknowns of first and second polyphase components of $\mathbf{h}_{HP}$ whilst other polyphase components in (4.33) are known from the solution of the previous step $l-1$ (i.e. $\mathbf{h}_i^{l-1}[n_i]$, $i = p_0+2, \cdots, q-1$ are known) . Other steps of the iterative algorithm remains the same. Such limit of j values in (4.33) improves the likelihood of convergence since the constraint is now relaxed from second order to first. However, at the same time we limit the number of variables contributing to satisfy PR conditions (only two polyphase components of $\mathbf{h}_{HP}$ are used as variables for PR condition) which leads to longer analysis filter $\mathbf{h}_{HP}$ required. Example 4.5.1 illustrates a case of $p_1 = 5$, designed base on the proposed modification.

Example 4.5.1. *RFB* $(8/13, 5/13)$ *with one regularity order is considered. Hence,* $p_1 = 5$ *in this example. The filter lengths are* $65, 110$*, dilation factor of* $13/8 = 1.625$*. The designed filters' responses and the corresponding constructed wavelet functions are illustrated in Fig. 4.12.*

4.6 Chapter summary

In this chapter, the design of bi-orthogonal two channel rational filter bank with arbitrary re-sampling ratios and multiple regularity orders is proposed, which is a generalisation of that of chapter 3. Thus, it began with a discussion of the more general conditions for imposing regularity on the filter bank structure. This enables the flexibility of quality factor Q in the resulting constant Q-transform or more general RADWTs. Local optimisation method as discussed in section 3.3.1 can be applied for all design parameters p_0, p_1, q that satisfy PR necessary conditions (2.1). Such method however relies much on a line-search algorithm to solve the nonlinear constraint optimisation

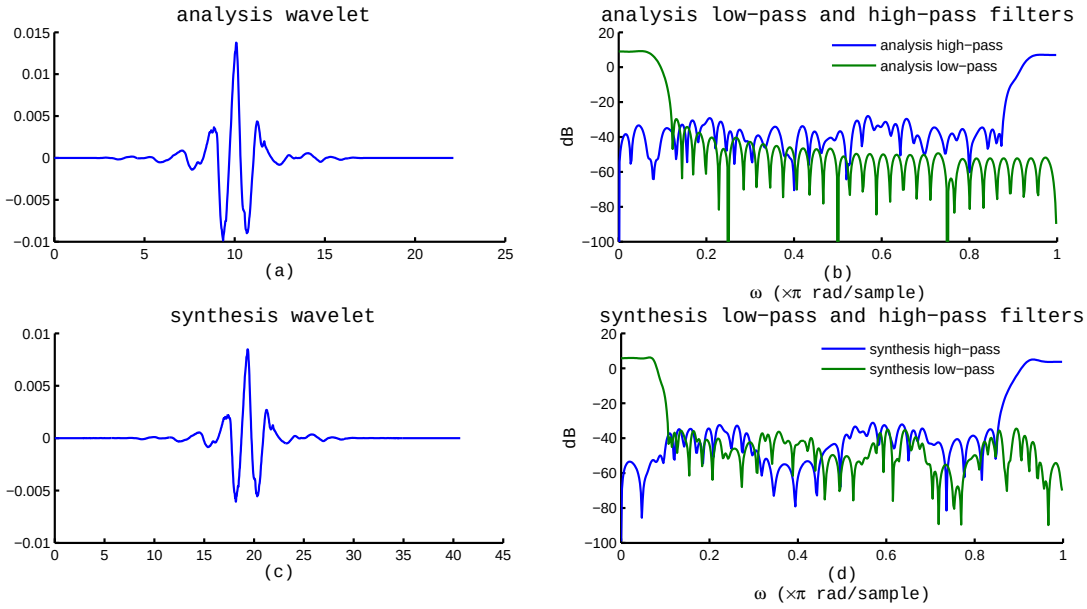

Figure 4.12. $(\frac{8}{13}, \frac{5}{13})$ RFB with one regularity order (modified iterative approach). Left panels: Analysis (a) and Synthesis (c) wavelet functions, respectively. Right panels show the analysis (b) and synthesis (d) low-pass and high-pass filters' frequency response, respectively.

problem, provided an approximate solution to the problem is pre-obtained to feed the algorithm. Thus, for high order q constraints and long filters, the algorithm complexity increases significantly. An iterative algorithm is proposed and presented in section 4.3.1. The algorithm decomposes the original nonlinear problem into a sequence of quadratic problems with linear constraints. Even though proof of the convergence is still an unsolved problem, we empirically investigated the iterative maximum error between successive steps against random initialisations. It shows that the the algorithm converges in less than 100 iterations in all design examples. Some experiments to demonstrate the use of our designed RADWTs in applications such as denoising and signal separations based on basis pursuit principle are presented in the next chapter.

Chapter 5

Biorthogonal RADWT: Applications and discussions

THIS chapter explores some applications for the RADWT designs presented in chapters 3 and 4. They apply to a wide variety of real-world signals, including speech and chirp signals. These signals share one common aspect: their bi-orthogonal RADWT representations are sparse. This property is exploited for denoising and signal separation based on basis pursuit (Chen *et al.* 2001). The presented experimental results show the effectiveness of using bi-orthogonal RADWTs with dyadic wavelet transforms to construct dictionary for the basis pursuit problem. Signal separation on chirp signals and narrow band interferences are used as illustrative examples of this technique.

5.1 Introduction

The topic of sparse signal representation has raised much interest from researchers (Akçakaya and Tarokh 2008b, Gribonval and Nielsen 2003) due to its fruitful application to areas such as signal compression and coding (Teschke 2007) which has enabled compact storage and rapid transmission of information. For example, if the signals to be compressed are known to have sparse representations in some transform domain, then they can be expressed or approximated by a small number of components in that domain. Many transform bases and frames have been used in search of sparsity for signals of various classes. Examples include short time Fourier transform (STFT), discrete cosine transform (DCT), wavelet transforms, ..., etc. Recently, Selesick (Selesnick 2011c) has adopted the RADWT in search for sparsity. It is expected that signals of an oscillatory nature, such as EEG, and speech are well-suited for decomposition into a dictionary containing low and high resonance components, which corresponds to RADWTs of low and high quality factors Q, respectively (Bayram and Selesnick 2009a, Selesnick 2011a). The transforms used in the existing literature are redundant and based on non-FIR filters.

In this chapter, we attempt to take advantage of the bi-orthogonal RADWTs designed in chapters 3 and 4 in attaining sparse representation of signals such as the TIMIT speech dataset (Garofolo *et al.* 1993). Denoising of TIMIT speech using the bi-orthogonal RADWT representation is presented, whose results are compared against other dyadic wavelet transforms. It is followed by some signal separation based on the *basis pursuit* principle, and uses a dictionary constructed from a concatenation of critically-sampled RADWTs of various Q factors. In the literature, over-complete RADWTs are used for constructing dictionaries for signal separation/decomposition based on *basis pursuit*. This was first investigated in (Selesnick 2011b), where it was termed *resonance based* signal separation. Here we construct our dictionary based on critically-sampled RADWTs in mixture with dyadic wavelet transforms to separate the oscillatory and non-oscillatory components of signals. Detailed work is discussed in section 5.2.3. In section 5.3, signal separation of chirp signals mixed with sinusoidal interferences is discussed. Section 5.4 provides the concluding remarks and chapter summary.

5.2 Speech signal processing

The speech signals used for the experiments in this section are from a corpus of phonemically and lexically transcribed speech of American English speakers of different sexes and dialects. The corpus is designed by Texas instruments and Massachusetts Institute of Technology (TIMIT) for automatic speech recognition research.

5.2.1 Comparing sparsity measures of TIMIT speech signals

RADWTs can be advantageous in representing signals of an oscillatory nature due to its flexible dilation factor over conventional dyadic wavelets. In assessing the suitability of different signal representations, the sparsity of appropriate classes of signals is usually a useful proxy for representational efficiency. Fundamentally, sparsity is a measure of how much of a signal's energy is packed into few coefficients. In this experiment, we apply two sparsity measures reported in (Hurley and Rickard 2009), namely *GINI index* and *pq-mean* (for $p = 1, q = 3$), on wavelet transformed speech signals. The sparsity measures are chosen as they are shown to satisfy all criteria for effective sparsity measures, as discussed by (Hurley and Rickard 2009). *GINI index* is defined as

$$GINI = 1 - 2\sum_{k=1}^{N} \frac{\mathbf{x}[k]}{\|\mathbf{x}\|_1}\Big(\frac{N-k+1/2}{N}\Big), \tag{5.1}$$

where $\mathbf{x}[n]$ represents ordered data such that $0 \leq \mathbf{x}[1] \leq \mathbf{x}[2] \leq \ldots \leq \mathbf{x}[N]$; *pq-mean* for $p = 1, q = 3$ can be expressed as

$$pq_{mean} = -\Big(\frac{1}{N}\sum_{k=1}^{N}\mathbf{x}[k]\Big)^{\frac{1}{3}}\Big(\frac{1}{N}\sum_{k=1}^{N}\mathbf{x}[k]^3\Big), \tag{5.2}$$

where $\mathbf{x}[n] \geq 0$ for $n = 1, \ldots, N$. The considered signals are taken from the commonly used TIMIT database (Garofolo *et al.* 1993) of phonemically and lexically transcribed speech of American English speakers. The quantification is performed on a set of 100 TIMIT signals from both male and female speakers, being analysed by our RADWT 6/5 as it can approximate the psychoacoustic bark scale (Fastl and Zwicker 2007). Comparisons are made with the dyadic wavelet transforms, `db5` and `db45`, the orthogonal Daubechies wavelet of 5, 45 regularity orders, discrete Meyer wavelet `dmey`, a FIR based approximation of the Meyer wavelet and bi-orthogonal spline wavelet with decomposition and reconstruction regularity orders of 8 and 6, respectively (`bior6.8`).

The choice of dyadic DWTs are made to be representative for different types of dyadic wavelets. They include low and high regularity order DWTs and orthogonal and bi-orthogonal DWTs. The discrete Meyer `dmey` is a dyadic DWT which uses filters with good frequency selectivity.

The rational 6/5 discrete wavelet transforms are iterated for 15 levels, and all dyadic wavelets are iterated for 4 levels, to equalise the range of resolutions captured by the two transforms, since $(\frac{5}{6})^{15} \approx (\frac{1}{2})^4$. To take into account the sub-band energy gained at each decomposition level due to the scale dependent norm of the designed RADWT, the wavelets coefficients of each sub-band are multiplied by a compensation constant defined as $\mathbf{b} \odot \mathbf{w}$; where $\mathbf{w}$ is the column vector representing the wavelets coefficients, $\odot$ denotes the element-wise multiplication of vectors $\mathbf{b}$ and $\mathbf{w}$; $\mathbf{b}$ is defined to take into account the scale dependent norm of the reconstruction wavelet functions such that for any index k such that the coefficient $\mathbf{w}(k)$ corresponds to the weight of any analysis wavelet function at level n_0; ψ_{n_0} is the synthesis wavelet function at the same level, defined by iterating the synthesis filters for n_0 times; $\|.\|_2$ denotes the l^2 norm. The *scale dependent norm* adjustment is verified using Gaussian noise signals, where the sparsity measures are compared between 4-level dyadic wavelet transforms, 15-level RADWT 6/5 and untransformed data.

$$\mathbf{b}[k] = \|\psi_{n_0}\|_2 \tag{5.3}$$

Fig. 5.1 illustrates the comparisons as the sparsity measures are approximately equal between transformed and non-transformed noise data. One hundreds white Gaussian noise signals of 0 mean and 1 variance is considered for the experiment. It should be noted that, for white Gaussian noise signals, the representation sparsity should not differ between transform and non-transform data. This is clearly shown in Fig. 5.1. The sparsity measures comparison of speech signal dataset is illustrated in Fig. 5.2 and 5.3. In Fig. 5.2, RADWT 6/5 outperforms dyadic wavelet transformed and non-transformed TIMIT signals, i.e. greater sparsity measures are attained for RADWT coefficients. To better illustrate the distribution of sparsity measure for each wavelet transform method, normalised histogram is constructed and shown in Fig. 5.3.

This experiment shows the RADWT 6/5 representation for TIMIT signals can achieve better sparsity when compared with existing dyadic DWTs. The normalised histograms in Fig. 5.3 shows RADWT coefficients distribute in greater value of sparsity measures

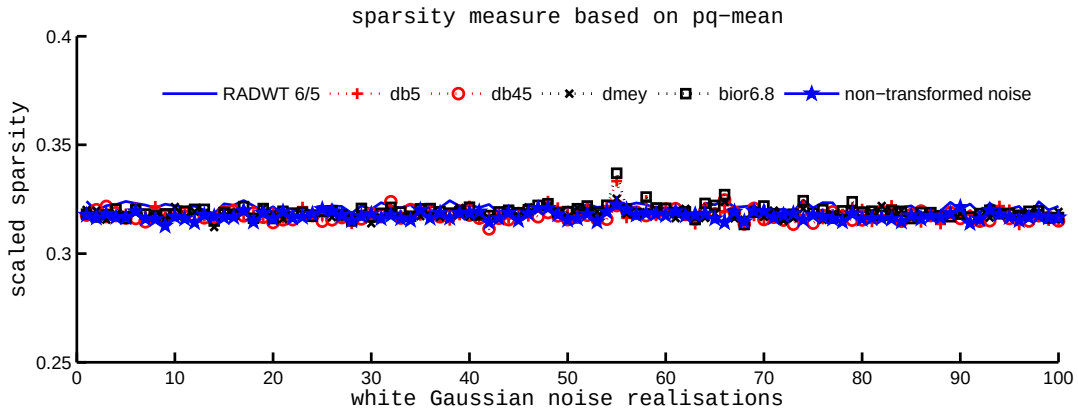

(a) Sparsity measure of Gaussian noise (based on pq-mean)

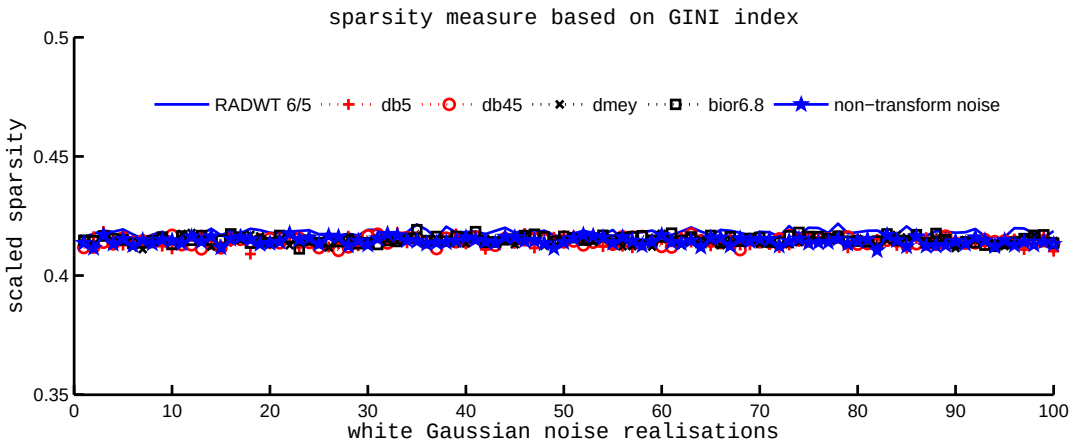

(b) Sparsity measure of Gaussian noise (based on GINI index))

Figure 5.1. Sparsity measures of white Gaussian noise based on pq-mean (a) and GINI index (b). For both plots, a higher numerical value indicates a greater sparsity in the representation. In the two plots: blue solid trace represents sparsity measures of the coefficients resulted from RADWT 6/5 transform on TIMIT signals; $+, \circ, \times, \diamond, \star$ traces represent the results of dyadic wavelets `db5`, `db45`, `dmey` and `bior6.8` on non-transform data, respectively.

as compared to other dyadic wavelet transform coefficients. The non-transformed data shows least sparse representation as expected.

5.2.2 Denoising of TIMIT speech signals based on RADWTs

In this experiment, the advantage of sparse representations for the TIMIT signals is directly exploited for denoising. Though there are more efficient techniques for speech denoising than wavelets (Chen and Selesnick 2013) which requires higher redundancy

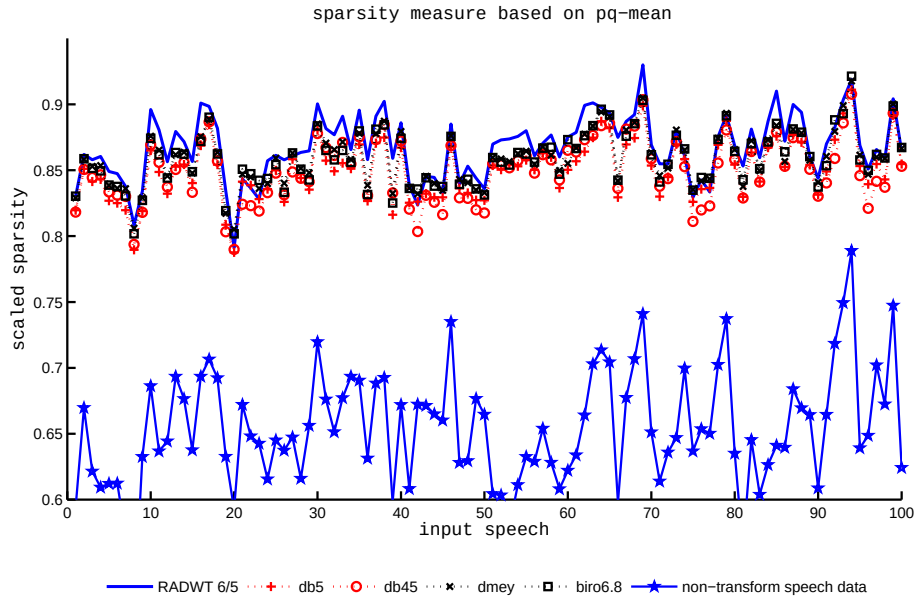

(a) Sparsity measure of speech signals (based on pq-mean)

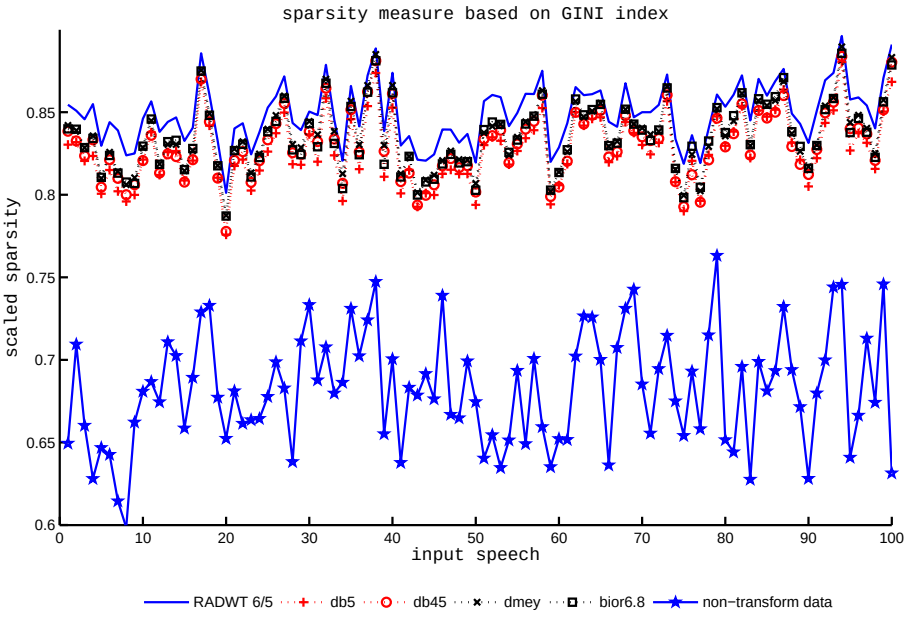

(b) Sparsity measure of speech signals (based on GINI index)

Figure 5.2. Sparsity measures of TIMIT speech signals based on pq-mean (a) GINI index (b). For both plots, a higher numerical value indicates a greater sparsity in the representation. In the two plots: blue solid trace represents sparsity measures of the coefficients resulted from RADWT $6/5$ transform on TIMIT signals; $+, \circ, \times, \diamond, \star$ traces represent the results of dyadic wavelets `db5`, `db45`, `dmey` and `bior6.8` on non-transform data, respectively.

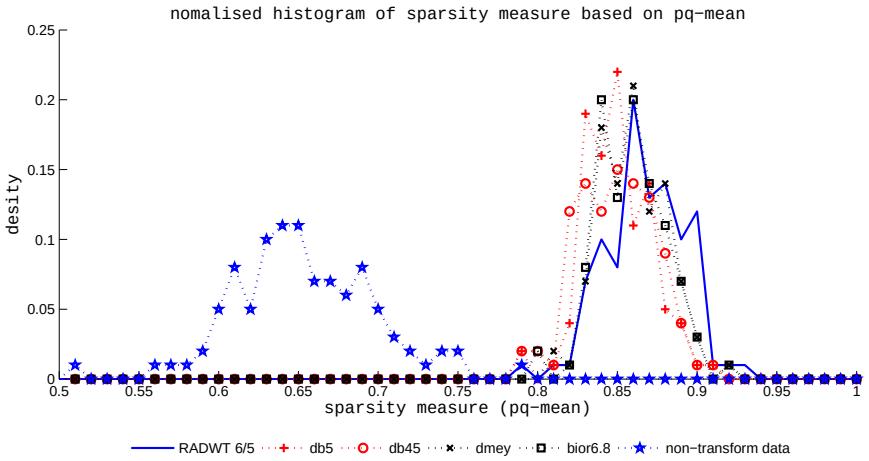

(a) normalised histograms of the signals' sparsity measure (pq mean)

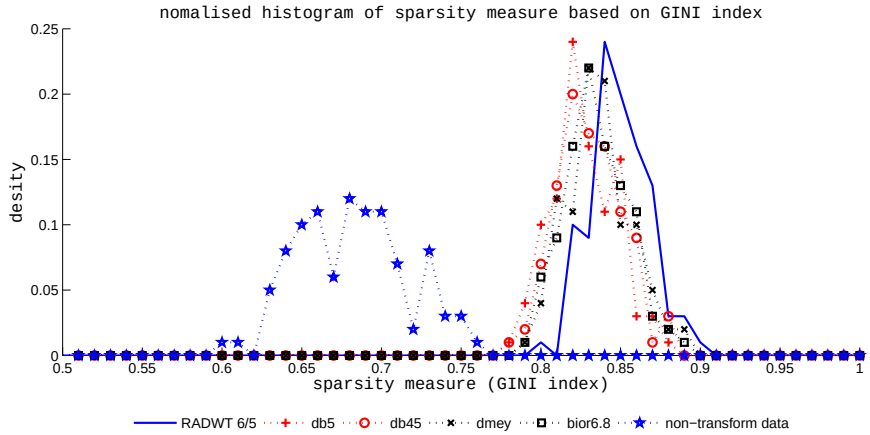

(b) normalised histograms of the signals' sparsity measure (GINI index)

Figure 5.3. The normalised histograms of the signals' sparsity measures. In the two plots: blue solid trace represents sparsity measures of the coefficients resulted from RADWT $6/5$ transform on TIMIT signals; $+, \circ, \times, \diamond, \star$ traces represent the results of dyadic wavelets `db5`, `db45`, `dmey` and `bior6.8`

transforms and computational complexity, the experiment simply compares RADWTs' performance with other wavelet bases for denoising speech signals. The designed RADWT with dilation factor $6/5 = 1.2$ is again used since the bandwidths of the corresponding transform approximate the psychoacoustic Bark scale (Fastl and Zwicker 2007) to compare with conventional dyadic wavelets. Soft thresholding and *Stein's*

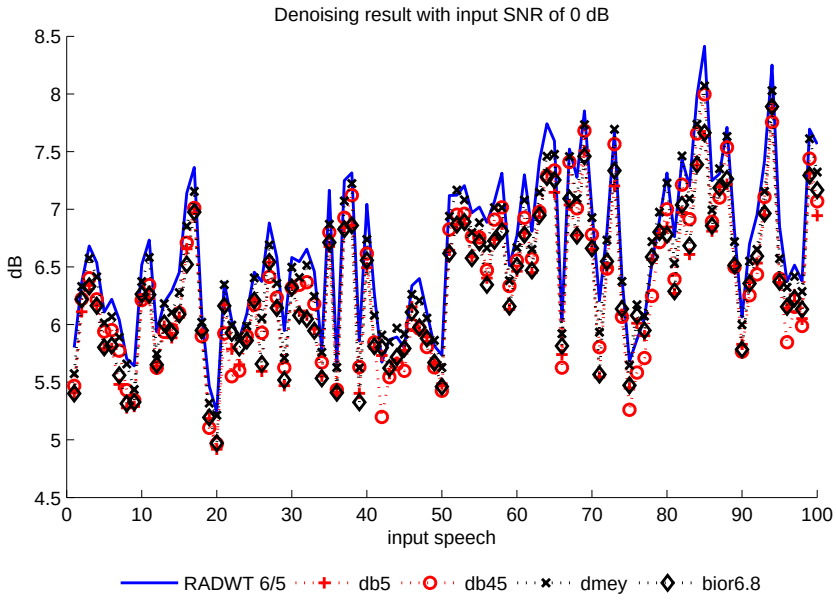

(a) output SNR for 0 dB input SNR

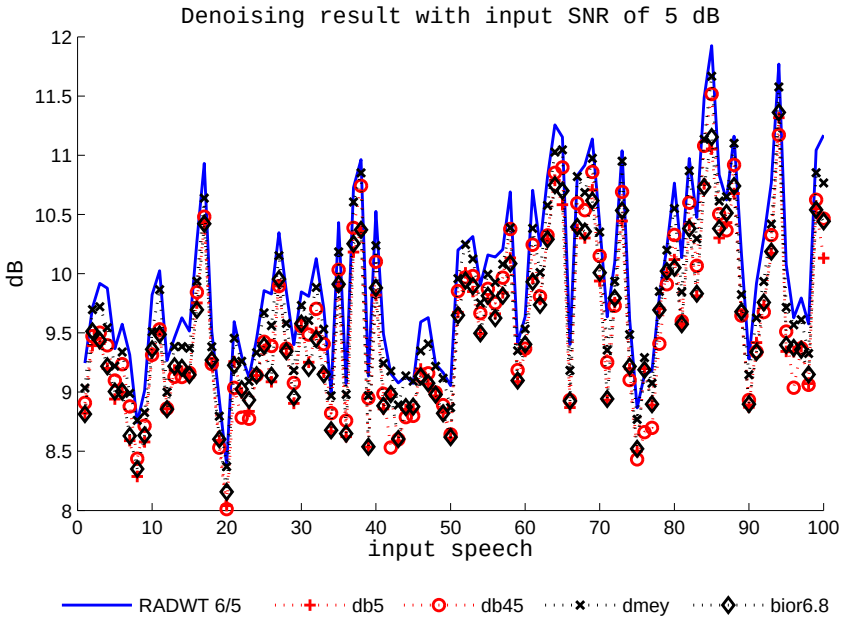

(b) output SNR for 5 dB input SNR

Figure 5.4. TIMIT speech signals denoising based on dyadic wavelet and RADWT $6/5$ on 100 different input speech signals of input SNR of $0, 5$ dB. In the two plots: blue solid trace represents denoising result of RADWT $6/5$; $+, \circ, \times, \diamond$ dotted traces represent the results of Daubechies wavelets $db5, db45, dmey, bior6.8$ respectively.

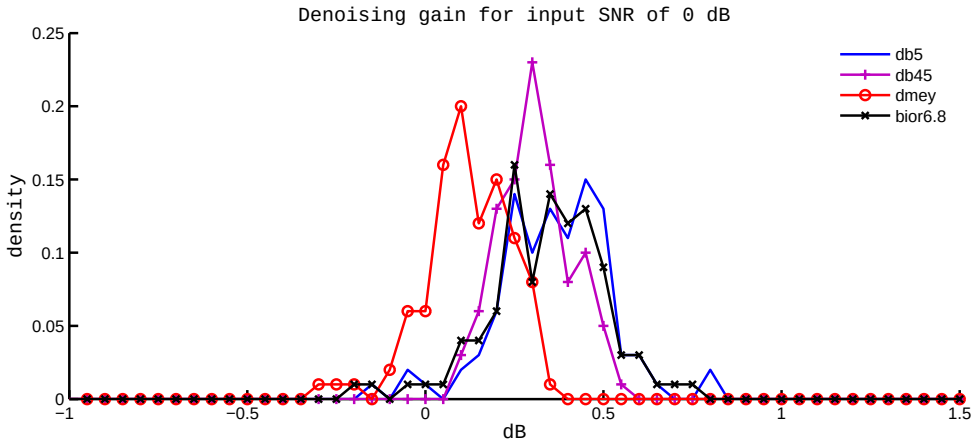

(a) histogram of the denoising gain for 0 dB input SNR

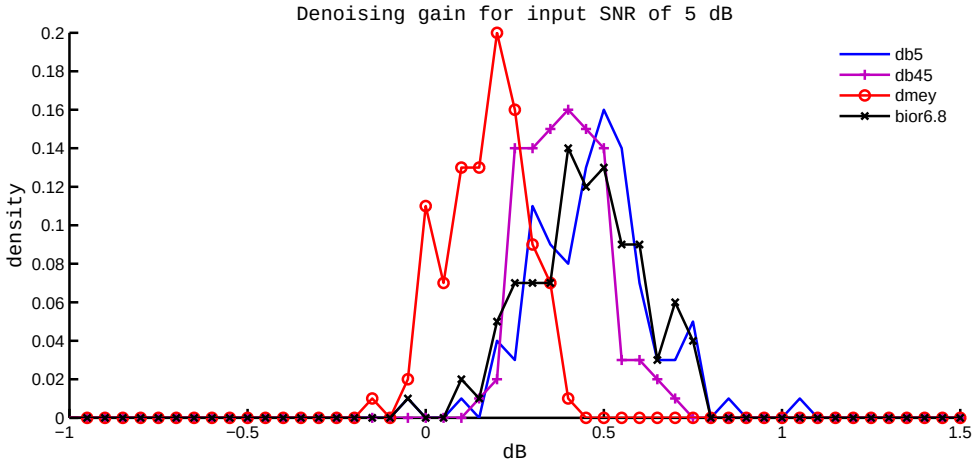

(b) histogram of the denoising gain for 5 dB input SNR

Figure 5.5. The normalised histograms of the denoising gain. In two plots: SNR of each input set resulted from RADWT 6/5 is subtracted by the corresponding SNR of dyadic DWTs `db5` (solid blue), `db45` (+ purple), `dmey` (∘ red) and `bior6.8` (× black), respectively. Top plot represents result of 0 dB input SNR while bottom corresponds to 5 dB input SNR. Positive gain denotes superior performance by RADWT and vice versa.

unbiased risk estimate-SURE (Stein 1981) are used for denoising operation and to estimate the threshold value at each level of the wavelet decompositions, respectively. These choices are empirically made to maximise the denoising performance. Other schemes are also considered such as hard thresholding and other threshold estimation techniques including fixed threshold estimate of $\sqrt{2\log l_x}$ (Donoho and Johnstone 1994) with l_x being the signal length and minimax threshold estimation (Donoho 1995).

Amongst the techniques, soft thresholding with SURE threshold estimate was found to give best SNR results. Hence, it is chosen for the denoising performance comparison.

The recovered signals' SNR, which associate to mean-squared error (MSE), is the measure for comparison. One hundred noise realisations are used and the average MSE is calculated for the final recovery signal SNR. Signals are corrupted by white Gaussian noise of input speech SNR of $0,5$ dB. The wavelet transforms are computed for $15,4$ levels for RADWT $6/5$ and dyadic transforms, respectively. The same set of TIMIT signals as in *experiment 1* is used for this experiment. The results are shown in Fig. 5.4, which demonstrates the denoising improvement. This is a result of the sparser representation property of RADWT $6/5$ as compared to dyadic DWTs, shown in *experiment 1*. To better illustrate the difference in denoising SNR for each dataset, the denoising SNR gain of RADWT compared to dyadic DWT is computed and defined as

$$G_{dyad}[i] = SNR_{RAD}[i] - SNR_{dyad}[i], \tag{5.4}$$

where $SNR_{RAD}[i], SNR_{dyad}[i]$ are the denoising output SNR of the RADWT and dyadic DWT of the speech dataset index $i = 1,\ldots,100$, respectively, subscript *dyad* represents the name of the dyadic DWT that is compared with the RADWT. In Fig. 5.5, normalised histogram of SNR difference $G_{dyad}[i], i = 1,\ldots,100$ between RADWT and dyadic DWTs are illustrated. Note that the positive dB gain ($G_{dyad} > 0$) denotes the superiority of RADWT over the dyadic DWT while negative gain shows otherwise. From the figure, it could be noted that the maximum attained gain for $0,5$ dB input SNR are $0.7, 1.05$ dB while the worst cases show losses of $0.3, 0.5$ dB, respectively. The RADWT outperforms dyadic DWTs in 87% and 93% of the testing signals in cases of $0,5$ dB input SNR, respectively.

5.2.3 Speech signal decomposition

In this experiment we demonstrate the use of RADWTs in signal decomposition based on the principle of *basis pursuit*. A speech signal is decomposed into separate oscillatory and non-oscillatory components for audio coding purpose, since such components can be more effectively modeled/encoded by mixed Q decompositions (Molla and Torrsani 2005). Similar decomposition is addressed in other papers in the literature (Levine 1998, Laurenti *et al.* 2007). In this thesis, the signals are decomposed based on based on constant Q transforms constructed from the designed bi-orthogonal RADWT.

In this experiment, our dictionary for the basis pursuit algorithm is constructed as a concatenation of our design design critically sampled two regularity order RADWT with dilation factor of 11/8 as reported in Example 3 of Sec. 4.4 and dyadic wavelet `db2`. One segment of speech signal (the word "I'm" spoken by a male speaker) is experimented with in a similar fashion as described in (Selesnick 2011b), to facilitate direct comparison. The resulting decomposition obtained is illustrated in Fig. 5.6. In our decomposition, the dictionary's redundancy is 2, which is much smaller than W. and Selesnick's. The decomposition is attained by finding minimal l^1 norm solutions for each wavelet representation as we optimise

$$\min_{\mathbf{w_1},\mathbf{w_2}} \lambda_1 \|\mathbf{b_1} \odot \mathbf{w_1}\|_1 + \lambda_2 \|\mathbf{b_2} \odot \mathbf{w_2}\|_1 \quad \text{subject to} \quad \Phi_{dy}^{-1}\mathbf{w_1} + \Phi_{RAD}^{-1}\mathbf{w_2} = \mathbf{s} \tag{5.5}$$

where Φ_{dy}, Φ_{RAD} are the square matrices representing the non-redundant wavelet transforms dyadic and RADWT 11/8, respectively; Φ_{dy}^{-1}, Φ_{RAD}^{-1} denote their inverse transform matrices. The transforms Φ_{dy}, Φ_{RAD} in (5.5) are selected to be sufficiently incoherent. In other words, the analysis/synthesis functions of the two wavelets have low correlation. The incoherence measure, defined as the maximum correlation between the wavelet functions from the two transforms, is proportional to the ratio between quality factors Q_1, Q_2 of the transforms Φ_{dy}, Φ_{RAD}. The measure is defined as (Selesnick 2011b)

$$\rho(Q_1, Q_2) = \sqrt{\frac{Q_1 + 1/2}{Q_2 + 1/2}}, \quad Q_2 > Q_1, \tag{5.6}$$

where Q_1, Q_2 are quality factors of the two transforms.

Wavelet decompositions are performed for 4 and 9 levels for dyadic and RADWT 11/8, respectively since $(\frac{1}{2})^4 \approx (\frac{8}{11})^9$; $\mathbf{w_1}, \mathbf{w_2}$ represent wavelet coefficient vectors of the dyadic transform and RADWT 11/8 , respectively; $\odot$ represents the element-wise multiplication of vectors $\mathbf{b_1}, \mathbf{b_2}$ and $\mathbf{w_1}, \mathbf{w_2}$, respectively; $\mathbf{b_1}, \mathbf{b_2}$ are the scale dependent norms of the reconstruction wavelet functions, constructed as in (5.3); $\mathbf{s}$ is the original speech signal; λ_1, λ_2 are scalar parameters, whose ratio determines the energy distribution between the two wavelet transforms. The l^1 minimisation problem in (5.5) is solved using the iterative SALSA algorithm (Afonso *et al.* 2010, Selesnick 2011c). The dyadic wavelet's role is to pick up the transient non-oscillatory component, which exhibits wide bandwidth and low Q factor characteristics while RADWT 11/8's role is to

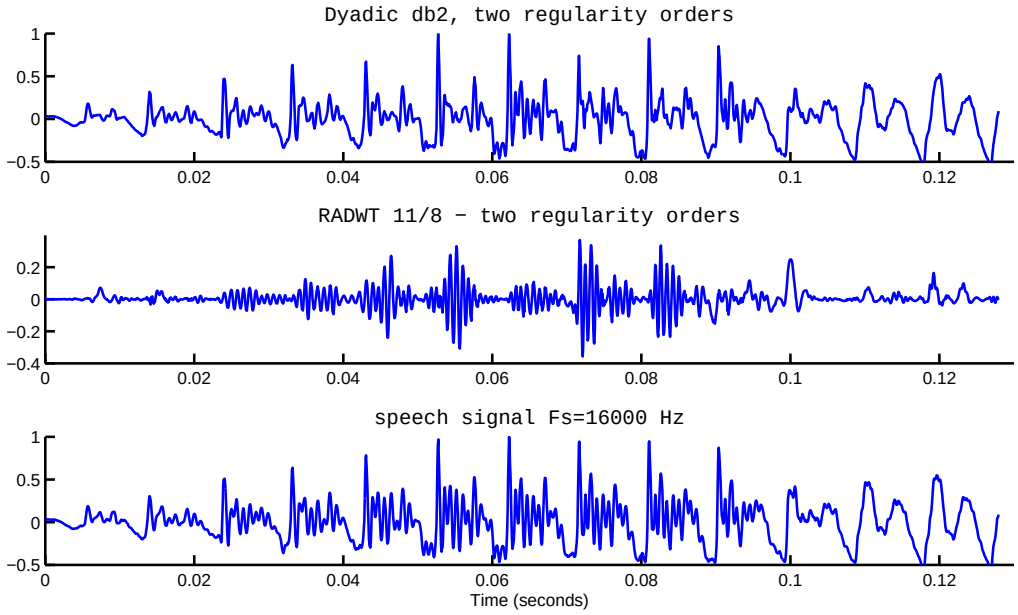

Figure 5.6. Speech signal decomposition (non-oscillatory and oscillatory components). Top panel represents the non-oscillatory components (picked up by dyadic wavelets transform) while middle panel shows the oscillatory part (picked up by the RADWT with dilation factor of $11/8$). Bottom is the original speech signal.

pick up the sustained oscillation counterpart of the signal, which exhibits narrow bandwidth and high Q characteristics [12]. It should be noted that in Fig. 5.6 middle panel, the oscillatory component exists as high frequency before $0.095s$ and low frequency after $0.095s$. This suggests that as a result of the l^1 minimisation in (5.5), the oscillatory characteristics of the signal are extracted out and not a simple frequency domain separation. Autoregressive (AR) model is then applied to both the oscillatory component and original speech signal for comparison. The signals are modeled with AR models, whose parameters are computed using *burg* (Burg 1968, Brockwell *et al.* 2005) and *covariance* (Marple Jr 1987) methods, with the ratio between standard deviations of the oscillatory component to original speech signal being 0.132 and a model order $p = 6$. Hence, the prediction error rate attained is slightly better than the reported value in the literature of 0.147, and with computational advantage of lower redundancy.

[12] In the extreme case, such two characteristics are the Dirac delta (non-oscillatory) and the sinusoidal (purely oscillatory) functions

In this experiment, we re-produce the speech decomposition described in literature (Selesnick 2011b) and demonstrate the use critically-sampled RADWT in signal separation based on basis pursuit principle. Slight improvement in prediction error in our case of 0.132 over the literature 0.147 with lower redundancy used for constructing the dictionary can be attained. Besides, critically-sampled RADWT is more suitable for use in conjunction with dyadic wavelet transforms in construction basis pursuit's dictionary. The dyadic wavelets possess various properties such as linear-phase (biorthogonal), existing from low to very high regularity orders (Daubechies), good frequency selectivity (discrete Meyer) which can be flexibly chosen for different types of signals.

5.3 Chirp signal separation from narrow band interference

5.3.1 Chirp signal separation from prolonged sinusoidal interference

The mixed Q signal separation in (5.5) can be applied for signal filtering, in situations which pure frequency domain filtering cannot be applied. In the following, we consider an example of a wide band signal interfered by narrow band sinusoids. Consider signal $s = s_I + s_S$, where s_I represents a low frequency sinusoidal interference with discrete frequency $\omega_d = .045\pi$ and s_S is a real linear chirp with instantaneous frequency ranging from $[0, \pi]$. We rewrite the equation (5.5) for this experiment as follows:

$$\min_{\mathbf{w_I}, \mathbf{w_S}} \lambda_I \|\mathbf{b_I} \odot \mathbf{w_I}\|_1 + \lambda_S \|\mathbf{b_S} \odot \mathbf{w_S}\|_1 \quad \text{subject to} \quad \Phi_S^{-1}\mathbf{w_S} + \Phi_I^{-1}\mathbf{w_I} = \mathbf{s}, \tag{5.7}$$

where Φ_S, Φ_I are dyadic `db1` DWT and RADWT 7/6, respectively. For such a mixture, purely frequency based analysis cannot separate s_I, s_S since they reside in the same frequency band at various times. Notch filter can possibly be used provided that we have knowledge about the discrete frequency (ω_d) and spectrum level of the sinusoid signal s_I. However, the notch filtering can partially or completely remove that frequency component from the original chirp signal. For unknown ω_d, l^1 minimisation, described in (5.7) can be used for the separation. The transforms' decomposition levels are 3 and 27, respectively. The time domain signal s and its spectrogram are illustrated in Fig. 5.7 (a) and Fig. 5.8, respectively. The resulting separated signals are illustrated in Fig. 5.7 (b), (c). In this experiment, the linear chirp behaves as a non-

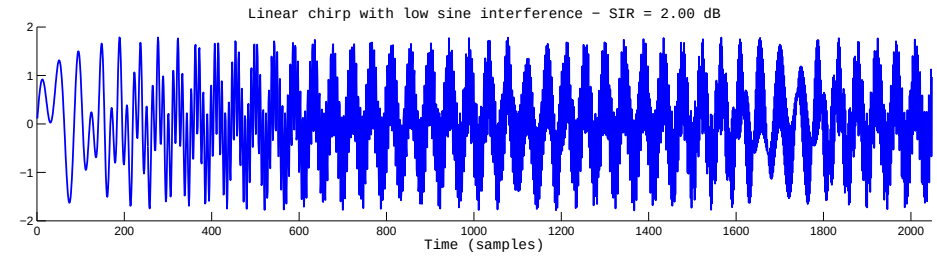

(a) The original interfered chirp signal

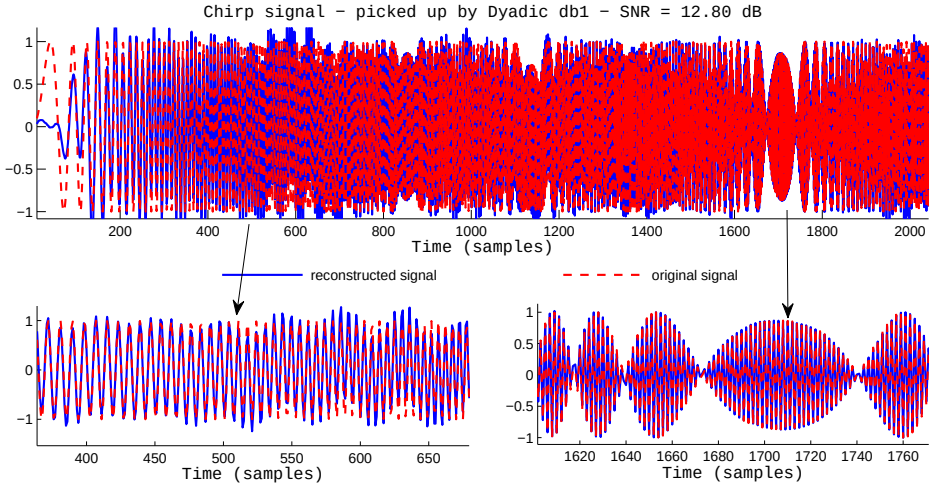

(b) Reconstructed chirp super-imposed with the original chirp signal

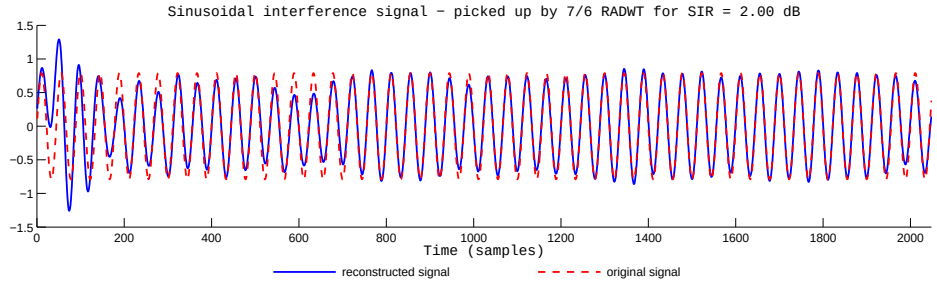

(c) Reconstructed interference super-imposed with the original interfered sinusoid

Figure 5.7. From top to bottom of (a) are: original signal s (mixture of chirp and sinusoid signal); (b) represents linear chirp signal and (c) is the sinusoid signal. Red dashed and solid blue traces are original and the reconstructed signals for in both (b) and (c), respectively.

oscillatory component in the sense that its constant frequency oscillations exist over infinitesimally short interval of time. It also exhibits wide bandwidth and low thus Q characteristic, which explains why it was well represented by the dyadic wavelet. The

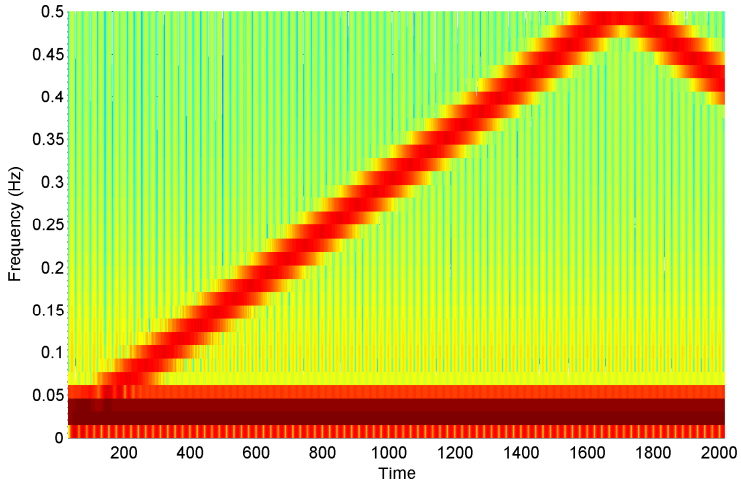

Figure 5.8. Spectrogram plot of signal s.

low frequency sinusoidal signal, on the other hand, has an oscillatory (high Q) characteristic and is therefore captured by the RADWT. This technique can thus be used to mitigate monochromatic interference at an unknown frequency. In this experiment,

Table 5.1. Reconstructed SNR versus SIR for linear chirp and prolonged sinusoidal signals separation

SIR	-13 dB	-8 dB	-3 dB	2 dB
$20\log_{10}\left(\frac{\lambda_I}{\lambda_S}\right)$	29.69 dB	35.04 dB	36.82 dB	38.56 dB
SNR	9.28 dB	10.6 dB	12.01 dB	12.80 dB

the choice of λ_I, λ_S of (5.7) is critical. These parameters vary depending on the input signal to interference ratio. Various signal to interference ratios (SIR) are tested and the recovered chirp signal to noise ratios (SNR) are computed. SIR is defined as the ratio of the original chirp's energy to the interference sinusoid's. The noise energy is defined as the square error between the original chirp signal and the reconstructed signal after the separation. For each case of input SIR the ratio λ_I/λ_S is empirically selected to attain optimal result of SNR. In table 5.1, the optimal resultant SNR versus input SIR and ratio λ_I/λ_S are shown. The results show how optimal choices of λ_I/λ_S vary with the input SIR. For example, greater SIR requires greater λ_I/λ_S ratio and vice versa which agrees well with the expression (5.7), i.e. when the ratio λ_I/λ_S increases less energy is distributed in $\mathbf{w_I}$ (interference) while more energy is distributed in $\mathbf{w_S}$ (signal).

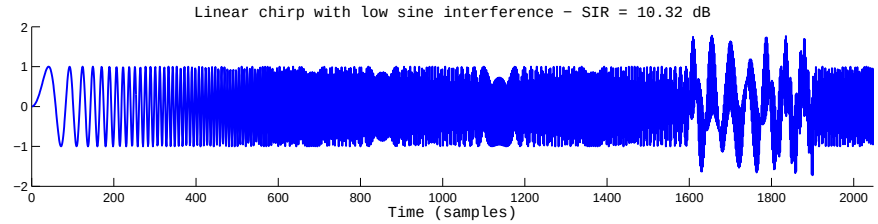

(a) The original interfered chirp signal

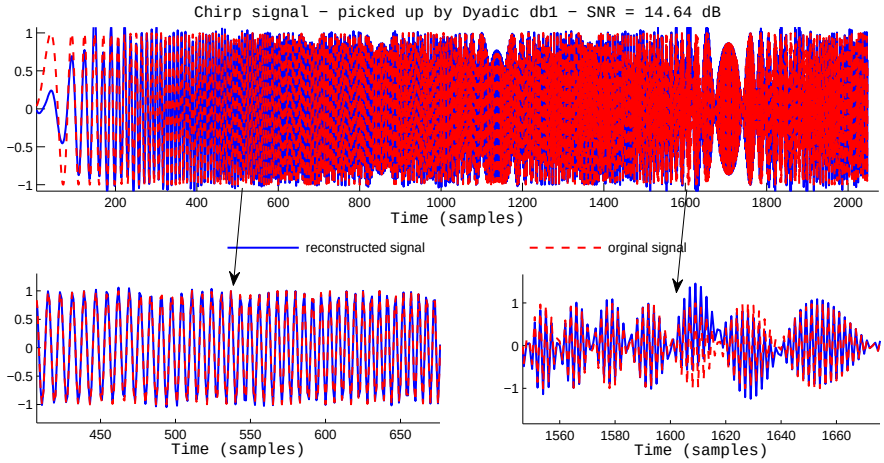

(b) Reconstructed chirp super-imposed with the original chirp signal

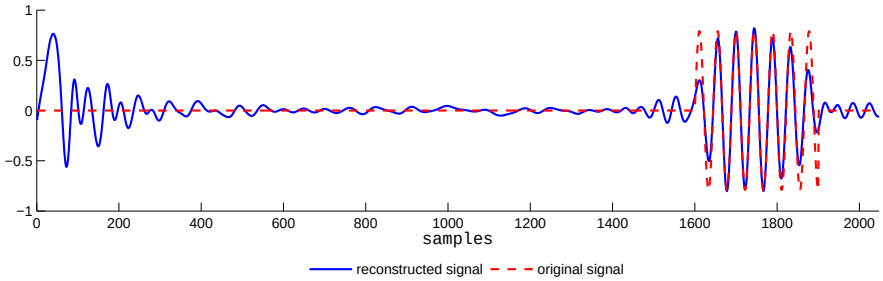

(c) Reconstructed short burst sinusoid super-imposed with the original interference

Figure 5.9. From top to bottom of (a) are: original signal s (mixture of chirp and sinusoid signal); (b) represents linear chirp signal and (c) is the sinusoid signal. Red dashed and solid blue traces are original and the reconstructed signals in both (b) and (c), respectively.

5.3.2 Chirp signal separation from short burst interference

As an extension of the previous experiment, we demonstrate in this experiment that a similar separation can be effective for wide bandwidth linear chirps suffering interference by *temporally sporadic* monochromatic source. In this situation, the sinusoid

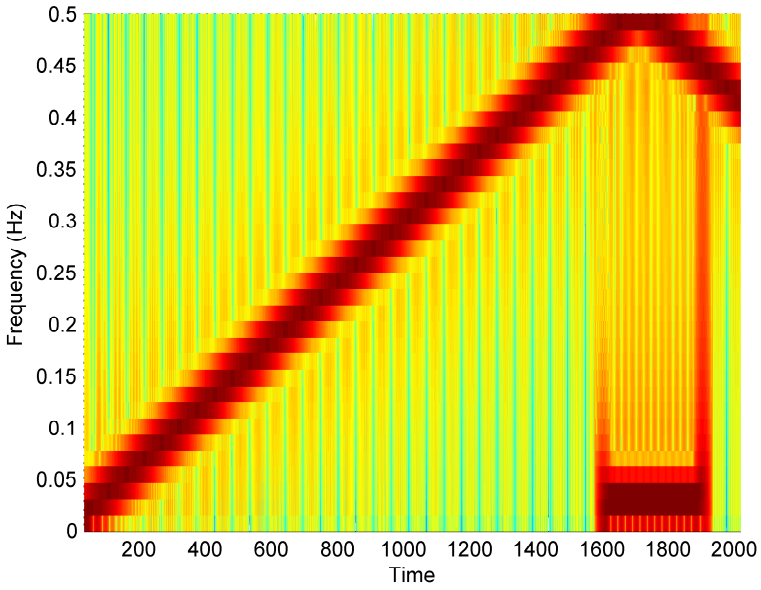

Figure 5.10. Spectrogram plot of signal s.

Table 5.2. Reconstructed SNR versus SIR for linear chirp and short burst sinusoid separation

SIR	-4.68 dB	0.32 dB	5.32 dB	10.32 dB
$20\log_{10}(\frac{\lambda_I}{\lambda_S})$	29.86 dB	35.37 dB	39.58 dB	44.58 dB
SNR	8.00 dB	10.18 dB	12.28 dB	15.41 dB

signal corresponding to one discrete frequency, exists only in a short interval of time as shown in Fig. 5.9 (c). The dictionary used for the signal separation consists of RADWT 7/6, and the dyadic `db1`.

The result illustrated in Fig. 5.9 (b) and (c) show that the RADWT can effectively extract the temporal sinusoid signal component from the mixture with linear chirp of 10.32 dB SIR to attain 14.64 dB output SNR. The decomposition levels are 27 and 3 for RADWT 7/6, and dyadic `db1`, respectively. The separated signals are plotted against their original expected signals, both are illustrated in Fig. 5.9 (b) and (c). The spectrogram of the original signal s is shown in Fig. 5.10. In table 5.2, the optimal resulted SNR versus input SIR and ratio λ_I/λ_S are shown. Again, the ratio λ_I/λ_S is empirically selected to attain optimal result SNR of each SIR case with some knowledge about the input SIR. In this experiment, it is more apparent how the optimal λ_I/λ_S varies with respect to the input SIR. It should be noted that the optimal ratio for $20\log_{10}(\lambda_I/\lambda_S)$ differs by approximately 5 dB from one case to the next, which equal to the difference in SIR

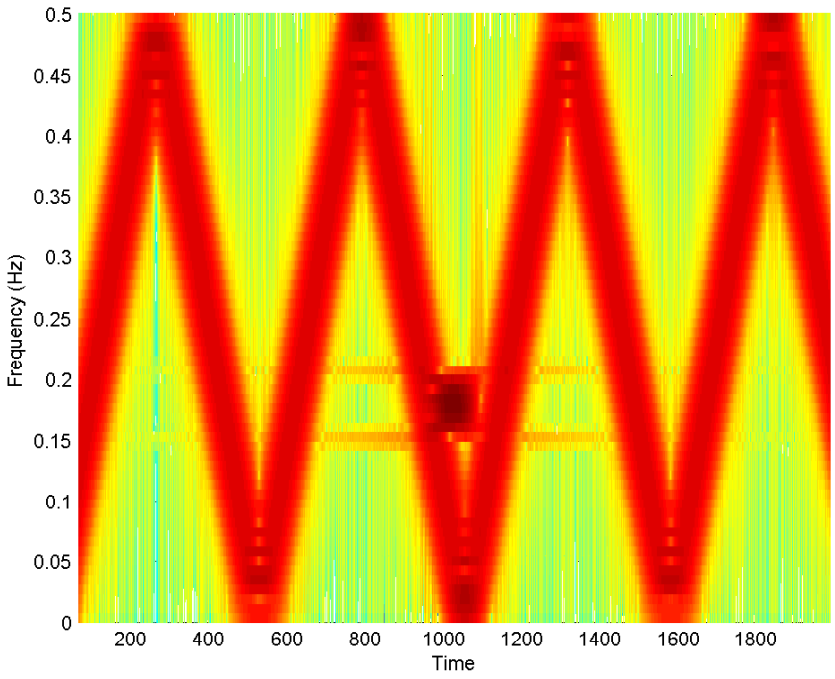

Figure 5.11. Spectrogram plot of signal s.

between two consecutive test cases. It is because λ_I/λ_S determines the energy ratio of the signal s_I, s_S resulting from the optimisation.

The experiments in section 5.3.1 and 5.3.2 show the effective separation of chirp signal from the low frequency sinusoid interference. However, if the narrow bandwidth interference is located in the middle or high frequency, the problem becomes more complicated. It is because to separate such high Q factor interference, a corresponding high Q RADWT is required. In the following, we present a similar separation with the narrow band interference locating approximately near the middle of the chirp bandwidth. The non-oscillatory behavior of the linear chirp signal can be made more significant by increasing the rate of frequency change over time, figure 5.11 illustrates the spectrogram of the analysed signal. The narrow band interference locating at near the middle of the chirp bandwidth requires a more oscillatory type of RADWT to pick up, hence the RADWT 11/10 of 3 regularity orders is used. The separation is shown in figure 5.12. It could be observed from figure 5.12 that the separation is possible in this case of mid-band interference even though the output SNR attained is 9.2 dB for 8 dB SIR which results in an approximate 4 dB loss compared to the low frequency short burst

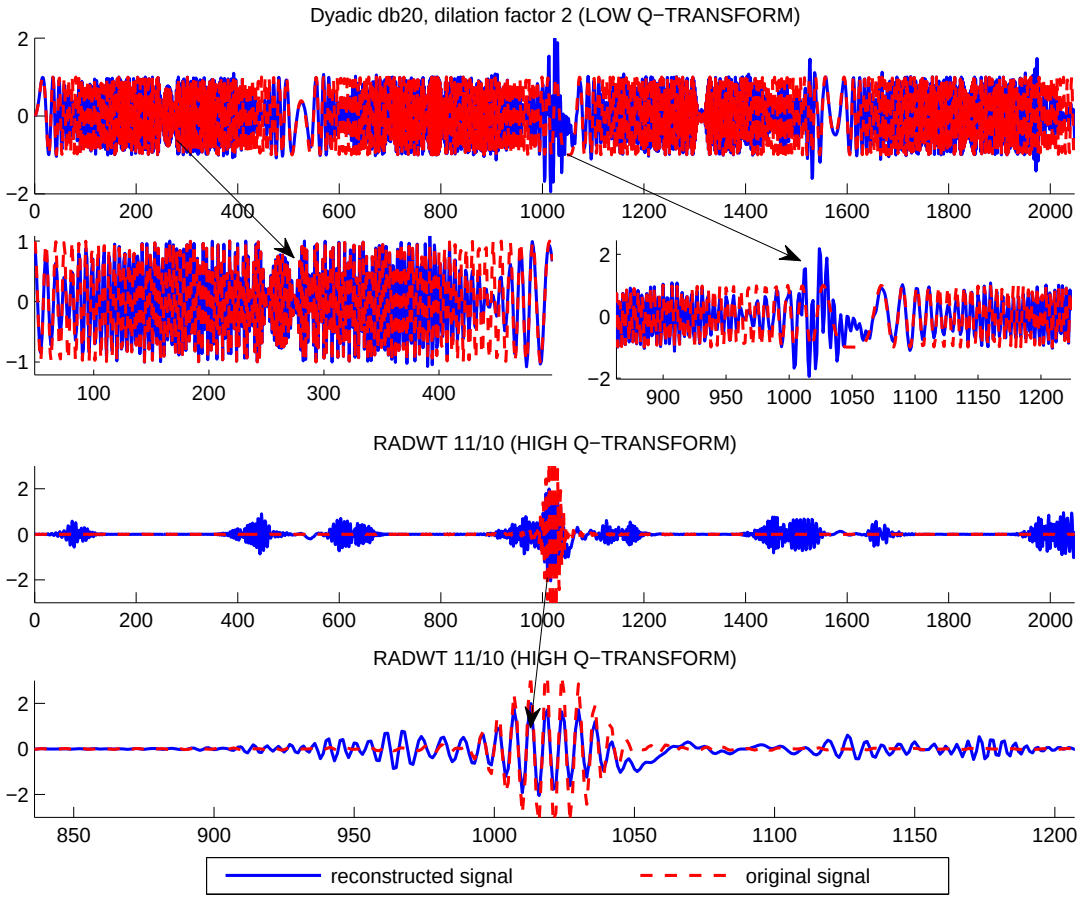

Figure 5.12. From top to bottom of are: original signal s (mixture of chirp and sinusoid signal); zoomed in region of the reconstructed linear chirp; the narrow band interfered signal and the zoomed in region of the narrow band interference. Red dashed and solid blue traces are original and the reconstructed signals, respectively.

case. Further study should be done for this case of interference since a more suitable transform should be used to extract the interference signal.

5.4 Concluding remarks and summary

From the experiments presented, we can summarise the key advantages of the RADWT designs as follow:

Constant Q-transform or wavelet transform with flexible Q-RADWTs are better suited to representing signals of an oscillatory nature with greater sparsity. This is shown in section 5.2.1 for TIMIT speech signals, which benefited from the bi-orthogonal RADWT

6/5. Bi-orthogonal RADWTs can effectively be used to separate sustained oscillation components of signals from the non-oscillatory ones based on l^1 minimisation as in (5.5), where they are used with dyadic wavelets to form the problems' dictionary.

In chirp signal separation experiments, basis pursuit problem with bi-orthogonal RADWT and dyadic DWTs dictionary have shown some effectiveness in recovering linear chirp signal from low frequency sinusoidal interference at an unknown frequency. However, the separation does not work in cases of high frequency sinusoidal interference since very high Q-RADWT is required to sparsely represent such signal. More appropriate bases/frames are required for such cases of interference. Experiments on the choices of λ_I/λ_S of (5.7) were considered. The results suggest that to find an optimal choice λ_I/λ_S, knowledge of the input SIR is required. The effect of regularity orders of the wavelets used in dictionary and the choice of decomposition levels are not yet investigated in this thesis due to scope limiting. The choices made in the experiments presented in this chapter are empirically based.

The experiments on chirp signal separation shows that such separation can be very useful in reconstructing wide-band signals corrupted by narrow-band interference sources which reside in the same frequency band. A similar demonstration was presented in (Duarte *et al.* 2006), in which *chirplet dictionary* (Baraniuk and Jones 1993) and *Fourier basis* were chosen to construct the incoherent bases dictionary. The presented method is based on *matching pursuit*, hence greedy algorithm, as differed from *basis pursuit* as presented in this paper, which can offer several advantages such as better sparsity and super-resolution over matching pursuit (Chen *et al.* 1998). Note that the re-sampling ratios of the RFB, and hence dilation factors, used in the basis pursuit algorithms are chosen to ensure incoherence between the transforms in the dictionaries.

In this chapter, *basis pursuit* algorithm is adopted for the signal separation experiments which allows inferring/separating signal in noiseless observations. However, in the presence of noise and exact representation could not be obtained, l^2-norm error can be imposed. The optimization can be formulated as

$$\min_{\mathbf{w}} \|\mathbf{w}\|_1 \quad \text{subject to} \quad \left\|\Phi^{-1}\mathbf{w} - \mathbf{x}\right\|_2^2 \leq \epsilon \tag{5.8}$$

where ϵ is a positive real parameter representing the l^2 penalty chosen in association with the noise level; Φ is a $N \times M$ matrix representing a redundant dictionary with $M > N$; (5.8) allows inferring $\mathbf{w}$ from the noisy observation as compared to the noiseless counterpart $\Phi^{-1}\mathbf{w} = \mathbf{x}$. Note that though Φ^{-1} represents a matrix, the

matrix is not explicitly stored since it is costly and impractical in problems involving long signals. However, the matrix-vector products $\Phi^{-1}\mathbf{w}$ can still be computed efficiently. For example, if Φ, Φ^{-1} represent a dyadic wavelet transform and the inverse transform matrices, a fast discrete wavelet and the inverse transform can be computed without requiring the actual transform and inverse matrices. In solving (5.8) (Figueiredo *et al.* 2007, Fuchs 2007), computation of the transposed matrix operation ${\Phi^{-1}}^t\mathbf{w}$ is required since the l^2 penalty can be expanded to

$$\left\|\Phi^{-1}\mathbf{w} - \mathbf{x}\right\|_2^2 \leq \epsilon \tag{5.9}$$

$$\Leftrightarrow \quad (\Phi^{-1}\mathbf{w} - \mathbf{x})^t(\Phi^{-1}\mathbf{w} - \mathbf{x}) \leq \epsilon \tag{5.10}$$

$$\Leftrightarrow \quad \mathbf{w}^t{\Phi^{-1}}^t\Phi^{-1}\mathbf{w} - \mathbf{w}^t{\Phi^{-1}}^t\mathbf{x} - \mathbf{x}^t\Phi^{-1}\mathbf{w} + \mathbf{x}^t\mathbf{x} \leq \epsilon \tag{5.11}$$

If Φ contains orthogonal bases or tight frames, the transposing operation simply involves the inverse operation. For dictionaries consisting of non-tight frames, explicitly defined matrix Φ^{-1} is required to compute its transposition. The proposed RADWTs are non-tight frames, hence its use the in constructing the redundant dictionary of (5.8) is limited to small scale problems when the stored and manipulated matrix can be within reasonable computational resources.

Chapter 6

Thesis conclusion and future work

THIS chapter summarises the key findings of the thesis and potential direction for future work.

6.1 Introduction

Since the discovery of dyadic wavelet transforms, the available literature has been dominated by studies on the construction of wavelet transforms from filter banks with various properties. Recently, finer frequency decomposition resulting from iterated rational rate filter banks or rational discrete wavelets have drawn greater attention. The rational structure leads to constant Q transforms whose Q factor is adjustable, which is a departure from conventional dyadic wavelets. The newly reported transform bases (frames), termed RADWTs in this thesis, enrich the existing bases in searching for sparse representation of signals from various classes. Representation sparsity is the key feature for many applications including compressive sensing (Candes and Romberg 2007, Candès 2006, Candes and Wakin 2008), denoising (Cands *et al.* 2008, Zhu 2008), signal separation (Selesnick 2010, O'Grady *et al.* 2005, He *et al.* 2007, Tropp 2006, Rickard 2007, Yilmaz and Rickard 2004), or in image processing (Mairal *et al.* 2008, Aharon and Elad 2008, Esther Leung *et al.* 2008), ...etc. Therefore, the design of rational discrete wavelet transforms has been addressed by many authors. The literature works are also categorised based on their approaches. This thesis investigates bi-orthogonal rational discrete wavelets, which has not been studied in the literature of RADWTs design. The resultant RADWTs are experimented with signals of oscillatory nature, which show encouraging results in applications such as signal coding and separation.

6.2 Thesis summary conclusion

In chapter 1, some background of time-frequency analysis and wavelet transform is discussed together with the motivation for developing rational dilation factor wavelets. The key issues to be addressed and contributions of the thesis are summarised.

In chapter 2, the design challenges of *iterated rational FBs* are discussed. The challenges prevent the iterated rational rate filter banks from behaving as the conventional dyadic transforms do in terms of multi-resolution analysis. Remedies for the issues are provided in this chapter. Necessary conditions for feasible FB parameters are provided and the literature works of designing iterated RFBs and their key features are outlined. Hence, the design challenges and research gap are underlined.

In chapter 3, a design of bi-orthogonal RFB with re-sampling rate satisfying $(\frac{q-1}{q}, \frac{1}{q})$ and multiple regularity orders is proposed. The issue of imposing regularity orders

on an bi-orthogonal structure is addressed. Two methods of solving the nonlinear constraint optimisation, which arises from the FB design problem, are proposed with some design examples.

In chapter 4, a design of bi-orthogonal RFB with re-sampling rate satisfying more general p, q parameters $(\frac{p}{q}, \frac{q-p}{q})$ is discussed with proof for imposing generalised regularity conditions for arbitrary p, q pair. An iterative procedure for solving the design problem is proposed, some design examples are provided. Mathematical proof for convergence of the iterative algorithm though is not addressed, empirical evidence and the affected factors to convergence of the algorithm are discussed.

In chapter 5, experiments on TIMIT and chirp signals using the designed bi-orthogonal RADWTs are investigated. Some sparsity advantage is shown by using the bi-orthogonal RADWTs for signals of oscillatory nature. Hence, the designed bi-orthogonal RADWTs can be used with dyadic wavelet in constructing incoherent dictionary for applications such as signal separation of chirp signals and narrow band interference.

6.3 Potential future work

In section 5.2, the proposed RADWTs and conventional dyadic wavelet transforms are concatenated to form a redundant dictionary for a *basis pursuit* problem, in which exact representation $\Phi^{-1}\mathbf{w} = \mathbf{x}$ is imposed as the linear constraints of the optimisation problem (5.5). However, a more flexible optimisation, which allows some l^2-norm error as in (5.8) can overcome the potential issue of ill-conditioned or singular matrix Φj, which arises in cases of exact representation $\Phi^{-1}\mathbf{w} = \mathbf{x}$ (Figueiredo *et al.* 2007). There have been many works investigating (5.8) in the literature including *basis pursuit denoising* (Chen *et al.* 2001), *regression shrinkage and selection via the lasso* (Tibshirani 1996), whose applications vary from signal reconstruction (Elad *et al.* 2006, Figueiredo and Nowak 2003, Figueiredo and Nowak 2005) to compressive sensing (Candes *et al.* 2006, Candes and Tao 2006). Hence, a potential direction for future work is to attain a tight-frame bi-orthogonal RADWTs. This will enable the use of RADWTs in problem as in (5.8) in seeking the spareness of signal representation in the presence of noise.

The signals in the presented experiments are one dimensional signals. In image and video coding, the spatial scalability factors for broadcasting applications is increasingly in demand. Hence, the adjustable re-sampling property of the proposed bi-orthogonal can be applied to increase the scalability of images, some relevant works are reported

in (Pau *et al.* 2006). Fractional scalability is important for aspects such as ratio adaption between wide-screen video formats. Besides, compressive sensing application using the designed RADWTs in images can be a topic of investigation, which can be applied in video coding.

6.4 Original contributions

We first provide a comprehensive summary of all design approaches to date regarding RADWT designs. From the summary and key features, the gap is found and hence the proposed design of bi-orthogonal RFB with multiple regularity orders. To achieve finer frequency decomposition as compared to existing dyadic wavelets is the primary motivation of the RADWTs. Thus, a design of RFB satisfying $(\frac{q-1}{q}, \frac{1}{q})$ is proposed, which maximises such fine decomposition property for a given integer parameter q. Flexibly adjusted Q factor, which is required to seek representation sparsity of many classes of signals, results in $(\frac{p}{q}, \frac{q-p}{q})$ RFB with more general parameters p, q being investigated. Thus, a general proposition of imposing regularity orders for the bi-orthogonal RFB is presented. The RFB design problem is formulated as a nonlinear constraint optimisation. Three approaches are proposed to solve such problem including *linearised method*, *local optimisation method* and *iterative method*.

- The first one, attains solution in two steps, each of which is to solve a quadratic problem with linear constraints. However, this approach only works for the design with $p = 1$.
- The second approach, *local optimisation* is applicable for all values p, q though running time increases significantly as q increases since it determines the highest order of the nonlinear constraints.
- The third approach solves the nonlinear constraint problem based on an iterative procedure. Proof of convergence was not addressed in the thesis even though extensive experiments of design examples suggest that the iterative algorithm converges in less that 100 iterations. The factors that affect convergence of the algorithm is discussed in section 4.5.

Finally, some application experiments inspired by the designed filters are presented to illustrate their uses.

6.5 In closing

The chapter summarises the key contributions of the thesis and suggesting directions for future work. The thesis investigates on bi-orthogonal rational rate filter banks with regularity orders, which fills in the gap in the area of designing iterated RFB. The advantages and disadvantages of the designs are compared against the existing designs. Together with the application experiments, the thesis has made contributions towards enriching the existing time-frequency transform bases (frames) in seeking representations sparsity, which promotes a property which can potentially benefit many applications in the field of signal processing.

Appendix A

THIS chapter presents proof of some claims and propositions from chapter 3 and 4.

A.1 Detailed derivation of the regularity condition relationship

Proof. Re-writing equation (3.18), we have

$$F(z) = \det \mathbf{A}_{-(0,0)}(z^{q-1}) - z^{-q} \det \mathbf{A}_{-(0,1)}(z^{q-1}) + \cdots + \\ + z^{-q(q-2)}(-1)^{q-2} \det \mathbf{A}_{-(0,q-2)}(z^{q-1}), \tag{A.1}$$

$\mathbf{A}$ is the AC matrix, defined as in (3.15); $\mathbf{A}_{-(0,k)}(z^{q-1})$ is a $q-1 \times q-1$ matrix, defined as matrix $\mathbf{A}$ with row 0 and column k being removed. We replace $\mathbf{A}_{-(0,k)}$ by $\mathbf{A_k}$ for $k = 0, \cdots, q-1$, apply Laplace's formula to the matrix determinants and re-arrange the factors, we have the followings:

$$F(z) = (-1)^{(q-2)} H_{q-1}(z^{q-1}W) \Big[\det \mathbf{A_0}_{-(0,q-2)} - z^{-q} \det \mathbf{A_1}_{-(0,q-2)} + \ldots + (-1)^{(q-2)} \times \\ z^{-q(q-2)} \det \mathbf{A_{q-2}}_{-(0,q-2)} \Big] + (-1)^{(1+q-2)} H_{q-1}(z^{q-1}W^2) \Big[\det \mathbf{A_0}_{-(1,q-2)} - \\ z^{q} \det \mathbf{A_1}_{-(1,q-2)} + \ldots + (-1)^{(q-2)} z^{-q(q-2)} \det \mathbf{A_{q-2}}_{-(1,q-2)} \Big] + \ldots + \\ (-1)^{(2q-4)} H_{q-1}(z^{q-1}W^{q-1}) \Big[\det \mathbf{A_0}_{-(q-2,q-2)} - z^{-q} \det \mathbf{A_1}_{-(q-2,q-2)} + \cdots \\ + (-1)^{(q-2)} z^{-q(q-2)} \det \mathbf{A_{q-2}}_{-(q-2,q-2)} \Big]. \tag{A.2}$$

If we define the matrix

$$\mathbf{B} = \begin{bmatrix} z^{0q} H_0(z^{q-1}W) & z^{1q} H_1(z^{q-1}W) & \cdots & z^{(q-2)q} H_{q-2}(z^{q-1}W) \\ \vdots & \vdots & \vdots & \vdots \\ z^{0q} H_0(z^{q-1}W^{q-1}) & z^{1q} H_1(z^{q-1}W^{q-1}) & \cdots & z^{(q-2)q} H_{q-2}(z^{q-1}W^{q-1}) \end{bmatrix}, \tag{A.3}$$

while the matrix $\mathbf{C}$ in (3.20) can be rewritten as

$$\mathbf{C} = \begin{bmatrix} H(zW^{q-1}) & H(zW^{q-1}W_p) & \cdots & H(zW^{q-1}W_p^{q-2}) \\ H(zW^{q-2}) & H(zW^{q-2}W_p) & \cdots & H(zW^{q-2}W_p^{q-2}) \\ \vdots & \vdots & \vdots & \vdots \\ H(zW) & H(zWW_p) & \cdots & H(zWW_p^{q-2}) \end{bmatrix}, \tag{A.4}$$

for $W = e^{j2\pi/q}$, $W_p = e^{j2\pi/(q-1)}$. The following relationship can therefore be derived in matrix forms as

$$\mathbf{B} \begin{bmatrix} 1 & 1 & 1 & \cdots & 1 \\ 1 & W_p & W_p^2 & \cdots & W_p^{(q-2)} \\ \vdots & \vdots & \vdots & \vdots & \vdots \\ 1 & W_p^{(q-2)} & W_p^{2(q-2)} & \cdots & W_p^{(q-2)(q-2)} \end{bmatrix} = \mathbf{C}$$

and

$$\det \mathbf{B}c = \det \mathbf{C}, \tag{A.5}$$

where $c = \det \begin{bmatrix} 1 & 1 & 1 & \cdots & 1 \\ 1 & W_p & W_p^2 & \cdots & W_p^{(q-2)} \\ \vdots & \vdots & \vdots & \vdots & \vdots \\ 1 & W_p^{(q-2)} & W_p^{2(q-2)} & \cdots & W_p^{(q-2)(q-2)} \end{bmatrix}$.

However, $\det \mathbf{B} =$

$$\det \underbrace{\begin{bmatrix} z^{0q}H_0(z^{q-1}W) + \cdots + & \cdots & z^{(q-2)q}\times \\ z^{(q-2)q}H_{q-2}(z^{q-1}W) & & H_{q-2}(z^{q-1}W) \\ \vdots & \vdots & \vdots \\ z^{0q}H_0(z^{q-1}W^{q-1}) + \cdots + & \cdots & z^{(q-2)q}\times \\ z^{(q-2)q}H_{q-2}(z^{q-1}W^{q-1}) & & H_{q-2}(z^{q-1}W^{q-1}) \end{bmatrix}}_{\text{first column of } \mathbf{B} \text{ is replaced by sum of all } \mathbf{B}\text{'s columns}} \tag{A.6}$$

From (A.5), we have

$$(q-1)\det \mathbf{B}c = (q-1) \times \det \mathbf{C} \tag{A.7}$$

Substitute (A.6) into the LHS of (A.7), we have

$$\begin{aligned}
\text{LHS} = & \\
& c\left\{ \det \begin{bmatrix} H(zW^{(q-1)}) & \cdots & z^{(q-2)q}H_{q-2}(z^{q-1}W) \\ \vdots & \vdots & \vdots \\ H(zW) & \cdots & z^{(q-2)q}H_{q-2}(z^{q-1}W^{q-1}) \end{bmatrix} \right. \\
& + \det \begin{bmatrix} z^{0q}H_0(z^{q-1}W) & H(zW^{(q-1)}) & \cdots \\ \vdots & \vdots & \vdots \\ z^{0q}H_0(z^{q-1}W^{q-1}) & H(zW) & \cdots \end{bmatrix} + \cdots \\
& \left. + \det \begin{bmatrix} z^{0q}H_0(z^{q-1}W) & \cdots & H(zW^{(q-1)}) \\ \vdots & \vdots & \vdots \\ z^{0q}H_0(z^{q-1}W^{q-1}) & \cdots & H(zW) \end{bmatrix} \right\} \\
& = (-1)^0 H(zW^{(q-1)}) \Big[z^{k_0} \det \mathbf{A_0}_{-(0,q-2)} - z^{k_0-q} \det \mathbf{A_1}_{-(0,q-2)} + \cdots + \\
& (-1)^{q-2} z^{k_0-q(q-2)} \det \mathbf{A_{q-2}}_{-(0,q-2)} \Big] + \cdots + (-1)^{q-2} H(zW) \times \\
& \Big[z^{k_n} \det \mathbf{A_0}_{-(q-2,q-2)} - z^{k_n-q} \det \mathbf{A_1}_{-(q-2,q-2)} + \cdots + \\
& (-1)^{q-2} z^{k_n-q(q-2)} \det \mathbf{A_{q-2}}_{-(q-2,q-2)} \Big]
\end{aligned}$$

while

$$\text{RHS} = (q-1) \times \Big[H(zW^{(q-1)}) \det \mathbf{C}_{-(0,0)} - H(zW^{(q-2)}) \det \mathbf{C}_{-(1,0)} + \cdots + (-1)^{q-2} H(zW) \det \mathbf{C}_{-(q-2,0)} \Big]$$

Equate LHS to RHS, we obtain

$$\begin{cases} \det \mathbf{C}_{-(0,0)} = & \frac{c}{q-1} z^{k_0} \big[\det \mathbf{A_0}_{-(0,q-2)} + \cdots + \\ & (-1)^{q-2} z^{-q(q-2)} \det \mathbf{A_{q-2}}_{-(0,q-2)} \big] \\ \det \mathbf{C}_{-(1,0)} = & \frac{c}{q-1} z^{k_1} \big[\det \mathbf{A_0}_{-(1,q-2)} + \cdots + \\ & (-1)^{q-2} z^{-q(q-2)} \det \mathbf{A_{q-2}}_{-(1,q-2)} \big] \\ \vdots & \\ \det \mathbf{C}_{-(q-2,0)} = & \frac{c}{q-1} z^{k_{q-2}} \big[\det \mathbf{A_0}_{-(q-2,q-2)} + \cdots + \\ & (-1)^{q-2} z^{-q(q-2)} \det \mathbf{A_{q-2}}_{-(q-2,q-2)} \big] \end{cases} \tag{A.8}$$

Substitute (A.8) into (A.2), we can find

$$\begin{aligned} F(z) = \frac{q-1}{c} \big[& z^{-k_0} (-1)^{(q-2)} H_{q-1}(z^{q-1} W) \det \mathbf{C}_{-(0,0)} \\ & + z^{-k_1} (-1)^{(1+q-2)} H_{q-1}(z^{q-1} W^2) \det \mathbf{C}_{-(1,0)} + \cdots \\ & + z^{-k_{q-2}} (-1)^{(2q-4)} H_{q-1}(z^{q-1} W^{q-1}) \det \mathbf{C}_{-(q-2,0)} \big] \end{aligned} \tag{A.9}$$

□

A.2 Relationship between filter's polyphase component and its passband flatness

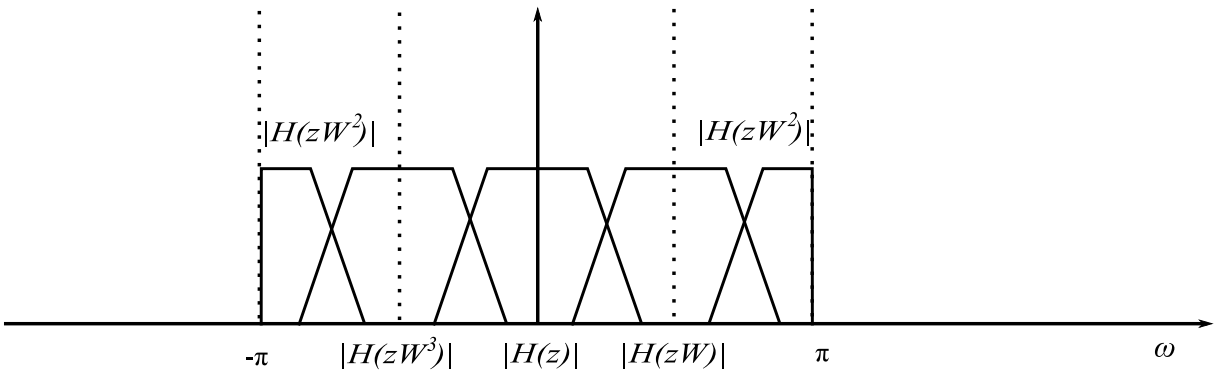

Figure A.1. The filter $H(z)$ and its frequency shifts magnitude response

Proof. Consider a special case of filter $H(z)$ with passband response in the frequency region of $[0, \pi/4]$ and $W = e^{-j2\pi/4}$. We have:

$$H_0(z) = H(z) + H(zW) + H(zW^2) + H(zW^3) \tag{A.10}$$

$$= h_0 + h_4 z^{-4} + h_8 z^{-8} + \cdots + h_{4n} z^{-4n}, \tag{A.11}$$

where $H(z) = h_0 + h_1 z^{-1} + \cdots + h_N z^{-N}$. Besides, we could observe from the figure that the polyphase component $|H_0(\omega)|$ magnitude response is strongly dominant by the passband response of the filter $|H(\omega)|$ except for the transition band and vice versa.

Similarly, if we have

$$\begin{aligned} H_3(z) &= H(z) + WH(zW) + W^2H(zW^2) + W^3H(zW^3) \\ &= h_3 z^{-3} + h_7 z^{-7} + h_1 1 z^{-11} + \cdots + h_{4n+3} z^{-4n+3} \end{aligned}$$

Since $|WH(zW)| = |H(zW)|$, $|W^2H(zW^2)| = |H(zW^2)|$, $|W^3H(zW^3)| = |H(zW^3)|$, we can claim that $|H_3(\omega)|$ response determines the flatness of the filter's passband response and vice versa. By induction, if the filter $H(z)$ has relatively flat pass band response in the region of $[0, \frac{\pi}{q}]$ or $[\frac{\pi(q-1)}{q}, \pi]$, the q polyphases of $H(z)$ is approximately flat across all frequency and vice versa. In the case when one of the q polyphases of $H(z)$ is a pure delay which is the case of a $q-$band filter, $H(z)$ is maximally flat in the passband region. □

Appendix B

Filter design results

THE appendix shows the responses of the designed filters that are mentioned in the thesis whose responses yet to be shown.

B.1 RFB designed by linearised method with parameters satisfying $(\frac{q-1}{q}, \frac{1}{q})$

Table B.1. The filter design parameters for appendices B.1.1-B.1.4.

	Linearised method			
	B.1.1 parameters: $(2/3, 1/3), K = 2$	B.1.2 parameters: $(3/4, 1/4), K = 2$	B.1.3 parameters $(6/7, 1/7), K = 4$	B.1.4 parameters $(9/19, 1/10), K = 3$
n_0, L_0, N_0	$42, 17, 35$	$50, 17, 33$	$63, 33, 65$	$96, 40, 79$
N_1	50	52	35	40
ϵ_{LP}	$\epsilon_{LP} = 0$	$\epsilon_{LP} = 0$	$\epsilon_{LP} = 0$	$\epsilon_{LP} = 0$
$\omega_{sLP}, \omega_{sHP}$	$0.388\pi, 0.592\pi$	$0.29\pi, 0.695\pi$	$0.193\pi, 0.787\pi$	$0.12\pi, 0.82\pi$

where n_0 determines the system's delay, N_0, N_1 are the analysis low-pass and high-pass filters' lengths, respectively; L_0, L_1 are the mid-point indices of the analysis low-pass and high-pass filters. If $\epsilon_{LP} = 0$, it is equivalent that the pre-designed analysis low-pass filter is an q^{th}-band filter.

B.1.1 Rational filter bank of $(\frac{2}{3}, \frac{1}{3})$

RFB of $(\frac{2}{3}, \frac{1}{3})$ with two regularity orders are designed based on linearised method. The analysis low-pass and high-pass filters are of $35, 50$ taps, respectively. The responses are shown in Fig. B.1

B.1.2 Rational filter bank of $(\frac{3}{4}, \frac{1}{4})$

RFB of $(\frac{3}{4}, \frac{1}{4})$ with two regularity orders are designed based on linearised method. The analysis low-pass and high-pass filters are of $33, 52$ taps, respectively. The responses are shown in Fig. B.2

B.1.3 Rational filter bank of $(\frac{6}{7}, \frac{1}{7})$

RFB of $(\frac{6}{7}, \frac{1}{7})$ with four regularity orders are designed based on linearised method. The analysis low-pass and high-pass filters are of $65, 35$ taps, respectively. The responses are shown in Fig. B.3

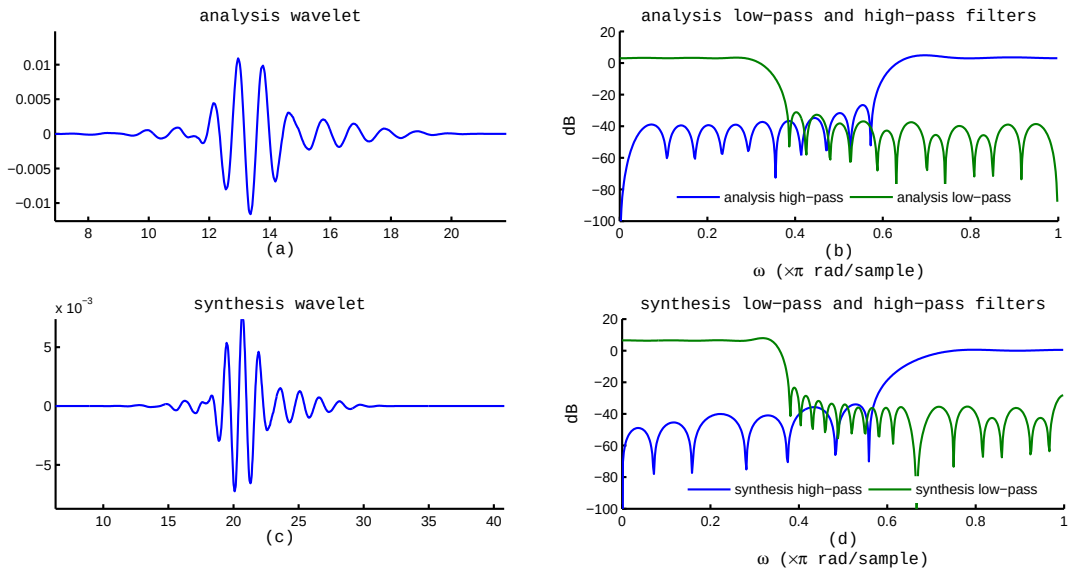

Figure B.1. $(\frac{2}{3}, \frac{1}{3})$ RFB with two regularity orders. Left panels: Analysis (a) and Synthesis (c) wavelet functions, respectively. Right panels show the analysis (b) and synthesis (d) low-pass and high-pass filters' frequency response, respectively.

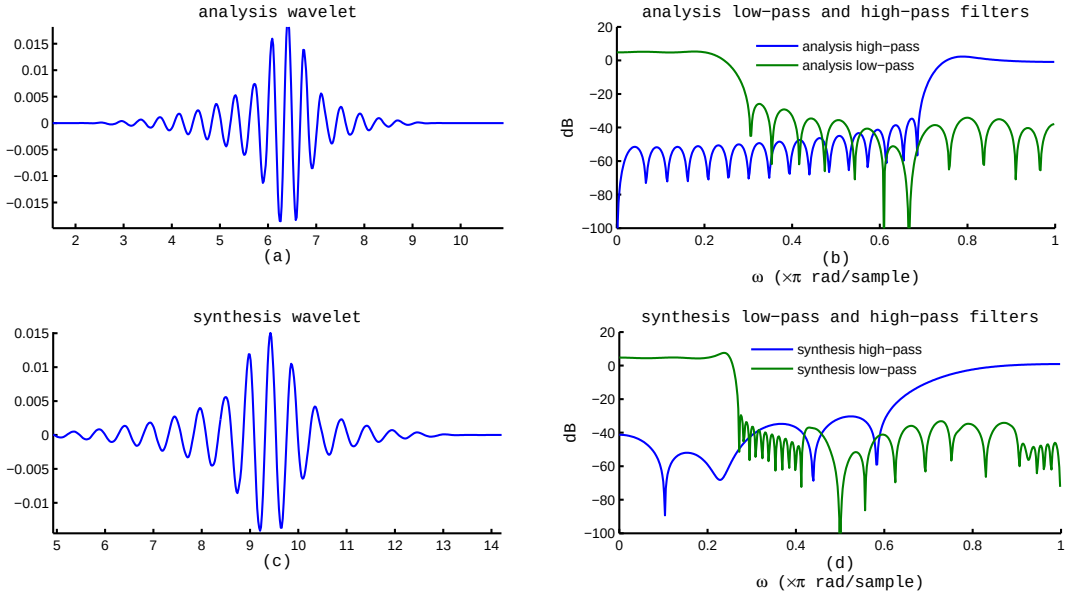

Figure B.2. $(\frac{3}{4}, \frac{1}{4})$ RFB with two regularity orders. Left panels: Analysis (a) and Synthesis (c) wavelet functions, respectively. Right panels show the analysis (b) and synthesis (d) low-pass and high-pass filters' frequency response, respectively.

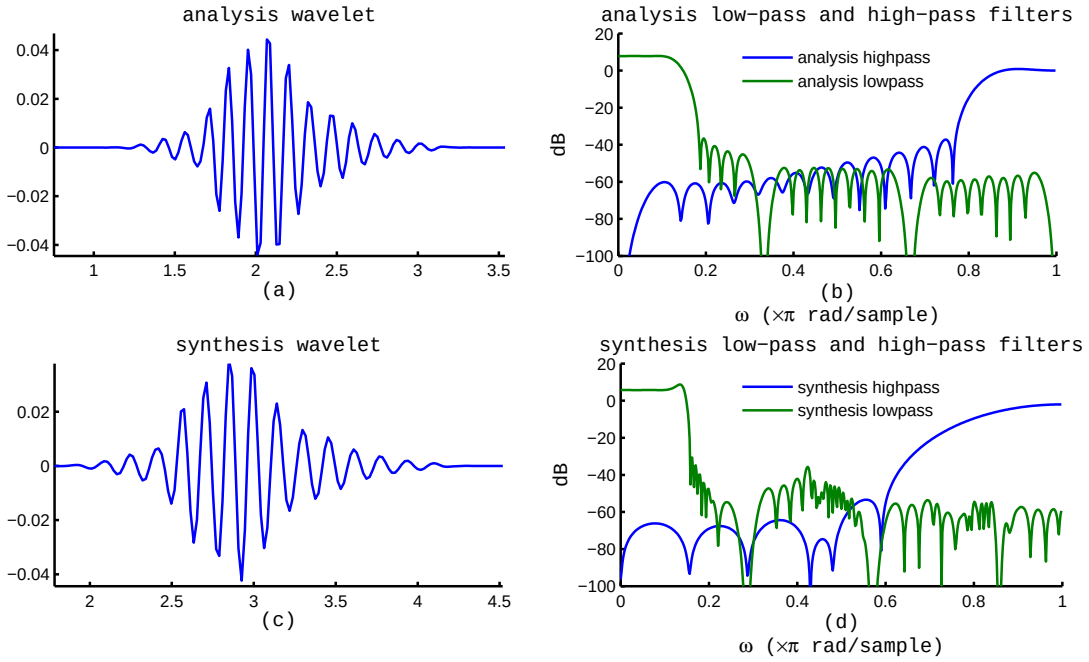

Figure B.3. $(\frac{6}{7}, \frac{1}{7})$ RFB with four regularity orders. Left panels: Analysis (a) and Synthesis (c) wavelet functions, respectively. Right panels show the analysis (b) and synthesis (d) low-pass and high-pass filters' frequency response, respectively.

B.1.4 Rational filter bank of $(\frac{9}{10}, \frac{1}{10})$

RFB of $(\frac{9}{10}, \frac{1}{10})$ with three regularity orders are designed based on linearised method. The analysis low-pass and high-pass filters are of $79, 40$ taps, respectively. The responses are shown in Fig. B.4

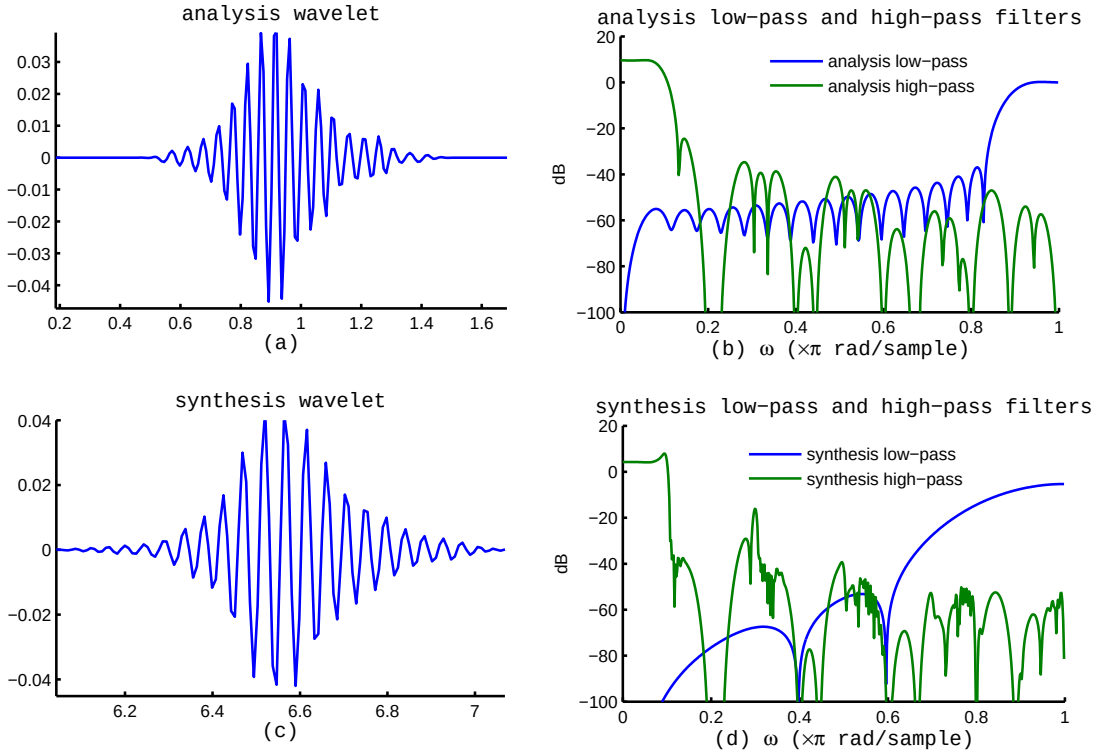

Figure B.4. $(\frac{9}{10}, \frac{1}{10})$ RFB with three regularity orders. Left panels: Analysis (a) and Synthesis (c) wavelet functions, respectively. Right panels show the analysis (b) and synthesis (d) low-pass and high-pass filters' frequency response, respectively.

Bibliography

AFONSO-M., BIOUCAS-DIAS-J., AND FIGUEIREDO-M. (2010). A fast algorithm for the constrained formulation of compressive image reconstruction and other linear inverse problems, *Acoustics Speech and Signal Processing (ICASSP), 2010 IEEE International Conference on*, pp. 4034 –4037.

AHARON-M., AND ELAD-M. (2008). Sparse and redundant modeling of image content using an image-signature-dictionary, *SIAM Journal on Imaging Sciences*, **1**(3), pp. 228–247.

AKÇAKAYA-M., AND TAROKH-V. (2008a). A frame construction and a universal distortion bound for sparse representations, *Signal Processing, IEEE Transactions on*, **56**(6), pp. 2443–2450.

AKÇAKAYA-M., AND TAROKH-V. (2008b). A frame construction and a universal distortion bound for sparse representations, *Signal Processing, IEEE Transactions on*, **56**(6), pp. 2443–2450.

AMIN-M., AND FENG-K. D. (1995). Short-time fourier transforms using cascade filter structures, *Circuits and Systems II: Analog and Digital Signal Processing, IEEE Transactions on*, **42**(10), pp. 631 –641.

ANTONIADIS-A. (1997). Wavelets in statistics: A review, *Statistical Methods & Applications*, **6**, pp. 97–130. 10.1007/BF03178905.

ANTONINI-M., BARLAUD-M., MATHIEU-P., AND DAUBECHIES-I. (1992). Image coding using wavelet transform, *Image Processing, IEEE Transactions on*, **1**(2), pp. 205 –220.

ARGENTI-F., AND DEL RE-E. (1998). Rational sampling filter banks based on IIR filters, *Signal Processing, IEEE Transactions on*, **46**(12), pp. 3403 –3408.

AUSCHER-P. (1992). Wavelet bases for $l^2(r)$ with rational dilation factor, *Wavelets and their applications*, Jones and Barlett, Boston, MA, USA, pp. 439–451.

BARANIUK-R. G., AND JONES-D. L. (1993). Shear madness: New orthonormal bases and frames using chirp functions, *IEEE Transactions on Signal Processing*, **41**(12), pp. 3543–3549.

BAUSSARD-A., NICOLIER-F., AND TRUCHETET-F. (2004). Rational multiresolution analysis and fast wavelet transform: application to wavelet shrinkage denoising, *Signal Processing*, **84**(10), pp. 1735–1747.

BAYRAM-I., AND SELESNICK-I. (2009a). Frequency-domain design of overcomplete rational-dilation wavelet transforms, *Signal Processing, IEEE Transactions on*, **57**(8), pp. 2957 –2972.

BAYRAM-I., AND SELESNICK-I. W. (2007). Design of orthonormal and overcomplete wavelet transforms based on rational sampling factors, *Wavelet Applications in Industrial Processing V*, Vol. 6763, SPIE, Boston, MA, USA, pp. 67630H–15.

BAYRAM-I., AND SELESNICK-I. W. (2009b). Orthonormal FBs with rational sampling factors and oversampled DFT-modulated FBs: A connection and filter design, *Signal Processing, IEEE Transactions on*, **57**(7), pp. 2515–2526.

BAYRAM-I., AND SELESNICK-I. W. (2009c). Overcomplete discrete wavelet transforms with rational dilation factors, *Signal Processing, IEEE Transactions on*, **57**(1), pp. 131–145.

BELOVA-N. Y., MIHAYLOV-S. V., AND PIRYOVA-B. G. (2007). Wavelet transform: A better approach for the evaluation of instantaneous changes in heart rate variability, *Autonomic Neuroscience*, **131**(1), pp. 107–122.

BLU-T. (1993). Iterated filter banks with rational rate changes connection with discrete wavelet transforms, *Signal Processing, IEEE Transactions on*, **41**(12), pp. 3232–3244.

BLU-T. (1998). A new design algorithm for two-band orthonormal rational filter banks and orthonormal rational wavelets, *Signal Processing, IEEE Transactions on*, **46**(6), pp. 1494–1504.

BLU-T., DRAGOTTI-P.-L., VETTERLI-M., MARZILIANO-P., AND COULOT-L. (2008). Sparse sampling of signal innovations, *Signal Processing Magazine, IEEE*, **25**(2), pp. 31–40.

BREGOVIC-R., LIM-Y. C., AND SARAMAKI-T. (2008). Frequency-response masking-based design of nearly perfect-reconstruction two-channel FIR filterbanks with rational sampling factors, *Circuits and Systems I: Regular Papers, IEEE Transactions on*, **55**(7), pp. 2002 –2012.

BROCKWELL-P. J., DAHLHAUS-R., AND TRINDADE-A. A. (2005). Modified burg algorithms for multivariate subset autoregression, *Statistica Sinica*, **15**(1), pp. 197–213.

BURG-J. P. (1968). A new analysis technique for time series data, *NATO Advanced Study Institute on Signal Processing with Emphasis on Underwater Acoustics*, pp. 12–23.

CANDES-E., AND ROMBERG-J. (2007). Sparsity and incoherence in compressive sampling, *Inverse problems*, **23**(3), p. 969.

CANDES-E., AND WAKIN-M. (2008). An introduction to compressive sampling, *Signal Processing Magazine, IEEE*, **25**(2), pp. 21 –30.

CANDÈS-E. J. (2006). Compressive sampling, *Proceedings oh the International Congress of Mathematicians: Madrid, August 22-30, 2006: invited lectures*, pp. 1433–1452.

CANDES-E. J., AND TAO-T. (2006). Near-optimal signal recovery from random projections: Universal encoding strategies?, *Information Theory, IEEE Transactions on*, **52**(12), pp. 5406–5425.

CANDES-E. J., ROMBERG-J. K., AND TAO-T. (2006). Stable signal recovery from incomplete and inaccurate measurements, *Communications on pure and applied mathematics*, **59**(8), pp. 1207–1223.

CANDS-E., WAKIN-M., AND BOYD-S. (2008). Enhancing sparsity by reweighted l1 minimization, *Journal of Fourier Analysis and Applications*, **14**, pp. 877–905. 10.1007/s00041-008-9045-x.

CHEN-P.-Y., AND SELESNICK-I. W. (2013). Translation-invariant shrinkage/thresholding of group sparse signals.

CHEN-S. S., DONOHO-D. L., AND SAUNDERS-M. A. (1998). Atomic decomposition by basis pursuit, *SIAM journal on scientific computing*, **20**(1), pp. 33–61.

CHEN-S. S., DONOHO-D. L., AND SAUNDERS-M. A. (2001). Atomic Decomposition by Basis Pursuit, *SIAM Review*, **43**, pp. 129–159.

CHEN-W., KEHTARNAVAZ-N., AND SPENCER-T. (1993). An efficient recursive algorithm for time-varying fourier transform, *Signal Processing, IEEE Transactions on*, **41**(7), pp. 2488 –2490.

CHUI.-C. K. (1992). *Wavelets: a tutorial in theory and applications*, Wavelet Analysis and Its applicatins, v. 2, Academic Press, San Diego, CA.

DAUBECHIES-I. (1988). Orthonormal bases of compactly supported wavelets, *Communications on Pure and Applied Mathematics*, **41**(7), pp. 909–996.

DAUBECHIES-I. (1990). The wavelet transform, time-frequency localization and signal analysis, *Information Theory, IEEE Transactions on*, **36**(5), pp. 961 –1005.

DAUBECHIES-I. (1992). *Ten Lectures on Wavelets*, CBMS-NSF, Siam.

DAVIS-M. J., AND HELLER-E. J. (1979). Semiclassical gaussian basis set method for molecular vibrational wave functions, *The Journal of Chemical Physics*, **71**(8), pp. 3383–3395.

DONOHO-D. L. (1995). De-noising by soft-thresholding, *Information Theory, IEEE Transactions on*, **41**(3), pp. 613–627.

DONOHO-D. L., AND JOHNSTONE-J. M. (1994). Ideal spatial adaptation by wavelet shrinkage, *Biometrika*, **81**(3), pp. 425–455.

DUARTE-M., DAVENPORT-M., WAKIN-M., AND BARANIUK-R. (2006). Sparse signal detection from incoherent projections, *Acoustics, Speech and Signal Processing, 2006. ICASSP 2006 Proceedings. 2006 IEEE International Conference on*, Vol. 3, p. III.

DURAK-L., AND ARIKAN-O. (2003). Short-time fourier transform: two fundamental properties and an optimal implementation, *Signal Processing, IEEE Transactions on*, **51**(5), pp. 1231 – 1242.

ELAD-M., MATALON-B., AND ZIBULEVSKY-M. (2006). Image denoising with shrinkage and redundant representations, *Computer Vision and Pattern Recognition, 2006 IEEE Computer Society Conference on*, Vol. 2, IEEE, pp. 1924–1931.

ESTHER LEUNG-K., VAN STRALEN-M., NEMES-A., VOORMOLEN-M. M., VAN BURKEN-G., GELEIJNSE-M. L., TEN CATE-F., REIBER-J., DE JONG-N., VAN DER STEEN-A. F ETXXXXX AL.. (2008). Sparse registration for three-dimensional stress echocardiography, *Medical Imaging, IEEE Transactions on*, **27**(11), pp. 1568–1579.

FAROOQ-O., AND DATTA-S. (2001). Mel filter-like admissible wavelet packet structure for speech recognition, *Signal Processing Letters, IEEE*, **8**(7), pp. 196 –198.

FASTL-H., AND ZWICKER-E. (2007). *Psychoacoustics: Facts and Models*, Springer, Berlin, Heidelberg.

FIGUEIREDO-M. A., AND NOWAK-R. D. (2003). An em algorithm for wavelet-based image restoration, *Image Processing, IEEE Transactions on*, **12**(8), pp. 906–916.

FIGUEIREDO-M. A., AND NOWAK-R. D. (2005). A bound optimization approach to wavelet-based image deconvolution, *Image Processing, 2005. ICIP 2005. IEEE International Conference on*, Vol. 2, IEEE, pp. II–782.

FIGUEIREDO-M., NOWAK-R., AND WRIGHT-S. (2007). Gradient projection for sparse reconstruction: Application to compressed sensing and other inverse problems, *Selected Topics in Signal Processing, IEEE Journal of*, **1**(4), pp. 586 –597.

FOLLAND-G. (2009). *Fourier Analysis and Its Applications*, The Wadsworth & Brooks/Cole Mathematics series, American Mathematical Society.

FUCHS-J. J. (2007). Convergence of a sparse representations algorithm applicable to real or complex data, *Selected Topics in Signal Processing, IEEE Journal of*, **1**(4), pp. 598–605.

GABOR-D. (1946). Theory of communication. part 1: The analysis of information, *Electrical Engineers - Part III: Radio and Communication Engineering, Journal of the Institution of*, **93**(26), pp. 429 –441.

GAROFOLO-J. S., LAMEL-L. F., FISHER-W. M., FISCUS-J. G., PALLETT-D. S., DAHLGREN-N. L., AND ZUE-V. (1993). TIMIT acoustic-phonetic continuous speech corpus, *Linguistic Data Consortium Philadelphia*.

GHINWA-F. C., AND JAMES-R. G. (2007). An implementation of rational wavelets and filter design for phonetic classification, *Audio, Speech, and Language Processing, IEEE Transactions on*, **15**(3), pp. 939–948.

GOPINATH-R., AND BURRUS-C. (1995). On cosine-modulated wavelet orthonormal bases, *Image Processing, IEEE Transactions on*, **4**(2), pp. 162–176.

GOYAL-V. K., FLETCHER-A. K., AND RANGAN-S. (2008). Compressive sampling and lossy compression, *Signal Processing Magazine, IEEE*, **25**(2), pp. 48–56.

GRIBONVAL-R., AND NIELSEN-M. (2003). Sparse representations in unions of bases, *Information Theory, IEEE Transactions on*, **49**(12), pp. 3320–3325.

HE-Z., XIE-S., DING-S., AND CICHOCKI-A. (2007). Convolutive blind source separation in the frequency domain based on sparse representation, *Audio, Speech, and Language Processing, IEEE Transactions on*, **15**(5), pp. 1551–1563.

HURLEY-N., AND RICKARD-S. (2009). Comparing measures of sparsity, *Information Theory, IEEE Transactions on*, **55**(10), pp. 4723 –4741.

JIAO-L., BO-L., AND WANG-L. (2007). Fast sparse approximation for least squares support vector machine, *Neural Networks, IEEE Transactions on*, **18**(3), pp. 685–697.

KOVACEVIC-J., AND VETTERLI-M. (1993). Perfect reconstruction filter banks with rational sampling factors, *Signal Processing, IEEE Transactions on*, **41**(6), pp. 2047–2066.

KUMAR-P., AND PRABHU-K. (1997). Simulation studies of moving-target detection: a new approach with wigner-ville distribution, *Radar, Sonar and Navigation, IEE Proceedings -*, **144**(5), pp. 259 –265.

KWOK-H., AND JONES-D. (2000). Improved instantaneous frequency estimation using an adaptive short-time fourier transform, *Signal Processing, IEEE Transactions on*, **48**(10), pp. 2964 –2972.

LAKSHMANAN-M., AND NIKOOKAR-H. (2006). A review of wavelets for digital wireless communication, *Wireless Personal Communications*, **37**, pp. 387–420. 10.1007/s11277-006-9077-y.

LAURENTI-N., DE POLI-G., AND MONTAGNER-D. (2007). A nonlinear method for stochastic spectrum estimation in the modeling of musical sounds, *Audio, Speech, and Language Processing, IEEE Transactions on*, **15**(2), pp. 531 –541.

LEVINE, SCOTT N.; SMITH III-J. O. (1998). A sines+transients+noise audio representation for data compression and time/pitch scale modifications, *Audio Engineering Society Convention 105*.

LIU-K. (1993). Novel parallel architectures for short-time fourier transform, *Circuits and Systems II: Analog and Digital Signal Processing, IEEE Transactions on*, **40**(12), pp. 786 –790.

MAIRAL-J., ELAD-M., AND SAPIRO-G. (2008). Sparse representation for color image restoration, *Image Processing, IEEE Transactions on*, **17**(1), pp. 53–69.

MALLAT-S. G. (1989a). Multiresolution apporximations and wavelet orthonormal bases of l2(r), *Transactions of the American Mathematical Society*, **315**(1), pp. 69–87.

MALLAT-S. G. (1989b). A theory for multiresolution signal decomposition: the wavelet representation, *Pattern Analysis and Machine Intelligence, IEEE Transactions on*, **11**(7), pp. 674–693.

MARPLE JR-S. L. (1987). Digital spectral analysis with applications, *Englewood Cliffs, NJ, Prentice-Hall, Inc., 1987, 512 p.*

MEYER-Y. (1989). Orthonormal Wavelets, *in* J.-M. Combes., A. Grossmann., and P. Tchamitchian. (eds.), *Wavelets. Time-Frequency Methods and Phase Space*, p. 21.

MOLLA-S., AND TORRSANI-B. (2005). A hybrid scheme for encoding audio signal using hidden Markov models of waveforms, *Applied and Computational Harmonic Analysis*, **18**(2), pp. 137 – 166.

NGUYEN-S., AND NG-B.-H. (2010). Critically sampled discrete wavelet transforms with rational dilation factor of 3/2, *Signal Processing (ICSP), 2010 IEEE 10th International Conference on*, pp. 199 –202.

NGUYEN-S. T. N., AND NG-B.-H. (2012). Design of two-band critically sampled rational rate filter banks with multiple regularity orders and associated discrete wavelet transforms, *Signal Processing, IEEE Transactions on*, **60**(7), pp. 3863 –3868.

NGUYEN-S. T. N., AND NG-B. W.-H. (2013). Bi-orthogonal rational discrete wavelet transform with multiple regularity orders and application experiments, *Signal Processing*, (0), pp. –.

O'GRADY-P. D., PEARLMUTTER-B. A., AND RICKARD-S. T. (2005). Survey of sparse and non-sparse methods in source separation, *International Journal of Imaging Systems and Technology*, **15**(1), pp. 18–33.

ORAINTARA-S., TRAN-T. D., HELLER-P. N., AND NGUYEN-T. Q. (2001). Lattice structure for regular paraunitary linear-phase filterbanks and m-band orthogonal symmetric wavelets, *Signal Processing, IEEE Transactions on*, **49**(11), pp. 2659–2672.

PAN-Q., ZHANG-L., DAI-G., AND ZHANG-H. (1999). Two denoising methods by wavelet transform, *Signal Processing, IEEE Transactions on*, **47**(12), pp. 3401 –3406.

PAU-G., PESQUET-POPESCU-B., AND PIELLA-G. (2006). Modified m-band synthesis filter bank for fractional scalability of images, *Signal Processing Letters, IEEE*, **13**(6), pp. 345–348.

PICHOT-V., BUFFIERE-S., GASPOZ-J.-M., COSTES-F., MOLLIEX-S., DUVERNEY-D., ROCHE-F., AND BARTHELEMY-J.-C. (2001). Wavelet transform of heart rate variability to assess autonomic nervous system activity does not predict arousal from general anesthesia, *Canadian Journal of Anesthesia*, **48**(9), pp. 859–863.

PICHOT-V., GASPOZ-J.-M., MOLLIEX-S., ANTONIADIS-A., BUSSO-T., ROCHE-F., COSTES-F., QUINTIN-L., LACOUR-J.-R., AND BARTHÉLÉMY-J.-C. (1999). Wavelet transform to quantify heart rate variability and to assess its instantaneous changes, *Journal of Applied Physiology*, **86**(3), pp. 1081–1091.

PORTNOFF-M. (1980). Time-frequency representation of digital signals and systems based on short-time fourier analysis, *Acoustics, Speech and Signal Processing, IEEE Transactions on*, **28**(1), pp. 55–69.

PRINCEN-J. (1994). The design of nonuniform modulated filter banks, *Time-Frequency and Time-Scale Analysis, 1994., Proceedings of the IEEE-SP International Symposium on*, pp. 112–115.

QIAN-S., AND CHEN-D. (1999). Joint time-frequency analysis, *Signal Processing Magazine, IEEE*, **16**(2), pp. 52 –67.

RAAB-R. E. (1982). Gabor's Signal Expansion and Degrees of Freedom of a Signal, *Optica Acta*, **29**, pp. 1223–1229.

RICKARD-S. (2007). The duet blind source separation algorithm, *Blind Speech Separation*, pp. 217–241.

ROTHWELL-E., CHEN-K., AND NYQUIST-D. (1998). An adaptive-window-width short-time fourier transform for visualization of radar target substructure resonances, *Antennas and Propagation, IEEE Transactions on*, **46**(9), pp. 1393 –1395.

SAADAT MEHR-A., AND CHEN-T. (2000). Design of nonuniform multirate filter banks by semidefinite programming, *Circuits and Systems II: Analog and Digital Signal Processing, IEEE Transactions on*, **47**(11), pp. 1311–1314.

SAGHIZADEH-P., AND WILLSON-A. N. (1998). A new approach to the design of critically sampled M-channel uniform-band perfect-reconstruction linear-phase FIR filter banks, *Signal Processing, IEEE Transactions on*, **46**(6), pp. 1544–1557.

SANDERCOCK-G. R., BROMLEY-P. D., AND BRODIE-D. A. (2005). The reliability of short-term measurements of heart rate variability, *International journal of cardiology*, **103**(3), pp. 238–247.

SELESNICK-I. (2010). A new sparsity-enabled signal separation method based on signal resonance, *Acoustics Speech and Signal Processing (ICASSP), 2010 IEEE International Conference on*, pp. 4150 –4153.

SELESNICK-I. (2011a). Wavelet transform with tunable Q-factor, *Signal Processing, IEEE Transactions on*, **59**(8), pp. 3560 –3575.

SELESNICK-I. W. (2011b). Resonance-based signal decomposition: A new sparsity-enabled signal analysis method, *Signal Processing*, **91**(12), pp. 2793 – 2809. ¡ce:title¿Advances in Multirate Filter Bank Structures and Multiscale Representations¡/ce:title¿.

SELESNICK-I. W. (2011c). Sparse signal representations using the tunable Q-factor wavelet transform, *in* M. Papadakis., D. V. D. Ville., and V. K. Goyal. (eds.), *Wavelets and Sparsity XIV*, Vol. 8138, SPIE, p. 81381U.

SMITH-M., AND BARNWELL-T. (1984). A procedure for designing exact reconstruction filter banks for tree-structured subband coders, *Acoustics, Speech, and Signal Processing, IEEE International Conference on ICASSP '84.*, Vol. 9, pp. 421–424.

STANKOVIC-L. (1994). A method for time-frequency analysis, *Signal Processing, IEEE Transactions on*, **42**(1), pp. 225 –229.

STEFFEN-P., HELLER-P. N., GOPINATH-R. A., AND BURRUS-C. S. (1993). Theory of regular m-band wavelet bases, *Signal Processing, IEEE Transactions on*, **41**(12), pp. 3497–3511.

STEIN-C. M. (1981). Estimation of the mean of a multivariate normal distribution, *The Annals of Statistics*, **9**(6), pp. pp. 1135–1151.

STRANG-G., AND NGUYEN-T. (1996). *Wavelets and Filter banks.*, Wellesley-Cambridge, Wellesley, MA.

TERRAS-A. (1999). *Fourier Analysis on Finite Groups and Applications*, London Mathematical Society Student Texts, Cambridge University Press.

TESCHKE-G. (2007). Multi-frame representations in linear inverse problems with mixed multi-constraints, *Applied and Computational Harmonic Analysis*, **22**(1), pp. 43–60.

TIBSHIRANI-R. (1996). Regression shrinkage and selection via the lasso, *Journal of the Royal Statistical Society. Series B (Methodological)*, pp. 267–288.

TROPP-J. (2006). Just relax: convex programming methods for identifying sparse signals in noise, *Information Theory, IEEE Transactions on*, **52**(3), pp. 1030 –1051.

UNSER-M., AND ALDROUBI-A. (1996). A review of wavelets in biomedical applications, *Proceedings of the IEEE*, **84**(4), pp. 626 –638.

VAIDYANATHAN-P. (1987a). Quadrature mirror filter banks, m-band extensions and perfect-reconstruction techniques, *ASSP Magazine, IEEE*, **4**(3), pp. 4–20.

VAIDYANATHAN-P. (1987b). Theory and design of m-channel maximally decimated quadrature mirror filters with arbitrary m, having the perfect-reconstruction property, *Acoustics, Speech and Signal Processing, IEEE Transactions on*, **35**(4), pp. 476–492.

VAIDYANATHAN-P. P. (1993). *Multirate systems and filter banks*, Prentice Hall.

VETTERLI-M. (1987). A theory of multirate filter banks, *Acoustics, Speech and Signal Processing, IEEE Transactions on*, **35**(3), pp. 356–372.

VETTERLI-M., AND HERLEY-C. (1992). Wavelets and filter banks: theory and design, *Signal Processing, IEEE Transactions on*, **40**(9), pp. 2207–2232.

VETTERLI-M., AND KOVACEVIC-J. (1995). *Wavelets and subband coding*, Prentice-Hall, Inc.

WADA-S. (1995). Design of nonuniform division multirate fir filter banks, *Circuits and Systems II: Analog and Digital Signal Processing, IEEE Transactions on*, **42**(2), pp. 115–121.

WISUTMETHANGOON-Y., AND NGUYEN-T. Q. (1999). A method for design of Mth-band filters, *Signal Processing, IEEE Transactions on*, **47**(6), pp. 1669–1678.

YILMAZ-O., AND RICKARD-S. (2004). Blind separation of speech mixtures via time-frequency masking, *Signal Processing, IEEE Transactions on*, **52**(7), pp. 1830–1847.

YU-L., AND WHITE-L. B. (2005). Broadband doppler compensation for rational wavelet-based uwa communication systems, *Communications, 2005 Asia-Pacific Conference on*, pp. 605–609.

YU-L., AND WHITE-L. B. (2006). Complex rational orthogonal wavelet and its application in communications, *Signal Processing Letters, IEEE*, **13**(8), pp. 477–480.

ZHONG-W., SHI-G., XIE-X., AND CHEN-X. (2010). Design of linear-phase nonuniform filter banks with partial cosine modulation, *Signal Processing, IEEE Transactions on*, **58**(6), pp. 3390 –3395.

ZHU-C. (2008). Stable recovery of sparse signals via regularized minimization, *Information Theory, IEEE Transactions on*, **54**(7), pp. 3364 –3367.

Glossary

AC	alias component
BPF	band-pass filter
DCT	discrete cosine transform
DWT	discrete wavelet transform
ECG	electrocardiographic
EEG	electroencephalography
FB	filter bank
FIR	finite impulse response
HPF	high-pass filter
IIR	infinite impulse response
LPF	low-pass filter
MRA	multi-resolution analysis
MSE	mean squared error
NUFB	nonuniform filter bank
PR	perfect reconstruction
Q-factor	quality factor
RADWT	rational discrete wavelet transform
RFB	rational rate filter bank
RHS	right hand side
SALSA	split augmented lagrangian shrinkage Algorithm
SIR	signal to interference ratio
SNR	signal to noise ratio
STFT	short time Fourier transform
TIMIT	Texas instruments and Massachusetts institute of technology
WVD	Wigner-ville distribution